2.5.4.7 Response of Soil and Rock to Dynamic Loading

LNP COL 2.5-2
LNP COL 2.5-6

This subsection presents a summary of information regarding the response of soil and rock to dynamic loading. Cross references to other subsections in this FSAR are provided herein.

Descriptions of investigations performed to identify surface faulting features in the LNP site and vicinity are presented in FSAR Subsection 2.5.3. As stated therein, there are no capable tectonic fault sources within the site area or vicinity. There is no evidence of Quaternary tectonic surface faulting or fold deformation within the LNP site location. The potential for nontectonic deformation at the site from phenomenon other than karst-related collapse or subsidence is negligible. The LNP site lies within a region susceptible to dissolution and karst development. The materials below the bottom of the nuclear island to an elevation of -30 m (-99 ft.) NAVD88 will be improved as described in FSAR Subsection 2.5.4.12.

Results of V_S and V_P surveys at the LNP site are presented in FSAR Subsection 2.5.4.4. Results of V_S from Suspension P-S velocity logging and downhole logging within boreholes at LNP 1 and LNP 2 are presented on Figures 2.5.4.2-204A, 2.5.4.2-204B, 2.5.4.2-205A, and 2.5.4.2-205B. Interpretations of these data relative to the site geologic conditions are presented in FSAR Subsection 2.5.4.4.2. These data were used to develop site-specific dynamic velocity profiles for site response analyses as presented in FSAR Subsection 2.5.2.5.

Dynamic triaxial shear tests and resonant column tests were not performed as part of the investigation because of the following:

- The basemats for the nuclear islands for LNP 1 and LNP 2 bear on RCC which in turn bears on rock. Considering the low seismic environment and the foundation configuration, no site specific soil structure interaction analysis for safety class structures is required and, therefore, no Modulus Degradation Curves or Damping Curves as typically measured by these types of tests were required.

- During the site investigation, it was extremely difficult to obtain quality undisturbed samples of the Quaternary and Tertiary sediments at the site and reconstituted samples from SPT samples would not be representative as the cementation effects would be lost. The uncertainty in the modulus reduction and damping relationship was incorporated in the site response analysis by modeling a range of behavior (relatively linear to relatively nonlinear) for the softer layers of weathered limestone/calcareous silts. The range in dynamic properties had only a small effect on the computed GMRS and an even smaller effect on the FIRS computed ground motion at the base of the excavation. Hence, it was judged that the EPRI curves would be suitable for site response analysis and nonsafety-related drilled shaft design. (Reference 2.5.2-260)

Structures adjacent to the nuclear island are founded on drilled shafts embedded in the rock. Both beneficial and adverse effects of soil will be considered in the design of drilled shafts to ensure no building interaction at the foundation level.

2.5.4.8 Liquefaction Potential

LNP COL 2.5-9 The potential for liquefaction of existing soils at LNP 1 and LNP 2 was evaluated by conducting liquefaction analyses using the following relationship stated in Regulatory Guide 1.198.

$$FS_{\text{against liquefaction}} = FS = CRR/CSR$$

where CRR (cyclic resistance ratio) is the available soil resistance and CSR (cyclic stress ratio) is the cyclic stress generated by the earthquake.

The CSR was determined using the empirical methods as cited in Regulatory Position 3.5. The SPT blow count method as cited in Regulatory Position 1.2 of Regulatory Guide 1.198 with corrections recommended in Youd et al (Reference 2.5.4.8-201) was used to determine the CRR.

The CSR was determined from Seismic Input Motions consistent with Regulatory Position 3.3.2 together with the empirical methods cited in Regulatory Position 3.5.

The following subsections identify the location of soils and groundwater at the LNP sites that were considered in the liquefaction evaluation, the procedures that were followed to assess liquefaction potential, and the results of the liquefaction evaluations.

2.5.4.8.1 Soil and Groundwater Conditions

Soil conditions at LNP 1 and LNP 2 generally consist of undifferentiated Quaternary and Tertiary sediments, which generally consist of sands, silts, and clays as described in FSAR Subsection 2.5.4.2.1.1.2. These sediments overly the Avon Park Formation. The density of the Quaternary and Tertiary granular soils ranges from relatively loose to very dense, based on SPT blow count measurements. Generally low SPT blow counts are recorded in the Quaternary Sands (e.g., N-values less than 10 blows per foot). Blow counts in the Tertiary sediments are generally above 20 blows per foot, except in isolated zones. These isolated zones are typically of limited thickness (e.g., less than 1.5 m [5 ft.]), and surrounding blow counts are usually greater than 20 blows per foot. High shear-wave velocity values plus very high blow counts at some elevations indicate that cementation exists in some of the Tertiary sediments at the site. Groundwater is typically located within 1 m (3 ft.) of the existing ground surface.

Construction of the LNP facilities will result in the following soil cases relative to liquefaction analysis:

- Soil beneath the foundation for the nuclear islands will be excavated and replaced with RCC as discussed in FSAR Subsection 2.5.4.3. Therefore, all SPT data from borings drilled within the nuclear island footprints were excluded from the liquefaction analysis. It is noted, however, that SPT data from borings drilled along the perimeter or just outside the nuclear islands were not excluded from the liquefaction analysis.

- Soil beyond the nuclear island perimeter, which will be left in place, was subject to liquefaction analysis except for soil within approximately 2.1 m (7 ft.) of existing grade which will be removed or improved to prevent liquefaction.

- Soil beyond the nuclear island perimeter that will be excavated as part of the overall plant construction (e.g., the Turbine Building Condenser Pit) was excluded from the analysis.

- Seismic Category II and nonsafety-related structures adjacent to the nuclear island will be supported on drilled shafts socketed into rock. Soil left in place that surrounds the shafts was addressed in the liquefaction analysis.

2.5.4.8.2 Liquefaction Analysis Procedure

As stated above, liquefaction analysis was conducted in accordance with the Regulatory Positions stated in Regulatory Guide 1.198 with SPT blow counts corrected as recommended in Youd et al (Reference 2.5.4.8-201).

The determination of CSR and CRR involved the following steps:

- CSR was determined from the seismic ground motions estimated for the site in terms of acceleration versus time. (Regulatory Position 3.3.2).

- CRR is estimated as a function of soil characteristics and field stress conditions. The soil characteristics include fine contents, SPT blow counts, soil type, and overburden pressure. The field stress conditions are determined by the groundwater locations and soil density. Various methods of evaluating CRR are available, including the SPT, the cone penetrometer test, the Becker penetration test, and shear-wave velocity procedures. The most common method involves the use of the SPT blow count. The blow counts used in the liquefaction analysis are adjusted for drilling and sampling equipment and method to obtain corrected N-values. The adjustments include borehole diameter, hammer transfer energy, sample liner characteristics, and length of rods.

Cohesive soils, such as fat clay (CH), lean clay (CL), and elastic silt (MH) are not considered to be liquefiable, following the guidance provided in Youd et al (Reference 2.5.4.8-201) and Regulatory Guide 1.198.

Cohesionless soils with low factors of safety against liquefaction (FS ≤ 1.1) are considered to be liquefiable under the design earthquake. Soils with intermediate factors of safety (FS ≈ 1.1 to 1.4) are considered to be non-liquefiable, but increased dynamic pore pressures should be taken into account. Soils with high factors of safety (FS ≥ 1.4) are generally not considered to be liquefiable under the design earthquake, but under certain circumstances would suffer relatively minor cyclic pore pressure generation that could result in some reduction in shear strength.

2.5.4.8.3 Cyclic Resistance of Soils

The Youd et al analysis procedure uses empirical relationships that correlate CRR of soils to the corrected SPT blow counts to evaluate liquefaction potential (Reference 2.5.4.8-201). The corrected SPT blow counts, or $(N_1)_{60}$, at the LNP sites, were obtained by applying correction factors to the field measured N-value, N_{field} as shown in Equation 2.5.4.8-201:

$$(N_1)_{60} = N_{field} * C_N * C_E * C_B * C_R * C_S \qquad \text{Equation 2.5.4.8-201}$$

Where C_N, C_E, C_B, C_R, and C_S are correction factors for overburden pressure, hammer transfer energy, borehole diameter, rod length, and sampler type (with and without liner). Additional correction factors were made for confining pressure (K_σ) and for earthquake magnitude. The ground surface at both of the LNP sites is relatively flat and therefore no adjustments were made for ground surface slope (K_α). The background for these correction factors is discussed in detail in Youd et al. (Reference 2.5.4.8-201)

A fines content correction was also applied to define a $(N_1)_{60\text{-}CS}$ value for use in the liquefaction evaluation. The fines content correction was based on the methods discussed in Youd et al (Reference 2.5.4.8-201) where grain-size information was available. In cases where grain-size information was not available, the fines content was based on visual descriptions and on lower-bound estimates from field logs.

2.5.4.8.4 Earthquake Induced Cyclic Stress

Earthquake-induced cyclic stresses within soils considered for liquefaction analysis were computed from the site response analyses used to develop the site amplification functions for the PBSRS profiles described in Subsection 2.5.2.5. The site response analyses were performed using 60 randomized soil profiles representing each PBSRS shear wave velocity profile and 30 acceleration time histories representing each deaggregation earthquake (DE) listed in Table 2.5.2-225. In each individual site response analysis effective cyclic shear strains and iterated shear modulus were computed for each layer of the profile. The effective cyclic shear stress for each layer ~~is~~was then taken as the product of the effective cyclic shear strain and the iterated shear modulus. The results of the 180 analyses (60 randomized profiles times three ~~3~~ deaggregation earthquakes) were then used to compute a weighted mean effective cyclic shear stress for each layer within each of the three PBSRS soil profiles and for the 10^{-4} and 10^{-5} exceedance level input motions. The weights used ~~a~~were the relative weights assigned to the DEs that are listed in Table 2.5.2-225.

The results of the site response analyses were used to produce peak ground acceleration (PGA) seismic hazard results at the finished graded elevation computed without CAV for the 10^{-4} and 10^{-5} exceedance levels. These values were used to compute a performance based PGA at the finished grade elevation using Equations 2.5.2-215 through 2.5.2-217. The resulting acceleration value is 0.118g. The corresponding PGA at the base of the excavation (-24 ft. NAVD88) is 0.071g. These values along with ~~the mean of the cyclic stress for each soil layer from the randomized set of soil profiles used to develop the PBSRS using the SHAKE program. The rock peak ground acceleration,~~ the site class and the value of F_a based on the International Building Code (2006)~~, and the horizontal peak ground surface acceleration for the North and the South reactor~~ are shown ~~o~~in Table 2.5.4.8-201.~~estimated based on the seismic ground motions, specifically horizontal ground accelerations versus time as identified on Table 2.5.4.8-201. These ground motions are based on the SHAKE analyses used to develop the GMRS, including the soil profile randomization procedure. The ground motions were scaled up to 0.10 g.~~

The development of the cyclic shear stress complies with the guidance in Regulatory Position 3.3.2 of Regulatory Guide 1.198 because an ensemble of time histories was used that represent the earthquakes contributing to the hazard at the LNP site. The development of the ensemble of time histories is described in Subsection 2.5.2.5.2. The time histories used to represent the DE were taken from NUREG/CR-6728 (Reference 2.5.2-263). The weighted~~ed~~ mean magnitude for the earthquake time histories representing the high frequency (HF) 10^{-4} and 10^{-5} DEs are 6.8 and 6.1, respectively. Thus, these time histories also satisfy the acceptance criteria in SRP Section 2.5.2 in that weighted mean magnitudes for the ensembles of time histories exceed magnitude 6. The associated number of equivalent cycles of loading was estimated using the relationship between earthquake magnitude and number of loading cycles provided in Reference 2.5.~~2~~4.8-203. The m_b magnitudes listed in Table 2.5.2-225 for the HF DEs were converted to moment magnitudes using the relationships given in Subsection 2.5.2.4.2.3 and the resulting average moment magnitude was used to estimate the number of cycles for each DE using Figure 12 in Reference 2.5.4.8-203. The resulting weighted mean values are 9.4 cycles and 6.5 cycles for the HF 10^{-4} and 10^{-5} hazard levels, respectively.

2.5.4.8.5 Results of Liquefaction Analysis

Soil characteristics obtained at various depths in applicable A-series and B-series boreholes were used to evaluate the liquefaction potential at the LNP sites. The analyses involved estimating CSR and CRR for cohesionless soil layers and then determining the FS from the following equation:

$$FS = (CRR_{7.5}/CSR) * MSF * K_{\sigma} * K_{\alpha} \qquad \text{Equation 2.5.4.8-202}$$

In Equation 2.5.4.8-202, $CRR_{7.5}$ is the empirical correlation between corrected blow count and CRR from the Youd et al paper (Reference 2.5.4.8-201), CSR is determined as described above, and MSF is the magnitude scaling factor. The MSF was determined using the MSF equation in Youd et al. This equation uses the moment magnitude for the site. A moment magnitude of 7.1 was used in the analysis based on the deaggregation results of the PSHA reported in Tables 2.5.2-221 and 2.5.2-225.

For borings where the liquefaction analysis shows potential for liquefaction, the borehole identification, bottom depth of the SPT sample, soil type, and the field SPT N-Value used in the liquefaction analysis are summarized in revised Tables 2.5.4.8-202A and 2.5.4.8-202B. The revised Tables 2.5.4.8-202A and 2.5.4.8-202B also present the results of the liquefaction analysis including the factors of safety against liquefaction and the depth of the postulated liquefiable zone. Figures 2.5.4.8-201A and 2.5.4.8-201B show, in plan and elevation respectively, the location of the liquefaction zones identified in revised Table 2.5.4.8-202A for LNP 1. Figure 2.5.4.8-202A and Figure 2.5.4.8-202B show, in plan and elevation view respectively, the liquefaction zones identified in revised Table 2.5.4.8-202B for LNP 2. In these figures, the liquefaction zones with a factor of safety of less than or equal to 1.1 are shown by circles with yellow infill. For LNP 1, liquefiable zones were postulated in boreholes O-2, A-15, A-18/O-4, and B-28. Boreholes O-2, A-15 and A-18/O-4 are in the nuclear island excavation zone. Borehole B-28 is under the Annex Building. For LNP 2, liquefiable zones were postulated for boreholes B-01, B-07, B-07A, B-31, and B-33. Borehole B-01 with liquefiable zones is well away from the AP1000 footprint. Boreholes B-07, B-07A, B-31, and B-33 are under the Turbine Building. Based on these figures, it was concluded that liquefiable zones under the LNP 1 and 2 footprints are confined to the northwest corner of the Unit 2 Turbine Building and in isolated random pockets under the remaining LNP 1 and 2 footprints.

Soil beneath the nuclear island foundation will be removed and replaced with Roller Compacted Concrete (RCC). Thus, the bearing stability of the nuclear island foundation is not affected by the postulated liquefaction. The random isolated pockets of liquefiable soils also do not affect the nuclear island sliding and overturning stability based on Westinghouse analysis. The Westinghouse analysis concludes that the nuclear island is stable against sliding, and there is no quality requirement for backfill adjacent to the nuclear island to maintain stability against sliding. The Westinghouse analysis also concludes that there is no passive pressure required to maintain stability against overturning.
For the area under the Annex, Turbine, and Radwaste building footprint, in-situ soil will be replaced or improved to a depth of approximately 2.1 m (7 ft.) below existing grade (elevation 12.8 m [42 ft.] NAVD88). The plant design grade will be established at elevation 15.5 m (51 ft.) NAVD88 by placing engineered fill above the improved / replaced in-situ material. In addition, the earthwork design incorporates vertical and horizontal drains to prevent buildup of excess pore

pressures that cause liquefaction as shown in Figures 2.5.4.8-205 and 2.5.4.8-206 for LNP 1 and 2 respectively.

2.5.4.8.6 Median Centered Liquefaction Evaluations for 10^{-5} UHRS

As a sensitivity analysis, the median centered liquefaction potential (factor of safety <1.0) for 10^{-5} UHRS was evaluated. The methodology and design parameters used for 10^{-5} UHRS liquefaction analysis were the same as that used for design basis liquefaction analysis described in FSAR Subsection 2.5.4.8 except liquefaction was postulated when the computed factor of safety was <1.0 and the soil cyclic shear stress were computed for the 10^{-5} UHRS ground motions and the median shear wave velocity soil profile derived from the randomized soil profiles used to compute the 10^{-5} UHRS. In addition, the equivalent number of stress cycles was computed for the weighted average moment magnitude of 5.74 for the site. Tables 2.5.4.8-203A and 2.5.4.8-203B present liquefaction analysis results for 10^{-5} UHRS for LNP 1 and 2 respectively. The results include the computed factors of safety against liquefaction and the depth below the Annex, Radwaste, or Turbine Building foundation mat where liquefaction is postulated. Figures 2.5.4.8-207 and 2.5.4.8-208 show, in plan and elevation respectively, the location of the liquefaction zones identified in Table 2.5.4.8-203A for LNP 1. Figure 2.5.4.8-209 and Figure 2.5.4.8-210 show, in plan and elevation view respectively, the liquefaction zones identified in Table 2.5.4.8-203B for LNP 2. In these figures, the liquefaction zones with a factor of safety of less than or equal to 1.0 are shown by circles with yellow infill. For Unit 1, liquefiable zones were postulated in boreholes O-2, A-15, A-18/O-4, A-13, and B-28. Boreholes O-2, A-15 and A-18/O-4 are in the nuclear island excavation zone. Borehole A-13 (factor of safety = 1.0) is under the Radwaste Building, and B-28 is under the Annex Building. For Unit 2, liquefiable zones were postulated for boreholes B-01, B-07, B-07A, B-31, and B-33. Borehole B-01 is well away from the AP1000 footprint. Boreholes B-07, B-07A, B-31, and B-33 are under the Turbine Building. Based on these figures, it can be concluded that liquefiable zones under the LNP 1 and 2 footprints are confined to the northwest corner of the LNP 2 Turbine Building and in isolated random pockets under the remaining LNP 1 and 2 footprints. These conclusions for median centered liquefaction potential for 10^{-5} UHRS are the same as the conclusions for the design basis liquefaction analysis described in FSAR Subsection 2.5.4.8.

2.5.4.8.7 Liquefaction Potential Evaluations for CEUS SSC

The soils under the Nuclear Island ~~(NI)~~ will be excavated and backfilled with ~~Roller Compacted Concrete~~ (RCC~~)~~; therefore~~. Thus~~, no liquefaction potential exists under the Nuclear Island~~I~~ foundation. For design basis evaluations of liquefaction potential of soils under the adjacent Annex, Turbine and Radwaste Buildings, earthquake--induced cyclic stresses in the soil column were based on ground motions computed for the PBSRS profile using the updated EPRI-SOG model. The associated PGA at the finished grade elevation is 0.118g (Table 2.5.4.8-201) and is based on the surface hazard curves computed without CAV. The PGA at the finished grade elevation computed without CAV using the CEUS SSC model is 0.091g. As the computed equivalent cyclic shear stresses are proportional to the PGA at the finished grade, the equivalent cyclic shear stresses based on the CEUS SSC model would be lower than those computed based on the updated EPRI-SOG model~~2.5.2-357RAI L-0998-3d~~. Therefore~~us~~, the liquefaction evaluations based on the updated EPRI--SOG LNP ground motions bound those from the CEUS SSC ground motions.

For the site specific seismic margins evaluation presented in Subsection 19.55.6.3, liquefaction potential of soils under the adjacent Annex, Turbine and Radwaste Buildings, earthquake--induced cyclic stresses in the soil column, based on ground motions consistent with the updated EPRI--SOG finished grade 10^{-5} UHRS, were used. As shown in Figures 3.7-228 and 3.7-229~~RAI L-0998-6 and RAI L-0998-7~~, 1.67*GMRS and 1.67*PBSRS developed using the CEUS SSC methodology and modified CAV filter are enveloped by the updated EPRI-SOG finished grade 10^{-5} UHRS. Furthermore, the PGA for the 10^{-5} PBSRS profile surface motions computed without CAV using the CEUS SSC model are lower than those computed using the updated EPRI-SOG model. Thus, the High Confidence Low Probability of Failure (HCLPF) capacity for liquefaction potential of soil under the Annex, Turbine, and Radwaste Buildings exceeds the 1.67*GMRS goal for the plant level HCLPF for the CEUS SSC ground motions.

LNP COL 2.5-9

Table 2.5.4.8-201
Summary of Peak Ground Acceleration Used for Liquefaction Analysis

Structure	Rock Peak Ground Acceleration (g)	Site Class	F_a	a_{max} (g)
North Reactor	0.071	C	1.2	0.118
South Reactor	0.071	C	1.2	0.118

Notes:

Site Class and F_a were estimated based on International Building Code (IBC) (2006).

a_{max} = Horizontal peak acceleration at ground surface for the PBSRS profile with no CAV or scaling. ~~A minimum value of 0.1 g was used, per 10 CFR 50.~~
g = gravity acceleration

LNP COL 2.5-9

Table 2.5.4.8-202A
Summary of Soil Layers Susceptible to Liquefaction in LNP 1 Site

Borehole	Bottom Depth of SPT Sample (ft.)[a]	Soil Type	Field SPT N-Value (bpf)	Factor of Safety (FS)
A-15	16	SP	5	1.0
A-15	21	SP	1	0.8
A-15	26	SC	2	1.1
A-18	20	NR	0	0.7
B-28	36.5	ML	0	0.9
O-2	9	SP-SC	2	0.9
O-2	10.5	SP-SC	2	0.9
O-2	12.0	SP-SC	1	0.8
O-4	24.0	ML	0	0.9

Notes:

a) Depth of SPT sample is relative to original site grade at approximately El 41-43 ft. NAVD88

BPF = Blows per Foot
SC = Clayey Sand
SM = Silty Sand
SP = Poorly Graded Sand
NR = Not Recorded
ML = Silt with Sand

LNP COL 2.5-9

Table 2.5.4.8-202B (Sheet 1 of 2)
Summary of Soil Layers Susceptible to Liquefaction in LNP 2 Site

Borehole	Bottom Depth of SPT Sample (ft.)[(a)]	Soil Type	Field SPT N-Value (bpf)	Factor of Safety (FS)
B-01	26.5	SM	2	0.8
B-01	31.5	SM	2	0.8
B-07	31.5	SP-SM	3	1.0
B-07	36.5	SP-SM	2	0.8
B-07	51.5	SP-SM	2	0.8
B-07	56.5	SP-SM	2	0.8
B-07	61.5	SP-SM	3	0.9
B-07	76.5	SP-SM	3	1.0
B-07A	26.5	SP-SM	5	1.0
B-07A	31.5	SM	4	1.1
B-07A	36.5	SP-SM	3	0.8
B-07A	41.5	SM	3	0.8
B-07A	51.5	SM	2	1.1
B-07A	76.5	SP-SM	6	0.9
B-31	40.5	SP	4	1.0
B-31	69.0	SP	5	1.0
B-31	70.5	SP	6	1.1
B-31	73.5	SP	5	1.0
B-31	76.5	SP	2	0.7
B-31	78.0	SP	6	1.1
B-31	79.5	SP	4	0.9
B-31	81.0	SP	2	0.7
B-31	82.5	SP	3	0.8
B-31	84.0	SP	3	0.8
B-31	85.5	SP	3	0.8
B-31	87.0	SP	2	0.7
B-31	88.5	SP	1	0.7
B-31	90.0	SP	0	0.7
B-31	91.5	SP	4	0.9
B-31	93.0	SP	3	0.8
B-31	94.5	SP	7	1.1
B-31	96.0	SP	0	0.6
B-31	97.5	SP	0	0.6
B-31	99.0	SP	1	0.6
B-31	103.5	SP-SM	7	1.1
B-31	109.5	SP-SC	5	0.9
B-31	118.5	SP-SM	0	0.7
B-31	120.0	SP-SM	0	0.7
B-31	121.5	SP-SM	0	0.7
B-31	123.0	SP-SM	0	0.7
B-31	124.5	SP-SM	0	0.7

LNP COL 2.5-9

Table 2.5.4.8-202B (Sheet 2 of 2)
Summary of Soil Layers Susceptible to Liquefaction in LNP 2 Site

Borehole	Bottom Depth of SPT Sample (ft.) [(a)]	Soil Type	Field SPT N-Value (bpf)	Factor of Safety (FS)
B-31	126.0	SP-SM	0	0.7
B-31	127.5	SP-SM, ML	0	1.0
B-31	129.0	SP-SM	0	0.7
B-31	130.5	SP-SM	0	0.7
B-33	28.5	SP	4	1.0
B-33	30.0	SP	5	1.2
B-33	31.5	SP	3	0.9
B-33	33.0	SP	2	0.8
B-33	34.5	SP	2	0.8
B-33	36.0	SP	1	0.7
B-33	37.5	SP	2	0.8
B-33	39.0	SP	2	0.8
B-33	40.5	SP	2	0.8
B-33	42.0	SP	1	0.7
B-33	43.5	SP	0	0.7
B-33	45.0	SP	0	0.7
B-33	46.5	SP	0	0.7
B-33	58.5	SP	5	1.1
B-33	66.0	SP	7	1.1

Notes:

a) Depth of SPT sample is relative to original site grade at approximately El 41-43 ft. NAVD88

BPF = Blows per Foot
SC = Clayey Sand
SM = Silty Sand
SP = Poorly Graded Sand
NR = Not Recorded
ML = Silt with Sand

LNP COL 2.5-9

Table 2.5.4.8-203A
Summary of Soil Layers Susceptible to Liquefaction in LNP 1 Site For 10^{-5} UHRS

Borehole	Bottom Depth of SPT Sample (ft.) [(a)]	Soil Type [(c), (d), (e) (f), (g)]	Field SPT N-Value (BPF) [(b)]	Factor of Safety (FS)
A-15	16.0	SP	5	0.8
A-15	21.0	SP	1	0.7
A-15	26.0	SC	2	1.0
A-18	20.0	NR	0	0.5
B-28	36.5	ML	0	0.8
O-2	9.0	SP-SC	2	0.8
O-2	10.5	SP-SC	2	0.8
O-2	12.0	SP-SC	1	0.6
O-4	24.0	ML	0	0.8
A-13	16.5	SM	3	1.0

Notes:

a) Depth of SPT sample is relative to original site grade at approximately El 41-43 ft. NAVD88
b) BPF = Blows per Foot
c) SC = Clayey Sand
d) SM = Silty Sand
e) SP = Poorly Graded Sand
f) NR = Not Recorded
g) ML = Silt with Sand

LNP COL 2.5-9

Table 2.5.4.8-203B (Sheet 1 of 3)
Summary of Soil Layers Susceptible to Liquefaction in LNP 2 Site For 10^{-5} UHRS

Borehole	Bottom Depth of SPT Sample (ft.) [(a)]	Soil Type, [(c), (d), (e) (f), (g)]	Field SPT N-Value (BPF) [(b)]	Factor of Safety (FS)
B-01	26.5	SM	2	0.7
B-01	31.5	SM	2	0.7
B-07	31.5	SP-SM	3	0.9
B-07	36.5	SP-SM	2	0.7
B-07	51.5	SP-SM	2	0.7
B-07	56.5	SP-SM	2	0.7
B-07	61.5	SP-SM	3	0.8
B-07	76.5	SP-SM	3	0.9
B-07A	26.5	SP-SM	5	0.9
B-07A	31.5	SM	4	1.0
B-07A	36.5	SP-SM	3	0.7
B-07A	41.5	SM	3	0.7
B-07A	51.5	SM	2	1.0
B-07A	76.5	SP-SM	6	0.8
B-31	40.5	SP	4	0.9
B-31	69.0	SP	5	0.9
B-31	70.5	SP	6	1.0
B-31	73.5	SP	5	0.9
B-31	76.5	SP	2	0.7
B-31	78.0	SP	6	1.0
B-31	79.5	SP	4	0.8

LNP COL 2.5-9

Table 2.5.4.8-203B (Sheet 2 of 3)
Summary of Soil Layers Susceptible to Liquefaction in LNP 2 Site For 10^{-5} UHRS

Borehole	Bottom Depth of SPT Sample (ft.) [(a)]	Soil Type, [(c), (d), (e) (f), (g)]	Field SPT N-Value (BPF) [(b)]	Factor of Safety (FS)
B-31	81.0	SP	2	0.7
B-31	82.5	SP	3	0.7
B-31	84.0	SP	3	0.7
B-31	85.5	SP	3	0.7
B-31	87.0	SP	2	0.7
B-31	88.5	SP	1	0.6
B-31	90.0	SP	0	0.6
B-31	91.5	SP	4	0.8
B-31	93.0	SP	3	0.7
B-31	94.5	SP	7	1.0
B-31	96.0	SP	0	0.6
B-31	97.5	SP	0	0.6
B-31	99.0	SP	1	0.6
B-31	103.5	SP-SM	7	1.0
B-31	109.5	SP-SC	5	0.8
B-31	118.5	SP-SM	0	0.6
B-31	120.0	SP-SM	0	0.6
B-31	121.5	SP-SM	0	0.6
B-31	123.0	SP-SM	0	0.6
B-31	124.5	SP-SM	0	0.6
B-31	126.0	SP-SM	0	0.6

LNP COL 2.5-9

Table 2.5.4.8-203B (Sheet 3 of 3)
Summary of Soil Layers Susceptible to Liquefaction in LNP 2 Site For 10^{-5} UHRS

Borehole	Bottom Depth of SPT Sample (ft.) [a]	Soil Type, [c], [d], [e], [f], [g]	Field SPT N-Value (BPF) [b]	Factor of Safety (FS)
B-31	127.5	SP-SM, ML	0	0.9
B-31	129.0	SP-SM	0	0.6
B-31	130.5	SP-SM	0	0.6
B-33	28.5	SP	4	0.9
B-33	30.0	SP	5	1.0
B-33	31.5	SP	3	0.8
B-33	33.0	SP	2	0.7
B-33	34.5	SP	2	0.7
B-33	36.0	SP	1	0.6
B-33	37.5	SP	2	0.7
B-33	39.0	SP	2	0.7
B-33	40.5	SP	2	0.7
B-33	42.0	SP	1	0.6
B-33	43.5	SP	0	0.6
B-33	45.0	SP	0	0.6
B-33	46.5	SP	0	0.6
B-33	58.5	SP	5	1.0
B-33	66.0	SP	7	1.0

Notes:

a) Depth of SPT sample is relative to original site grade at approximately El 41-43 ft. NAVD88
b) BPF = Blows per Foot
c) SC = Clayey Sand
d) SM = Silty Sand
e) SP = Poorly Graded Sand
f) NR = Not Recorded
g) ML = Silt with Sand

2.5.4.9 Earthquake Site Characteristics

LNP COL 2.5-2 The methods used to calculate site amplification at the GMRS elevation (top of competent layer) are presented in FSAR Subsection 2.5.2.5. Methods for calculation of the LNP site GMRS and FIRS are presented in FSAR Subsection 2.5.2.6. The site amplification functions for LNP 1 and LNP 2 were enveloped to calculate the LNP site GMRS.

The horizontal and vertical LNP site GMRS are presented on Figure 2.5.2-296.

2.5.4.10 Static Stability

LNP COL 2.5-10 The static stability of the LNP 1 and LNP 2 nuclear islands was evaluated for foundation bearing capacity, sliding, foundation settlement, and lateral pressures against below-grade walls. These evaluations are presented in FSAR Subsections 2.5.4.10.1, 2.5.4.10.2, 2.5.4.10.3, and 2.5.4.10.4, respectively. As described in FSAR Subsection 2.5.4.5.3, suitable foundation material is present at LNP 1 and LNP 2 nuclear islands subgrade elevation of -7.3 m (-24 ft.) NAVD88. Infilling and voids associated with joints, fractures, and bedding planes have been conservatively modeled in these evaluations. The source and derivation of the subsurface materials engineering properties used in these evaluations are described in FSAR Subsection 2.5.4.2.

2.5.4.10.1 Bearing Capacity

The bearing capacities at the LNP nuclear island subgrades under static and dynamic loading conditions have been evaluated as presented in this subsection. The resulting bearing capacities exceed the demand for the AP1000 nuclear islands, as listed in the DCD, and therefore satisfy safety requirements. A conservative method was used in this analysis, and appropriate FS values for static and dynamic loading conditions were considered, as summarized in FSAR Subsection 2.5.4.10.1.3.

2.5.4.10.1.1 Bearing Capacity Analysis Methodology

Rock mass properties and compressive strength values from the North and South Reactor Avon Park Formation Profiles were used to calculate the bearing capacity of the RCC and subsurface limestone formation. These rock profiles included the lower-strength zones located below elevation -180 ft. NAVD88 for LNP 1 and below elevation -150 ft. NAVD88 for LNP 2. Bearing capacity results were compared with the static and dynamic allowable load bearing pressures.

The subsurface at LNP consists of limestone formations that extend to a depth of more than 450 ft. below plant grade, beneath about 67 ft. of undifferentiated Quaternary and Tertiary sediments. Beneath the nuclear island basemat, the undifferentiated sediments will be replaced by a

35-ft.-thick RCC Bridging Mat. Beneath the RCC, 75 ft. of limestone will be grouted for dewatering purposes.

A nominal rock profile was developed which considered plant site-specific rock properties.

The bearing capacity of the RCC Bridging Mat was calculated using the ACI 318-89 (Reference 2.5.4.10-201) permissible service load stresses on concrete. The bearing capacity of the subsurface limestone formation was calculated using two different methods: a simplified American Association of State Highway and Transportation Officials (AASHTO) formulation for footings on broken or jointed rock; and the U.S. Army Corps of Engineers formulation for two different failure modes of rock subsurface, considering both static and dynamic loads.

The shear strength of the subsurface limestone formation, based on the rock mass strength parameters (cohesion and friction angle) was compared to the shear stresses calculated with a Finite Element Model.

The factors of safety comparing the bearing capacity of the RCC with the subsurface limestone formation were calculated using static and dynamic allowable bearing pressures.

The gross bearing pressures to be imposed on the RCC are 0.43 MPa (8.9 kips per square foot [ksf]) for static loading and 1.15 MPa (24.0 ksf) for dynamic loading. The dynamic allowable bearing pressure corresponds to the maximum subgrade pressure at the basemat that results from a time-history analysis on soft rock. For the subsurface rock bearing capacity calculations, the RCC self weight was included as an additional bearing pressure load of 5.16 ksf. The buoyancy effects due to the hydrostatic pressure acting at the bottom of the RCC were considered in this analysis. For conservative buoyancy effects, the water table was considered to be at elevation 38 ft. NAVD88.

The compressive strength of the RCC was considered to be 2500 psi, which is considered to occur after one year of the concrete placement.

The dynamic forces and moments at the basemat that were used in this analysis to estimate the dynamic eccentricities of the North and South Reactors correspond to the maximum seismic reactions at the center line of the Containment Building that result from a time-history analysis.

The factors of safety for static and dynamic loading of the RCC are above the minimum requirements, and the RCC bearing capacity is adequate to accommodate the static and dynamic pressures that were considered in this analysis. The estimated factors of safety resulted in 12.1 for static loading and 4.5 for dynamic loading. The calculated factors of safety are significantly larger than the acceptable factors of safety of 3.0 for static loading and 2.0 for dynamic loading.

The incremental shear stresses induced at or below elevation -150 ft. NAVD88 (where a lower-strength zone exists) were found to be less than 2 psi (less than 25 percent of the incremental shear stress induced at the nuclear island basemat). For this reason, characterization of the subsurface conditions below elevation -150 ft. NAVD88 was determined to be adequate.

2.5.4.10.1.1.1 Allowable Bearing Stresses

The allowable bearing stresses in concrete on a loaded area shall not exceed the following value under both static and dynamic loading conditions, as shown in Equation 2.5.4.10-201 (Reference 2.5.4.10-201):

$$B_c \leq 0.3 f_c^{'} \qquad \text{Equation 2.5.4.10-201}$$

In Equation 2.5.4.10-201, B_c is the allowable bearing capacity and f'_c is the concrete compressive strength.

The corresponding static and dynamic factors of safety were determined by dividing the ultimate bearing capacity by the bearing pressures used in this analysis,

$$FS = B_c/q \qquad \text{Equation 2.5.4.10-202}$$

where q is the AP1000 bearing demand.

Appropriate FS under static and dynamic loading are discussed in FSAR Subsection 2.5.4.10.1.2.

2.5.4.10.1.2 Bearing Capacity Results and Design Criteria

Table 2.5.4.10-201 presents the bearing capacities calculated using the ACI 318-89 criteria for allowable bearing stresses in concrete described in FSAR Subsection 2.5.4.10.1.1.1. The resulting FS based on the design static load of 0.43 MPa (8.9 ksf) and design dynamic load of 1.15 MPa (24 ksf) are also presented for each result.

Minimum FS of 3.0 for static loads (dead plus live loads) and 2.0 for dynamic or seismic loads are commonly considered acceptable (Reference 2.5.4.10-202). As shown in Table 2.5.4.10-201, these minimum FS are satisfied by each of the presented cases for LNP 1 and LNP 2.

2.5.4.10.1.3 Bearing Capacity of Adjacent Buildings

The LNP 1 and LNP 2 Annex Buildings (seismic Category II structures) will be founded on deep foundations (4000-psi concrete drilled shafts) that are socketed into the Avon Park Formation limestone. The Turbine Buildings, Radwaste Buildings, and Diesel Generator Buildings will be founded on similar deep foundations (4000-psi concrete drilled shafts). Socket design and shaft spacing will be finalized with formal AP1000 building foundation bearing loads and pressures, including appropriate provisions for resistance to liquefaction. Prior to the construction of each drilled shaft, a pilot hole will be drilled to verify the capacity of the rock to resist the imposed loads.

2.5.4.10.2 Resistance to Sliding

LNP COL 2.5-6

The LNP 1 and LNP 2 nuclear islands will each be founded on a roller compacted concrete bridging mat, which will be founded on suitable rock. During excavation, loose material at the subgrade elevation will be removed, resulting in a relatively clean, exposed layer of rock, as discussed in FSAR Subsection 2.5.4.5.3. The RCC will interlock with the rock subgrade, and the concrete mudmat and nuclear island foundation will be placed over the RCC fill. While the RCC will adhere to the rock subgrade, the adhesion of the RCC to the rock subgrade is conservatively ignored when addressing sliding stability. Friction alone, between the rock and the RCC, will be capable of resisting sliding, as concrete on rock generally has a friction angle in the range of 48 to 60 degrees.

The weakest interface beneath the nuclear island foundation will be the lift joints within the RCC, when no bedding mix is used. Direct shear testing will be conducted prior to construction of the RCC bridging mat to ensure an adequate friction angle. On large-scale RCC projects, 42-degree friction angles are typically achieved, which would exceed the 35-degree requirement set forth by the DCD.

As described in FSAR Subsection 2.5.4.5.4, the space between the diaphragm wall and the nuclear island sidewall will be filled with concrete fill.

2.5.4.10.3 Settlement

LNP COL 2.5-12
LNP COL 2.5-16

The LNP nuclear islands will be founded on a roller compacted concrete bridging mat, which will be founded on suitable rock. As described in this subsection, elastic settlement of the rock under foundation loads is proportional to the elastic modulus of the rock mass, and the total settlements and differential settlements computed for the LNP 1 and LNP 2 nuclear islands are small and within tolerable limits. In light of the small total settlements calculated (less than 0.8 cm [0.3 in.]), any recompression settlement or heave is regarded as negligible.

2.5.4.10.3.1 Elastic (Total) Settlement under Foundation Loads

The elastic settlements of the subsurface, due to the weight of the RCC and the total construction loads applied to the nuclear island, were calculated.

The subsurface at LNP consists of limestone formations that extend to a depth of more than 450 ft. below plant grade, beneath about 67 ft. of undifferentiated Quaternary and Tertiary sediments. Beneath the nuclear island basemat, the undifferentiated sediments will be replaced by a

35-ft.-thick RCC Bridging Mat. The upper 75 ft. of limestone will be grouted for dewatering purposes.

Nominal rock profiles were developed for both the North and South Plant Units using LNP site-specific rock properties and layering information. These rock profiles included the lower-strength zones located below elevation -180 ft. NAVD88 for LNP 1 and below elevation -150 ft. NAVD88 for LNP 2. A SAP2000 elastic Finite Element Model of the RCC, nuclear island basemat, and the subsurface rock was developed using the design geometry, the rock profile configuration beneath the RCC, and the total loads applied on the nuclear island. The method that was used to determine the rock mass elastic modulus was based on shear-wave velocity measurements (Reference 2.5.4.10-203).

Three different methods were used to calculate the elastic settlements under static loading beneath the nuclear island basemat and beneath the RCC:

- Finite Element Model
- AASHTO 2002
- Elastic Theory

For the first method, a 3-D Elastic Finite Element Model (FEM) using solid elements was developed using SAP2000 verified and validated software. Settlements of the RCC Bridging Mat were calculated using the FEM. Two cases were analyzed: Case A: Settlements correspond to elevation -24 ft. NAVD88 (bottom of RCC); and Case B: Settlements correspond to elevation 11 ft. NAVD88 (top of RCC). This model included the in-place rock mass properties beneath the RCC bridging mat down to elevation -139.6 m (-458 ft.) NAVD88. The average settlements at the nuclear island basemat and the bottom of the RCC are presented in Table 2.5.4.10-202.

The elastic settlement results of the FEM Case A were compared with the results from two analytical procedures.

- Elastic settlement calculation using the subgrade modulus at three different locations: center, border midpoint, and corner of the RCC Bridging Mat.
- The elasticity deformation theory, considering a constrained rock mass elastic modulus and the Boussinesq solution for vertical stress distribution.

Subgrade Modulus is the ratio of bearing pressure (psf) over the settlement (ft.) (Reference 2.5.4.10-204). Subgrade modulus values for LNP 1 and LNP 2 are reported in FSAR Subsection 2.5.4.10.3.4. The elastic settlements can be calculated by using the following expression:

$$\delta = q / K_s \qquad \text{Equation 2.5.4.10-203}$$

In Equation 2.5.4.10-203, δ is the elastic settlement, q is the bearing pressure and considered as $q = q_{NI} + q_{RCC}$, and K_s is the subgrade modulus. q_{NI} is the nuclear island construction loads and q_{RCC} is the load due to the RCC selfweight. The RCC area is considered to be an equivalent rectangle. Using the Equation 2.5.4.10-203, elastic settlements were calculated at three points (center [internal], midpoint [south] and corner [north]) of the RCC.

In the third method, the relationship between the settlement of a rock interval, the stress increase, and the elastic modulus is based on simple elastic theory (Reference 2.5.4.10-205), as presented in Equation 2.5.4.10-204:

$$\Delta S = \sum_i H_i \Delta\sigma_i \Big/ M_i \qquad \text{Equation 2.5.4.10-204}$$

In Equation 2.5.4.10-204, ΔS is the total elastic settlement for all rock layers below the foundation, H_i is the thickness of the i^{th} layer, M_i is the constrained modulus (related to the elastic modulus) of the i^{th} layer, and $\Delta\sigma_i$ is the change in vertical stress at the i^{th} layer due to foundation loading. The total elastic settlement of all layers within the depth of influence below the foundation is summed to calculate the overall foundation settlement.

The resulting elastic foundation settlements under static loading using the three methods presented above are small, as listed in Table 2.5.4.10-202. These settlements would occur as the nuclear island facilities are constructed. No additional elastic settlements would occur after construction, when foundation loading is constant.

The average settlements predicted by the FEM analysis were in agreement with the results of the two alternative analytical procedures. For the FEM analysis, the average settlement at elevation -24 ft. NAVD88 (bottom of RCC) resulted in approximately 0.2 inches at both the North and South Reactors.

The differences in settlements predicted by the FEM and by the analytical methods are negligible. The analytical equations consistently lead to slightly lower settlement values.

In Case B of the FEM analysis, settlement results at elevation 11 ft. NAVD88 (top of RCC) are reported in order to assess RCC deformation due to the applied loads. The average difference between values at this elevation and at elevation -24 ft. NAVD88 is approximately 0.01 inches.

Given the small incremental shear stresses being induced below elevation -150 ft. NAVD88, as well as the small predicted settlement values, the characterization of the subsurface below elevation -150 ft. NAVD88 (approximately 200 ft. below final plant grade) performed was determined to be adequate.

Elastic settlements calculated by the first method (Finite Element Model) are considered the "best estimates" of settlement, as the Finite Element Model best accounts for the distribution of the stresses, and all of the stresses are relatively low (in the elastic range).

The total settlements listed in Table 2.5.4.10-202 are within the range of acceptable settlement limits for the AP1000.

2.5.4.10.3.2 Differential Settlement

The potential differential settlement across the nuclear island basemats is calculated using the 3-D finite element model. The maximum settlement is shown to occur in the middle of the nuclear island. Based on conservative estimates of total settlements, the slope associated with this settlement is expected to be less than 0.00083 (or 1:1200), which is within the acceptable range for the AP1000 under both LNP 1 and LNP 2 as defined in FSAR Subsection 2.5.4.10.3.3.

Adjacent nonsafety-related structures will be founded on deep foundations (4000-psi concrete drilled shafts) that are socketed into the Avon Park Formation. While foundation bearing loads and pressures for AP1000 structures are not yet finalized, conservative settlement analyses indicate that these structures will exhibit very little total settlement (less than 25 mm [1 in.]), and therefore, any potential for differential settlement is negligible. The results of the differential settlement analysis are presented in Table 2.5.4.10-203. Once AP1000 foundation bearing loads and pressures for structures adjacent to the nuclear island are finalized, a detailed analysis of differential settlements between the nuclear islands and adjacent structures will be performed, which will account for differential settlement of the nuclear island.

2.5.4.10.3.3 Design Criteria for Foundation Settlement

The following design criteria are tolerable values for the AP1000 nuclear island, as listed in Table 2.5-1 of the DCD and Revision 1 of TR85 (Reference 2.5.4.10-209):

- Total settlement of the nuclear island foundation mat: up to 76 mm (3 in.).
- Differential settlement across the nuclear island foundation mat: up to 13 mm (0.5 in.) per 15.2 m (50 ft.) (slope of 1:1200).
- Differential settlement between nuclear island and adjacent structures: up to 76 mm (3 in.).

As discussed in FSAR Subsections 2.5.4.10.1, 2.5.4.10.2, and 2.5.4.10.3, the engineering analyses indicate that these design criteria will be satisfied at LNP 1 and LNP 2. Conservative methods of settlement analyses and design parameters were used, as described in those subsections.

2.5.4.10.3.4 Subgrade Modulus

The subgrade modulus (K_s) for the LNP nuclear islands is given as:

$K_s = q / \delta$ Equation 2.5.4.10-205

where q is the bearing pressure (psf) and δ is the elastic settlement of the mat (ft.).

The relationship between bearing pressure and the elastic settlement of mat foundation is defined by Equation 2.5.4.10-206 (Reference 2.5.4.10-205):

$K_s = q / \delta = 1 / (B' (1- \mu_{av}^2) I_s I_f / E_{rm\ av})$ Equation 2.5.4.10-206

where B' is the least lateral dimension contributing basemat area, and I_s and I_f are the influence factors from chart solutions of Steinbrenner equations for deformation under a rectangular elastic half space. $E_{rm\ av}$ is the weighted average rock mass modulus of the subsurface and μ_{av} is the weighted average Poisson's ratio. In order to calculate K_s, terms in Equation 2.5.4.10-206 are determined as follows:

1. The subgrade modulus is a function of the soil parameters and foundation dimensions. These geometrical parameters are used to calculate the influence factors. K_s values are determined at the center, at the corner, and the edge midpoints of the RCC mat equivalent rectangle. A compressible rock thickness of 3B was considered to determine K_s.

2. The influence factors I_s and I_f were determined. The influence factor, I_s, was given with the following expression from Bowles (Reference 2.5.4.10-205).

   $I_s = I_1 + ((1-2\mu) / (1-\mu)) I_2$ Equation 2.5.4.10-207

   All I_1 and I_2 values are shown in Bowles (Reference 2.5.4.10-205).

3. Young's modulus (E_{max}) and rock mass modulus (E_{rm}) are used in the evaluation of the subgrade modulus. Young's modulus values were determined from shear-wave velocity measurements from suspension loggings. The E_{rm} for each rock layer was calculated by reducing E_{max} by 50 percent. This reduction reflects the strain degradation effects recommended by Mayne et al. (Reference 2.5.4.10-203) and is appropriate for these subgrade modulus calculations.

4. The effect of horizontal layering beneath the RCC mat is assessed in principle by taking a weighted average of the elastic modulus of each layer, and taking into account the influence of the distribution of the stresses beneath the foundation. The stress distribution for the layered system is considered to be the same as that for a homogeneous half space. It is further considered that the contribution to the stiffness of the composite system

made by an individual layer is directly proportional to the strain energy contained in that layer. Based on this principle, the equivalent elastic modulus for the layered system is evaluated as the weighted average of the elastic modulus of each layer in accordance with the strain energy in the layer.

The weighted averages of the E_{rm} and μ_{av} values were computed in order to include the variations in the soil profile along the influence depth of 3B. The weighted averages of E_{rm} were calculated by using the following expression:

$$E_{rm\ av} = \frac{E_{rm1}L_1 + E_{rm2}L_2 + \cdots\cdots + E_{rmn}L_n}{H} \qquad \text{Equation 2.5.4.10-208}$$

where E_{rmn} and L_n represent rock mass modulus value and depth of each rock layer. H is the depth of influence. $E_{rm\ av}$ values were computed for both reactors.

Similar to E_{rm} weighted average calculation, weighted average Poisson's ratios (μ □$_{av}$) were calculated with the same approach. The results of the weighted average rock mass modulus and Poisson's ratio computations are shown in Table 2.5.4.10-204.

5. Terzaghi and Peck (Reference 2.5.4.10-208) suggested to determine the distribution of the K_S (i.e., at the center and at the corner of basemat) if the load distribution is not uniform on the basemat. With this in mind, the nuclear island loads are higher under the Containment Building and lower around the edges (i.e., not uniform). Therefore, K_S values at four locations under the basemat are calculated by using Equation 2.5.4.10-206. In order to determine the K_S for the center of the RCC mat, by following the principle of super-position, the area is divided into four sections and 4q is used in Equation 2.5.4.10-206 to account for four contributing corners. Similarly, K_S values at Point B and Point D (midpoints of the edges) were determined by following the principle of super-position, where the area is divided into two sections and 2q is used in Equation 2.5.4.10-206 to account for two contributing corners. The K_S value at the corner was calculated by considering the equivalent rectangle as one contributing area.

6. The average subgrade moduli for each unit were calculated by including effect (weight) of subgrade modulus under each location, as explained by Bowles (Reference 2.5.4.10-205). The weighted average subgrade modulus was calculated as follows:

$$K_{s\ av} = (4x\ K_{s\ center} + K_{s\ corner}) / 5 \qquad \text{Equation 2.5.4.10-209}$$

The subgrade modulus for each reactor is also presented in Table 2.5.4.10-204.

2.5.4.10.3.5 Subsurface Instrumentation

LNP COL 2.5-13 Settlement of the nuclear island will be monitored throughout construction. A detailed settlement monitoring program will be developed prior to construction.

As presented in FSAR Subsection 2.5.4.10.3.3, nuclear island foundation settlements on the sound rock subgrade are expected to be small. The settlement monitoring program will be implemented to monitor settlement and heave with two primary elements: water pressure monitoring and settlement (heave) monitoring.

With respect to water pressures, the following activities are planned:

- Monitoring the head outside the perimeter of the diaphragm wall with 10 piezometers (open standpipes) installed to elevation -24ft. NAVD88.

- Monitoring the head with piezometers (a) within the excavation at elevation 0 ft. NAVD88 (~2/3 depth of excavation) with 6 piezometers (b) at elevation -29 ft. NAVD88 (5 ft. below the bottom of the excavation) with 6 piezometers and (c) at elevation -99 ft. NAVD88 (immediately below the grouted zone) with 3 piezometers.

- Settlement monuments, currently expected to be telltales at elevation -24 ft. NAVD88 to monitor heave and settlement as the excavation proceeds.

Settlement monuments will likely be installed and monitored throughout the construction process as follows:

- Settlement bench marks will be installed within the subgrade mudmat (at approximate elevation 3.4 m [11 ft.] NAVD88) at the four corners of each nuclear island and at the (plant) northernmost point of each Containment Building. These will be monitored before and periodically during construction of the nuclear island basemats and sidewalls prior to placement of backfill materials.

- Additional bench marks will be installed approximately 1 m (3 ft.) above site grade (at approximate elevation 16.5 m [54 ft.] NAVD88) and connected to the sidewalls of the nuclear island, directly above the deeper bench mark locations described previously. These bench marks will be monitored during backfilling operations and, periodically, during and after construction of the nuclear island structures.

Settlement bench marks will be installed approximately 1 m (3 ft.) above site grade (at approximate elevation 16.5 m (54 ft.] NAVD88) on the turbine buildings, annex buildings, and radwaste buildings, at the corners of these buildings that abut the nuclear islands. These bench marks, used to measure the differential settlement between the nuclear islands and the adjacent buildings, will be monitored during and after the construction of the nuclear island and adjacent structures.

Monitoring will be continued until at least 90 percent of expected settlement has occurred or the rate of settlement has virtually stopped. This will be evaluated by review of the settlement versus time curves at the bench mark locations.

A monitoring program will be implemented after construction to monitor any long-term settlement. While long-term settlement is expected to be minimal, the settlement bench marks installed during the construction phase (connected to the sidewalls of the nuclear islands) will be used post-construction to monitor settlement of the nuclear island structures.

2.5.4.10.4 Lateral Earth Pressures

LNP COL 2.5-7
LNP COL 2.5-11

Lateral earth pressures will develop against below-grade nuclear island sidewalls due to placement of concrete fill in the annular space between the diaphragm wall and the nuclear island sidewall, in addition to the soil backfill materials above the diaphragm wall. The earth pressure calculation considers the pressure imposed during construction and the long-term condition when construction has been fully completed. The pressure on the nuclear island wall is calculated as the maximum value at any elevation either during construction or operation. For the case during construction, the pressure on the nuclear island wall is calculated, including hydrostatic pressure, crane loads, a 3 m (10 ft.) lift of wet concrete fill at any elevation, and the compaction equipment (tamper) used for construction.

The following subsections describe the basic design input and calculation methodology for the lateral earth pressure calculation.

2.5.4.10.4.1 Design Input

The following loads were applied in the lateral pressure determination:

- Live Load on the ground surface is 250 psf.
- Crane Surcharge Load at a distance of 15 ft. from the wall.
- Water Table at elevation 43 ft. NAVD88.
- Pseudo static earthquake load coefficient is 0.1g.
- Density of concrete fill is 150 pcf.
- Moist/Saturated density of natural soil/compacted granular backfill is 125 pcf.

- Shear strength of natural soil/compacted granular backfill (ϕ') is 34 degrees, c is 0 psf.

The backfill adjacent to the nuclear island sidewalls will be placed as described in FSAR Subsection 2.5.4.5.4. In addition, light, hand-operated compaction equipment will be used to compact the soil adjacent to the nuclear island sidewalls. This will render compaction-induced soil stresses against the sidewalls to be small at the ground surface, decreasing to insignificant with depth.

2.5.4.10.4.2 Methodology

The relationship between each material and the corresponding lateral pressure is defined as follows (Reference 2.5.4.10-206):

- Lateral hydrostatic pressure coefficient for plastic concrete fill (K) = 1.
- Lateral pressure coefficient for hardened concrete fill (k) =$\mu/(1- \mu)$.
- The at-rest earth pressure coefficient (Ko) for natural soil/compacted granular backfill.

$$K_o = 1\text{-}\sin(\phi'); = 0.44 \qquad \text{Equation 2.5.4.10-210}$$

The lateral pressure, P against the nuclear island sidewalls at any depth is calculated as follows:

$$P = \sigma'_v{*}K_L + P_h + P_c + P_s{*}K_o + P_{Eq} \qquad \text{Equation 2.5.4.10-211}$$

Where σ'_v is the effective overburden pressure at the depth z, P_h is the groundwater pressure, P_c is pressure due to crane loading, P_s is the earth pressure due to the surface surcharge, and P_{Eq} is due to earthquake loading, and other terms are as defined previously.

The lateral earth pressure coefficient (K_L) could be due to either plastic concrete lift (K), hardened concrete (k), or earth pressure at rest.

The lateral earthquake load includes seismic lateral earth pressure for at-rest conditions and hydrodynamic water thrust. The seismic at-rest pressure is calculated from the Woods' method and hydrodynamic pressure is calculated from the Westergaard method (Reference 2.5.4.10-207).

- Hydrostatic pressures and hydrodynamic water thrust will act against the sidewalls during seismic loading conditions.
- Structures adjacent to the nuclear islands can potentially increase the at-rest pressures that develop against the nuclear island sidewalls. However, these adjacent structures will be founded on drilled piers socketed into sound rock, which is much stiffer than the soil adjacent to nuclear islands. Due to this

difference in rock and soil stiffness, it is anticipated that these adjacent structure foundation loads will not be transferred to the soil. Therefore, loads from structures adjacent to nuclear islands were considered insignificant in the calculation of the at-rest pressure distributions.

- Surface surcharges from live loads, and lateral loads for the crane, can potentially increase the at-rest pressures that develop against the nuclear island sidewalls; these are added to the static and earthquake lateral loads.

The resulting at-rest lateral pressure profiles for the soil backfill, concrete fill, and natural soil are presented for representative sidewall elevations in Table 2.5.4.10-205.

LNP COL 2.5-10

Table 2.5.4.10-201
Summary of Bearing Capacity Analyses at Nuclear Islands – Static and Dynamic Loading

Bearing Capacity Analysis Results			
Loading Conditions for Analyses		Concrete Allowable Stresses Method (ACI-318-89)	
Unit	**Load Condition**	**Bearing Capacity (ksf)**	**Factor of Safety[a]**
LNP 1	Static	108	12.1
LNP 1	Dynamic	108	4.5
LNP 2	Static	108	12.1
LNP 2	Dynamic	108	4.5

Notes:

a) Factor of safety for static and dynamic load conditions are calculated as ultimate bearing capacity divided by 8.9 ksf and 24 ksf, respectively.

ksf = kips per square foot

LNP COL 2.5-16

Table 2.5.4.10-202
Elastic Settlement under Nuclear Islands

Location	Elastic Settlements Based on (in.)		
	FEM SAP2000	Subgrade Modulus	Elastic Theory
LNP 1 - West Side	0.2	-	-
LNP 1 - Internal	0.2	0.3	-
LNP 1 - North Side	0.1	0.1	-
LNP 1 - South Side	0.1	0.1	-
LNP 1 - East Side	0.2	-	-
LNP 1 Average	0.2	0.2	0.2
LNP 2 - West Side	0.2	-	-
LNP 2 - Internal	0.3	0.3	-
LNP 2 - North Side	0.1	0.1	-
LNP 2 - South Side	0.1	0.1	-
LNP 2 - East Side	0.2	-	-
LNP 2 Average	0.2	0.2	0.2

LNP COL 2.5-16

Table 2.5.4.10-203
Differential Settlement under Nuclear Islands

Differential Settlement Location			Total Settlement at 1st Point (in.)	Total Settlement at 2nd Point (in.)	Distance Between Boreholes	Range in Differential Settlement (Slope) [(a)]
First Point	Second Point	Description	Best Estimate	Best Estimate	(ft.)	Best Estimate
Based on Settlement Results at Specific Points:						
4	8	LNP 2, West-East	0.2	0.2	174	0.0000045
2	6	LNP 2, North-South	0.1	0.1	268	0.0000031
4	8	LNP 1, West-East	0.2	0.2	174	0.0000023
2	6	LNP 1, North-South	0.1	0.1	268	0.0000026
Based on Maximum Differential Settlements:						
6	9	LNP 2	0.1	0.3	130	0.000085
6	9	LNP 1	0.1	0.2	130	0.000074

Notes:

The results correspond to the FEM analysis.

a) The differential settlement (slope) is defined as the difference in total settlement at two locations divided by the horizontal distance between those two locations (based on estimated settlements to third decimal place).

in. = inch, ft. = foot,

LNP COL 2.5-7

Table 2.5.4.10-204
Subgrade Modulus Based on Seismic Wave Velocity

Reactor	Weighted Average Rock Mass Modulus (ksf)	Weighted Average Poisson's Ratio	Location[(a)]	Subgrade Modulus, K_S (kcf) [(b)]
LNP-1	7.94E+05	0.39	Center	610
			Corner	1630
			Midpoint B	1220
			Midpoint D	850
			Average	814
LNP-2	8.41E+05	0.39	Center	587
			Corner	1568
			Midpoint B	1174
			Midpoint D	818
			Average	783

Notes:

a) Subgrade Modulus is calculated for center and corners of the basemat.
b) A compressible rock thickness of 3B (where B is width of basemat) was considered to determine subgrade modulus.

kcf = kilopound per cubic foot
ksf = kilopound per square foot

LNP COL 2.5-11

Table 2.5.4.10-205
Lateral Earth Pressures on Nuclear Island Sidewalls

Elevation (ft. NAVD88)	Lateral Earth Pressure (ksf)			
	Case 1[(a)]	Case 2[(b)]	Case 3[(c)]	Case 4[(d)]
51	0.61	0.61	0	0.61
43	1.26	1.37	1.17	0.95
33	2.38	2.20	2.67	1.70
11	3.74	3.56	1.99	3.52

Notes:

a) In Case 1, the lateral earth pressures due to 8 ft. of live load (250 psf), crane load, hydrostatic load, and earthquake load are evaluated.
b) In Case 2, the lateral earth pressures due to failure of the two rows of anchors supporting the diaphragm wall are evaluated.
c) In Case 3, the lateral earth pressures during the concrete fill placement are evaluated.
d) In Case 4, the lateral earth pressures induced by post construction loads (8 ft. backfill, 32 ft. concrete fill, hydrostatic, live load, and earthquake loads) are evaluated.

ft. NAVD88 = feet North American Vertical Datum 1988
ksf = kilopound per square foot

2.5.4.11 Design Criteria

LNP COL 2.5-3 This subsection summarizes the design criteria and methods used in the stability evaluations for safety-related structures, including factors of safety, assumptions, and conservatism used in the analyses. Cross references to subsections where these items are described are provided.

FSAR Table 2.0-201 compares the DCD site geotechnical parameter criteria with the corresponding site characteristics at LNP 1 and LNP 2, including the following items:

- Average Allowable Static Bearing Capacity.
- Maximum Allowable Dynamic Bearing Capacity for Normal plus SSE.
- Shear-Wave Velocity.
- Lateral Variability.
- Liquefaction Potential.

LNP COL 2.5-11 Design criteria and methods used in the evaluations of safety-related structures are found in the following subsections:

- Criteria for selection of borehole locations and depths are presented in FSAR Subsections 2.5.4.2.1.1.1 and 2.5.4.2.1.1.2, respectively.
- Criteria for selection of soil samples and rock core for laboratory testing are presented in FSAR Subsections 2.5.4.2.1.5.2 and 2.5.4.2.1.5.3, respectively.
- Criteria for selection of rock and soil properties used in the engineering analyses are presented in FSAR Subsection 2.5.4.2.4.
- Criteria for selection of geophysical survey results as design parameters are presented in FSAR Subsection 2.5.4.4.2.8.
- Criteria for evaluation of nuclear island subgrade conditions and identification of the need for subgrade improvement are presented in FSAR Subsection 2.5.4.5.3.
- Criteria for groundwater elevations are presented in FSAR Subsection 2.5.4.6.1. Selection of construction dewatering methods is presented in FSAR Subsection 2.5.4.6.2.

- Criteria for determination of nuclear island allowable bearing pressures, including analysis methods and selection of conservative rock strength parameters, are presented in FSAR Subsection 2.5.4.10.1. Selection of static and dynamic factors of safety is presented in FSAR Subsection 2.5.4.10.1.
- Criteria for determination of nuclear island settlement and subgrade rebound, including analysis methods and selection of conservative rock and soil parameters, are presented in FSAR Subsection 2.5.4.10.3. Tolerable settlement limits are presented in FSAR Subsection 2.5.4.10.3.3.
- Criteria for estimation of nuclear island sidewall lateral earth pressures are presented in FSAR Subsection 2.5.4.10.4.

For engineering analyses supporting the design and evaluation of safety-related structures, each software package used was validated and verified to operate properly on the computers used for the analyses in accordance with the Paul C. Rizzo Associates, Inc., Quality Assurance program. Specific software packages used for these analyses are described in the above-referenced design criteria subsections.

2.5.4.12 Techniques to Improve Subsurface Conditions

LNP COL 2.5-7 Major structures will derive support from the Avon Park Formation, at elevation -7.3 m (-24 ft.) NAVD88. Prior to excavation, grouting will be performed between this foundation elevation and elevation -30.2 m (-99 ft.) NAVD88 to create a relatively impervious zone of limestone to facilitate dewatering during construction.

Prior to the excavation of the nuclear island foundations, grout holes will be drilled from the existing ground surface to the proposed bottom of the targeted grout zone (elevation -32 m [-99 ft.] NAVD88). Grouting will be performed using a suite of mixes developed in the Grout Test Program. Primary grout holes will be spaced on a 4.8 m (16 ft.) hexagonal pattern, and split-spaced with secondary grout holes to achieve "no take" conditions. Provisions will be in place to perform additional split-spacing to tertiary grout holes, as dictated by the performance of the production grouting. This hole spacing was developed based on the results of the Grout Test Program conducted in early 2009. State-of-the-practice computerized monitoring of all grouting will take place, including the measurement of grout take in terms of pressure and volume.

Grouting will reduce the gross porosity and the gross permeability of the Avon Park Formation in this grouted zone. An additional benefit of this grouting is the long-term reduction of groundwater flow through the formation and the consequential reduction in the potential for renewed solution activity. This grouting program is not intended to strengthen the formation. However, the improved strength of the Avon Park Formation will add conservatism to the design. Grouting is nonsafety-related; however, it will be performed under a quality program.

Upon completion of the grout program and dewatering effort, the nuclear island foundations will be excavated to the interpreted top of the Avon Park Formation at elevation -7.3 m (-24 ft.) NAVD88. Sound rock is present at this elevation, which is capable of supporting the structures with surface repairs and dental concrete as necessary to level this erosional surface. Criteria for acceptable subgrade conditions are presented in FSAR Subsection 2.5.4.5.3. Rock that does not satisfy the criteria will be removed and replaced with concrete or grout.

Subsequent to the excavation described in FSAR Subsection 2.5.4.5.3, a RCC Bridging Mat will be constructed at elevation -24 ft. The mat will be installed in 1-ft. lifts to elevation 11 ft. The extent that the RCC placement is shown on Figure 2.5.4.5-201A and Figure 2.5.4.5-201B for LNP 1, and Figure 2.5.4.5-202A and Figure 2.5.4.5-202B for LNP 2.

The RCC will be placed in lift thicknesses of approximately 1 ft. Bedding Mix will be used over each entire lift surface for the RCC bridging mat construction. The Pre-COL RCC testing performed and the Post-COL RCC Testing planned is described in FSAR Subsection 3.8.5.11.

The specified density of RCC is in the range 143 to 153 pcf. During the construction of the RCC Bridging Mat, field measurements of RCC density will be performed using a "single-probe nuclear densometer" for each 1-ft. lift during placement of the RCC.

Verification laboratory tests will be performed to confirm that the compressive strength of the RCC is satisfactory. The tests will be conducted using six-inch cylindrical test specimens molded during construction, in accordance with ASTM C 1435/C 1434M-05: "Standard Practice for Molding Roller-Compacted Concrete in Cylinder Molds Using a Vibrating Hammer". Concrete to make the test specimens will be taken from six different locations for each 1-ft. lift of the RCC. Three samples will be taken at each of the six locations. The compressive strength tests will be conducted within 1 year of placement of the RCC. Compressive strength testing will be performed in accordance with ASTM C 39 "Test Method for Compressive Strength of Cylindrical Concrete Specimens." All laboratory testing will conform to NQA-1 quality requirements. The strength level of RCC, adjusted for aging, will be considered satisfactory if either conditions 1 and 2 or conditions 1 and 3 are satisfied:

1) The average of compressive strength from three cylinders molded at a location equals or exceeds f'c.

2) No individual strength test (average of two cylinders) falls below f'c by more than 500 psi.

3) If individual strength tests (average of two cylinders), adjusted for aging, fall below f'c by more than 500 psi, a minimum of three cores drilled from the area in question shall be tested. The cores shall be drilled in accordance with ASTM C42: "Method of Obtaining and Testing Drilled Cores and Sawed Beams of Concrete." RCC in areas represented by core tests shall be considered adequate if the average of compressive strength from three cores is equal to at least 85 percent of f'c and if no individual core compressive strength is less than 75 percent of f'c.

If these acceptance criteria are not met, an evaluation of the acceptability of the RCC for its intended function shall be performed before acceptance.

A detailed excavation, subgrade improvement, and verification program will be developed prior to and during construction. Subgrade improvement and verification methods summarized in FSAR Subsections 2.5.4.5.3 and 3.8.5.11, or equivalent, will be included in this program. The operational monitoring program for LNP 1 and LNP 2 is described in FSAR Subsection 2.4.12.4.

2.5.4.12.1 Impact of Dissolution Rate

As discussed in FSAR Subsection 2.5.4.1.2.1.1.1, the current dissolution rate of the Avon Park Formation is insignificant with regards to the foundation design. The operation of LNP's production wells, after full installation of the AP1000 basemat, RCC Bridging Mat, and grouted zone, was shown to have little significant impact on the groundwater regime of the site. Compared to the natural regime at the site, the LNP construction was shown to impact the hydrology approximately the same as the seasonal fluctuations. Given this and the very low expected dissolution rates described in FSAR Subsection 2.5.4.1.2.1.1.1, the potential for increased dissolution as a result of construction is also insignificant.

2.5.5 STABILITY OF SLOPES

LNP COL 2.5-14 The nominal plant grade floor elevation at the LNP site will be at 15.5 m (51 ft.) NAVD88, with minor variations to allow drainage for an area of about 370 m by 390 m (1210 ft. by 1280 ft.) around the nuclear island. No permanent slopes will be present at the site that could adversely affect safety-related structures.

LNP COL 2.5-15 The AP1000 does not utilize safety-related dams or embankments, and there are no existing upstream or downstream dams that could affect the LNP site safety-related facilities.

Attachment F

Revised Subsection 2.5.7 Text

[35 pages following this cover page]

2.5.7 REFERENCES

2.5.1-201 Florida Power Corporation, "Site and Environment," Chapter 2, *Crystal River Final Safety Analysis Report*, 1976.

2.5.1-202 Electric Power Research Institute and Seismic Owners Group (EPRI-SOG), "Seismic Hazard Methodology for the Central and Eastern United States," Technical Report NP-4726-A, 1988, Vols. 1 – 10.

2.5.1-203 Electric Power Research Institute (EPRI), "Probabilistic Seismic Hazard Evaluations at Nuclear Power Plant Sites in the Central and Eastern United States: Resolution of Charleston Earthquake Issue," Technical Report NP-6395-D, 1989.

2.5.1-204 Scott, T.M., "Text to Accompany the Geologic Map of Florida," Florida Geological Survey Open-File Report 80, 2001.

2.5.1-205 Hine, A.C., "Structural and Paleogeographic Evolution of the Margins of the Florida Platform," in Randazzo, A.F., and D.S. Jones, eds., *The Geology of Florida*, University Press of Florida, 1997, pp. 169 – 194.

2.5.1-206 Smith, D.L., "Review of the Tectonic History of the Florida Basement," *Tectonophysics*, 1982, Vol. 88, pp. 1 – 22.

2.5.1-207 Faill, R.T., "A Geologic History of the North-Central Appalachians. Part 1: Orogenesis from the Mesoproterozoic through the Taconic Orogeny," *American Journal of Science*, 1997, Vol. 297, pp. 551 – 619.

2.5.1-208 Withjack, M.O., R.W. Schlische, and P.E. Olsen, "Diachronous Rifting, Drifting, and Inversion on the Passive Margin of Central Eastern North America: An Analog for Other Passive Margins," *American Association of Petroleum Geologists Bulletin*, 1998, Vol. 82, No. 5A, pp. 817 – 835.

2.5.1-209 Fenneman, N., "Physiographic Subdivision of the United States," *Proceedings of the National Academy of Sciences*, 1916, Vol. 3, pp. 17 – 22.

2.5.1-210 Thornbury, W.D., *Regional Geomorphology of the United States*, Chapters 3: The Coastal Plain Province, 4: Appalachian Highlands, 5: Piedmont Province, 6: Blue Ridge Province, 7: Ridge and Valley Province, 8: Appalachian Plateaus Province, 11: Interior Low Plateaus Province, and 17: Rocky Mountain System, John Wiley & Sons, Inc., 1965.

2.5.1-211 Randazzo, A.F., and D.S. Jones, eds., *The Geology of Florida*, University Press of Florida, 1997, 327 pp.

2.5.1-212 White, W.A., "The Geomorphology of the Florida Peninsula," *Geological Bulletin* No. 51, 1970.

2.5.1-213 Davis, R.A., A.C. Hine, and E.A. Shinn, "Holocene Coastal Development on the Florida Peninsula," in Fletcher, C.H., III, and J.F. Wehmiller, eds., *Quaternary Coasts of the United States: Marine and Lacustrine Systems*, Society for Sedimentary Geology, Special Publication No. 48, 1992, pp. 193 – 212.

2.5.1-214 Schmidt, W., "Geomorphology and Physiography of Florida," in Randazzo, A.F., and D.S. Jones, eds., *The Geology of Florida*, University Press of Florida, 1997, Chapter 1, pp. 1 – 12.

2.5.1-215 Healy, H.G., "Terraces and Shorelines of Florida," Florida Geological Survey, Map Series No. 71, 1975.

2.5.1-216 Bryant, W.R., J. Lugo, C. Cordova, and A. Salvador, "Physiography and Bathymetry," Chapter 2 in A. Salvador, ed., "The Gulf of Mexico Basin," *The Geology of North America*, 1991, Vol. J, The Geological Society of America, Boulder, Colorado, pp. 13 – 30.

2.5.1-217 Rankin, D.W., "Continental Margin of the Eastern United States: Past and Present," in Speed, R.C., ed., *Phanerozoic Evolution of North American Continent-Ocean Transitions*, Geological Society of America, DNAG Continent-Ocean Transect Volume, 1994, Chapter 3, pp. 129 – 218.

2.5.1-218 Hatcher, R.D., Jr., "Tectonic Synthesis of the U.S. Appalachians," in Hatcher, R.D., Jr., W.A. Thomas, and G.W. Viele, eds., "The Appalachian-Ouachita Orogen in the United States," *The Geology of North America*, Volume F-2, The Geological Society of America, 1989, Chapter 14, pp. 511 – 535.

2.5.1-219 Hatcher, R.D., Jr., "Appalachians Introduction," in Hatcher, R.D., Jr., W.A. Thomas, and G.W. Viele, eds., "The Appalachian-Ouachita Orogen in the United States," *The Geology of North America*, Volume F-2, The Geological Society of America, 1989, Chapter 1, pp. 1 – 6.

2.5.1-220 Dalziel, I.W.D., L.H. Dalla Salda, and L.M. Gahagan, "Paleozoic Laurentia-Gondwana Interaction and the Origin of the Appalachian-Andean Mountain System," *Geological Society of America Bulletin*, Vol. 106, February 1994, pp. 243 – 252.

2.5.1-221 Rankin, D.W., A.A. Drake, L. Glover III, et al., "Pre-Orogenic Terranes," in Hatcher, R.D., Jr., W.A. Thomas, and G.W. Viele, eds., "The Appalachian-Ouachita Orogen in the United States," *The Geology of North America*, Geological Society of America, Vol. F-2, 1989, Chapter 2, pp. 7 – 100.

2.5.1-222 Thomas, W.A., T.M. Chowns, D.L. Daniels, T.L. Neathery, L. Glover III, and R.J. Gleason, "The Subsurface Appalachians beneath the Atlantic and Gulf Coastal Plains," in Hatcher, R.D., Jr., W.A. Thomas, and G.W. Viele, eds., "The Appalachian-Ouachita Orogen in the United States," *The Geology of North America*, Geological Society of America, Vol. F-2, 1989, Chapter 10, pp. 445 – 458.

2.5.1-223 Klitgord, K.D., P. Popenoe, and H. Schouten, "Florida: A Jurassic Transform Plate Boundary," *Journal of Geophysical Research*, Vol. 89, No. B9, 1984, pp. 7753 – 7772.

2.5.1-224 Smith, D.L., A.L. Heatherington, and P.A. Mueller, "Configuration and Geochemistry of Triassic Basins in Florida: Basement Controls," *GSA Abstracts with Programs*, Vol. 24, No. 2, March 1992, p. 65.

2.5.1-225 Smith, D.L., and K.M. Lord, "Tectonic Evolution and Geophysics of the Florida Basement," in Randazzo, A.F., and D.S. Jones, eds., *The Geology of Florida*, University Press of Florida, 1997, Chapter 2, pp. 13 – 26.

2.5.1-226 Pindell, J.L., "Alleghenian Reconstruction and Subsequent Evolution of the Gulf of Mexico, Bahamas, and Proto-Caribbean," *Tectonics*, January 1985, Vol. 4, No. 1, pp. 1 – 39.

2.5.1-227 Christenson, G., "The Florida Lineament," *Transactions Gulf Coast Association of Geological Societies*, 1990, Vol. XL, pp. 99 – 115.

2.5.1-228 Nelson, K.D., J.H. McBride, J.A. Arnow, J.E. Oliver, L.D. Brown, and S. Kaufman, "New COCORP Profiling in the Southeastern United States. Part II: Brunswick and East Coast Magnetic Anomalies, Opening of the North-Central Atlantic Ocean," *Geology*, October 1985, Vol. 13, pp. 718 – 721.

2.5.1-229 Thomas, W.A., "Early Mesozoic Faults of the Northern Gulf Coastal Plain in the Context of Opening of the Atlantic Ocean," in Manspeizer, W., ed., *Triassic-Jurassic Rifting: Continental Breakup and the Origin of the Atlantic Ocean and Passive Margins, Part A*, Elsevier, 1988, pp. 463 – 476.

2.5.1-230 Peel, F.J., C.J. Travis, and J.R. Hossack, "Genetic Structural Provinces and Salt Tectonics of the Cenozoic Offshore U.S. Gulf of Mexico: A Preliminary Analysis," in Jackson, M.P.A., D.G. Roberts, and S. Snelson, eds., *Salt Tectonics: A Global Perspective*, AAPG Memoir 65, Chapter 7, 1995, pp. 153 – 175.

2.5.1-231 Randazzo, A.F., "The Sedimentary Platform of Florida: Mesozoic to Cenozoic," in Randazzo, A.F., and D.S. Jones, eds., *The Geology of Florida*, University Press of Florida, 1997, Chapter 4, pp. 39 – 56.

2.5.1-232 Steckler, M.S., A.B. Watts, and J.A. Thorne, "Subsidence and Basin Modeling at the U.S. Atlantic Passive Margin," in Sheridan, R.E., and J.A. Grow, eds., "The Atlantic Continental Margin, U.S.," *The Geology of North America,* Geological Society of America, 1988, Vol. I-2, Chapter 18, pp. 399 – 416.

2.5.1-233 Halley, R.B., H.L. Vacher, and E.A. Shinn, "Pleistocene Geology," section of "Geology and Hydrogeology of the Florida Keys," originally published in Vacher, H.L., and T. Quinn, eds., "Geology and Hydrology of Carbonate Islands," 1997, available at South Florida Information Access (SOFIA) Websites: sofia.usgs.gov/publications/papers/keys_geohydro/index.html and sofia.usgs.gov/publications/papers/keys_geohydro /pleistocene.html, accessed September 22, 2008.

2.5.1-234 Peltier, W.R., "Deglaciation-Induced Vertical Motion of the North American Continent and Transient Lower Mantle Rheology," *Journal of Geophysical Research*, August 1986, Vol. 91, No. B9, pp. 9099 – 9123.

2.5.1-235 Scott, T.M., "Miocene to Holocene History of Florida," in Randazzo, A.F., and D.S. Jones, eds., *The Geology of Florida*, University Press of Florida, 1997, Chapter 5, pp. 57 – 68.

2.5.1-236 Muhs, D.R., B.J. Szabo, L. McCartan, P.B. Maat, C.A. Bush, and R.B. Halley, "Uranium-Series Age Estimates of Corals from Quaternary Marine Sediments of Southern Florida," in Scott, T.M., and W.D. Allmon, eds., *Plio-Pleistocene Stratigraphy and Paleontology of Southern Florida*, Florida Geological Survey, Special Publication No. 36, 1992, pp. 41 – 50.

2.5.1-237 Muhs, D.R., J.F. Wehmiller, K.R. Simmons, and L.L. York, "Quaternary Sea-Level History of the United States," in Gillespie, A.R., S.C. Porter, and B.F. Atwater, eds., "The Quaternary Period in the United States," *Developments in Quaternary Science*, Vol. 1, Elsevier, 2004.

2.5.1-238 Salvador, A., "Introduction," Chapter 1 in A. Salvador, ed., "The Gulf of Mexico Basin," *The Geology of North America*, Vol. J, The Geological Society of America, 1991, pp. 1 – 12.

2.5.1-239 Barnett, R.S., "Basement Structure of Florida and Its Tectonic Implications," *Transactions Gulf Coast Association of Geological Societies*, 1975, Vol. XXV, pp. 122 – 142.

2.5.1-240 Miller, J.A., "Hydrogeologic Framework of the Floridan Aquifer System in Florida and in Parts of Georgia, Alabama, and South Carolina," Regional Aquifer-System Analysis, U.S. Geological Survey Professional Paper 1403-B, 1986 (includes 33 plates).

2.5.1-241 Perkins, R.D., "Depositional Framework of Pleistocene Rocks in South Florida," in Enos, P., and R.D. Perkins, eds., *Quaternary Sedimentation in South Florida*, 1977, pp. 131 – 198.

2.5.1-242 Fullerton, D.S., C.A. Bush, and J.N. Pennell, "Map of Surficial Deposits and Materials in the Eastern and Central United States (East of 102° West Longitude)," U.S. Geological Survey Geologic Investigations Series Map I–2789, 2003.

2.5.1-243 DeMets, C, R.G. Gordon, D.F. Argus, and S. Stein, "Effect of Recent revisions to the Geomagnetic Reversal Time Scale on Estimates of Current Plate Motions," *Geophysical Research Letters*, Vol. 21, No. 20, October 1994, pp. 2191 – 2194.

2.5.1-244 National Aeronautics and Space Administration, Crustal Dynamics Data Information Systems, "Tectonic Plate Motion," Website, www.cddis.nasa.gov/926/slrtecto.html, accessed November 9, 2007, and "Tectonic Motion in North America," Website, www.cddis.nasa.gov/926/noamtect.html, accessed November 9, 2007.

2.5.1-245 Johnston, A.C., K.J. Coppersmith, L.R. Kanter, and C.A. Cornell, "The Earthquakes of Stable Continental Regions," Final Report submitted to Electric Power Research Institute, TR-102261, Vols. 1 and 3, 1994.

2.5.1-246 Crone, A.J., M.N. Machette, and J.R. Bowman, "Episodic Nature of Earthquake Activity in Stable Continental Regions Revealed by Palaeoseismicity Studies of Australian and North American Quaternary Faults," *Australian Journal of Earth Sciences*, Vol. 44, 1997, pp. 203 – 214.

2.5.1-247 Zoback, M.L., and M.D. Zoback, "Tectonic Stress Field of the Continental United States," in L.C. Pakiser and W.D. Mooney, eds., *Geophysical Framework of the Continental United States*, Geological Society of America Memoir 172, 1989, pp. 523 – 541.

2.5.1-248 Richardson, R.M., and L.M. Reding, "North American Plate Dynamics," *Journal of Geophysical Research*, Vol. 96, No. B7 1991, pp. 12,201 – 12,223.

2.5.1-249 Zoback, M.L., and M. Zoback, "State of Stress in the Conterminous United States," *Journal of Geophysical Research*, Vol. 85, No. B11, 1980, pp. 6,113 – 6,156.

2.5.1-250 Zoback, M.L., "Stress Field Constraints on Intraplate Seismicity in Eastern North America," *Journal of Geophysical Research*, Vol. 97, No. B8, 1992, pp. 11,761 – 11,782.

2.5.1-251 Trehu, A.M., K.D. Klitgord, D.S. Sawyer, and R.T. Buffler, "Atlantic and Gulf of Mexico Continental Margins," in L.C. Pakiser and W.D. Mooney, eds., *Geophysical Framework of the Continental United States*, Geological Society of America Memoir 172, 1989, pp. 349 – 382.

2.5.1-252 Ewing, T.E., "Structural Framework," Chapter 3 in A. Salvador, ed., "The Gulf of Mexico Basin," *The Geology of North America*, Vol. J, The Geological Society of America, 1991, pp. 31 – 52.

2.5.1-253 Dater, D., D. Metzger, and A. Hittelman (comps.), "Land and Marine Gravity CD-ROMS," U.S. Department of Commerce, National Oceanic and Atmospheric Administration, Nation Geophysical Data Center, 1999.

2.5.1-254 Jachens, R.C., R.W. Simpson, R.J. Blackely, and R.W. Saltus, "Isostatic Residual Gravity and Crustal Geology of the United States," in L.C. Pakiser and W.D. Mooney, eds., *Geophysical Framework of the Continental United States*, Geological Society of America Memoir 172, Chapter 19, 1989, pp. 405 – 424.

2.5.1-255 Sawyer, D.S., R.T. Buffler, and R.H. Pilger, Jr., "The Crust under the Gulf of Mexico Basin," Chapter 4 in A. Salvador, ed., "The Gulf of Mexico Basin," *The Geology of North America*, Vol. J, The Geological Society of America, 1991, pp. 53 – 72.

2.5.1-256 North American Magnetic Anomaly Group (NAMAG), "Magnetic Anomaly Map of North America," Sponsored by the Geological Survey of Canada, U.S. Geological Survey, and Consejo de Recursos Minerales de Mexico, 2002.

2.5.1-257 Smith, D.L., "Basement Model for the Panhandle of Florida," *Transactions of the Gulf Coast Association of Geological Societies*, Vol. XXXIII, 1983, pp. 203 – 208.

2.5.1-258 Gough, D.I., "Magnetic Anomalies and Crustal Structure in Eastern Gulf of Mexico," *The American Association of Petroleum Geologists Bulletin*, Vol. 51, No. 2, 1967, pp. 200 – 211.

2.5.1-259 Applin, P.L., and E.R. Applin, "The Comanche Series and Associated Rocks in the Subsurface in Central and South Florida," U.S. Geological Survey Professional Paper 447, 1965.

2.5.1-260 Applin, P.L., "Preliminary Report on Buried Pre-Mesozoic Rocks in Florida and Adjacent States," U.S. Geological Survey Circular No. 91, 1951.

2.5.1-261 Scott, T.M., "The Lithostratigraphy of the Hawthorn Group (Miocene) of Florida," Florida Geological Survey Bulletin No. 59, 1988.

2.5.1-262 Vernon, R.O., "Geology of Citrus and Levy Counties, Florida," Geological Bulletin No. 33, 1951.

2.5.1-263 Carr, W.J., and D.C. Alverson, "Stratigraphy of Middle Tertiary Rocks in Part of West-Central Florida," U.S. Geological Survey Bulletin 1092, 1959.

2.5.1-264 Pride, R.W., F.W. Meyer, and R.N. Cherry, "Hydrology of Green Swamp Area in Central Florida," Florida Geological Survey, Report of Investigations No. 42, 1966.

2.5.1-265 Sproul, C.R., D.H. Boggess, and H.J. Woodard, "Saline-Water Intrusion from Deep Artesian Sources in the McGregor Isles Area of Lee County, Florida," U.S. Geological Survey and Florida Department of Natural Resources, Information Circular No. 75, 1972.

2.5.1-266 Hutchinson, C.B., "Assessment of Hydrogeologic Conditions with Emphasis on Water Quality and Wastewater Injection, Southwest Sarasota and West Charlotte Counties, Florida," U.S. Geological Survey Water-Supply Paper 2371, 1992.

2.5.1-267 Winston, G.O., "Paleogene Zones of the Southwestern Peninsula," in *The Boulder Zone Dolomites of Florida*, Volume 2, 1996, Miami Geological Society.

2.5.1-268 Scott, T.M., "Faults of Florida or Whose Fault Is This Fault?" Abstract in *Florida Scientist*, Vol. 39, Supplement 1, 1976, p. 14.

2.5.1-269 Crone, A.J., and R.L. Wheeler, "Data for Quaternary Faults, Liquefaction Features, and Possible Tectonic Features in the Central and Eastern United States, East of the Rocky Mountain Front," U.S. Geological Survey Open-File Report 00-260, 2000.

2.5.1-270 Wheeler, R.L., "Known or Suggested Quaternary Tectonic Faulting, Central and Eastern United States — New and Updated Assessments for 2005," U.S. Geological Survey Open-File Report 2005-1336, 2005.

2.5.1-271 Bechtel Corporation, Southern Nuclear Company ALWR ESP Application – 25144-002, "Update of Charleston Seismic Source and Integration with EPRI Source Models," 25144-006-V14-CY06-0006, Revision 002, 2006.

2.5.1-272 Southern Nuclear Company (SNC), Vogtle Early Site Permit Application, Part 2 – Site Safety Analysis Report, Revision 2, April 2007.

2.5.1-273 Marple, R.T., and P. Talwani, "Evidence of Possible Tectonic Upwarping along the South Carolina Coastal Plain from an Examination of River Morphology and Elevation Data," *Geology*, Vol. 21, 1993, pp. 651 – 654.

2.5.1-274 Marple, R.T., and P. Talwani, "Evidence for a Buried Fault System in the Coastal Plain of the Carolinas and Virginia—Implications for Neotectonics in the Southeastern United States," *GSA Bulletin*, Vol. 112, No. 2, 2000, pp. 200 – 220.

2.5.1-275 Marple, R.T., and P. Talwani, "Proposed Shenandoah Fault and East Coast-Stafford Fault System and Their Implications for Eastern U.S. Tectonics," *Southeastern Geology*, Vol. 43, No. 2, 2004, pp. 57 – 80.

2.5.1-276 Weems, R.E., E.M. Lemon, Jr., M. S. Nelson, "Geology of the Pringletown, Ridgeville, Summerville, and Summerville Northwest 7.5-Minute Quadrangles, Berkeley, Charleston and Dorchester Counties, South Carolina," U.S. Geological Survey, Booklet to accompany Map I-2502, 1994.

2.5.1-277 Weems, R.E., and W.C. Lewis, "Structural and Tectonic Setting of the Charleston, South Carolina, Region: Evidence from the Tertiary Stratigraphic Record," *GSA Bulletin*, Vol. 114, No. 1, 2002, pp. 24 – 42.

2.5.1-278 Talwani, P., and M. Katuna, "Macroseismic Effects of the 1886 Charleston Earthquake," in *Carolina Geological Society Field Trip Guidebook*, 2004.

2.5.1-279 Wildermuth, E., and P. Talwani, "Tectonic Observations of a Pull-Apart Basin in the South Carolina Coastal Plain," *Seismological Research Letters*, 2002, Vol. 73, No. 3, p. 420.

2.5.1-280 Behrendt, J.C., R.M. Hamilton, H.D. Ackermann, V.J. Henry, and K.C. Bayer, "Marine Multichannel Seismic-Reflection Evidence for Cenozoic Faulting and Deep Crustal Structure near Charleston, South Carolina," in G.S. Gohn, ed., "Studies Related to the Charleston, South Carolina, Earthquake of 1886; Tectonics and Seismicity," U.S. Geological Survey Professional Paper 1313, 1983, pp. J1 – J29.

2.5.1-281 Behrendt, J.C., and A. Yuan, "The Helena Banks Strike-Slip (?) Fault Zone in the Charleston, South Carolina, Earthquake Area: Results from a Marine, High-Resolution, Multichannel, Seismic-Reflection Survey," *GSA Bulletin*, Vol. 98, No. 5, 1987, pp. 591 – 601.

2.5.1-282 Bakun, W.H., and M.G. Hopper, "Magnitudes and Locations of the 1811-1812 New Madrid, Missouri, and the 1886 Charleston, South Carolina, Earthquakes," *Bulletin of the Seismological Society of America*, Vol. 94, No. 1, 2004, pp. 64 – 75.

2.5.1-283 Dutton, C.E, "The Charleston Earthquake of August 31, 1886," in "U.S. Geological Survey Ninth Annual Report: 1887 – 88," 1889, pp. 203 – 528.

2.5.1-284 Obermeier, S.F., R.E. Weems, R.B. Jacobson, and G.S. Gohn, "Liquefaction Evidence for Repeated Holocene Earthquakes in the Coastal Region of South Carolina," *Annals New York Academy of Sciences*, Vol. 558, 1989, pp. 183 – 195.

2.5.1-285 Obermeier, S.F., R.B. Jacobson, J.P. Smoot, R.E. Weems, G.S. Gohn, J.E. Monroe, and D.S. Powars, "Earthquake-Induced Liquefaction Features in the Coastal Setting of South Carolina and in the Fluvial Setting of the New Madrid Seismic Zone," U.S. Geological Survey Professional Paper 1504, 1990.

2.5.1-286 Amick, D., "Paleoliquefaction Investigations along the Atlantic Seaboard with Emphasis on the Prehistoric Earthquake Chronology of Coastal South Carolina," 1990, Ph.D. dissertation, University of South Carolina.

2.5.1-287 Amick, D., R. Gelinas, G. Maurath, R. Cannon, D. Moore, E. Billington, and H. Kemppinen, "Paleoliquefaction Features along the Atlantic Seaboard," U.S. Nuclear Regulatory Commission, NUREG/CR-5613 RA, 1990.

2.5.1-288 Amick, D., G. Maurath, and R. Gelinas, "Characteristics of Seismically Induced Liquefaction Sites and Features Located in the Vicinity of the 1886 Charleston, South Carolina Earthquake," *Seismological Research Letters*, Vol. 61, No. 2, 1990, pp. 117 – 130.

2.5.1-289 Talwani, P., and W.T. Schaeffer, "Recurrence Rates of Large Earthquakes in the South Carolina Coastal Plain Based on Paleoliquefaction Data," *Journal of Geophysical Research*, Vol. 106, No. B4, 2001, pp. 6621 – 6642.

2.5.1-290 Obermeier, S.F., E.C. Pond, and S.M. Olson, "Paleoliquefaction Studies in Continental Settings: Geologic and Geotechnical Factors in Interpretations and Back-Analysis," U.S. Geological Survey Open-File Report 01-29, 2001.

2.5.1-291 Bollinger, G.A., "Reinterpretation of Intensity Data for the 1886 Charleston, South Carolina, Earthquake," in D. W. Rankin, ed., "Studies Related to the Charleston, South Carolina, Earthquake of 1886—A Preliminary Report," U.S. Geological Survey Professional Paper 1028-B, 1977, pp. 17 – 32.

2.5.1-292 Tarr, A.C., and S. Rhea, "Seismicity near Charleston, South Carolina, March 1973 to December 1979," in G.S. Gohn, ed., "Studies Related to the Charleston, South Carolina, Earthquake of 1886 — Tectonics and Seismicity," U.S. Geological Survey Professional Paper 1313, 1983, pp. R1 – R17.

2.5.1-293 Bollinger, G.A., A.C. Johnston, P. Talwani, L.T. Long, K.M. Shedlock, M.S. Sibol, and M.C. Chapman, "Seismicity of the Southeastern United States: 1698 – 1986," in D.B. Slemmons, E.R. Engdahl, M.D. Zoback, and D.D. Blackwell, eds., *Neotectonics of North America, Decade Map Volume to Accompany the Neotectonic Maps*, 1991, pp. 291 – 308.

2.5.1-294 Madabhushi, S., and P. Talwani, "Fault Plane Solutions and Relocations of Recent Earthquakes in Middleton Place Summerville Seismic Zone near Charleston, South Carolina," *Bulletin of the Seismological Society of America*, Vol. 83, No. 5, 1993, pp. 1442 – 1466.

2.5.1-295 Talwani, P., "Internally Consistent Pattern of Seismicity near Charleston, South Carolina," *Geology*, 1982, Vol. 10, pp. 654 – 658.

2.5.1-296 Gangopadhyay, A., and P. Talwani, "Fault Intersections and Intraplate Seismicity in Charleston, South Carolina: Insights from a 2-D Numerical Model," *Current Science*, Vol. 88, No. 10, 2005, pp. 1609 – 1616.

2.5.1-297 Johnston, A.C., "Seismic Moment Assessment of Earthquakes in Stable Continental Regions—III. New Madrid 1811 – 1812, Charleston 1886 and Lisbon 1755," *Geophysical Journal International*, 1996, Vol. 126 pp. 314 – 344.

2.5.1-298 Martin, J.R., and G.W. Clough, "Seismic Parameters from Liquefaction Evidence," *Journal of Geotechnical Engineering*, Vol. 120, No. 8, 1994, pp. 1345 – 1361.

2.5.1-299 Ishihara, K., "Stability of Natural Deposits during Earthquakes," *Proceedings of the Second International Conference on Soil Mechanics and Foundation Engineering, San Francisco*, A. A. Balkema, Rotterdam/Boston, Vol. 1, 1985, pp. 321 – 376.

2.5.1-300 Seed, H.B., K. Tokimatsu, L.F. Harder, and R.M. Chung, "Influence of SPT Procedures in Soil Liquefaction Resistance Evaluations," *Journal of Geotechnical Engineering*, Vol. 111, No. 12, 1985, pp. 1425 – 1445.

2.5.1-301 Bakun, W.H., and A. McGarr, "Differences in Attenuation among the Stable Continental Regions," *Geophysical Research Letters*, Vol. 29, No. 23, 2002, pp. 2121 – 2124.

2.5.1-302 Bakun, W.H., A.C. Johnston, and M.G. Hopper, "Estimating Locations and Magnitudes of Earthquakes in Eastern North America from Modified Mercalli Intensities," *Bulletin of the Seismological Society of America*, Vol. 93, No. 1, 2003, pp. 190 – 202.

2.5.1-303 Hu, K., S.L. Gassman, and P. Talwani, "In-situ Properties of Soils at Paleoliquefaction Sites in the South Carolina Coastal Plain," *Seismological Research Letters*, Vol. 73, No. 6, 2002, pp. 964 – 978.

2.5.1-304 Hu, K., S.L. Gassman, and P. Talwani, "Magnitudes of Prehistoric Earthquakes in the South Carolina Coastal Plain from Geotechnical Data," *Seismological Research Letters*, Vol. 73, No. 6, 2002, pp. 979 – 991.

2.5.1-305 Leon, E., "Effect of Aging of Sediments on Paleoliquefaction Evaluation in the South Carolina Coastal Plain," 2003, Ph.D. dissertation, University of South Carolina.

2.5.1-306 Leon, E., S.L. Gassman, and P. Talwani, "Effect of Soil Aging on Assessing Magnitudes and Accelerations of Prehistoric Earthquakes," *Earthquake Spectra*, Vol. 21, No. 3, 2005, pp. 737 – 759.

2.5.1-307 Spencer, S.M., "Geology of Citrus County, Florida," Florida Geological Survey Open-File Report 5, 1984.

2.5.1-308 Rupert, F.R., "Geology and Geomorphology of Levy County, Florida," Florida Geological Survey Open-File Report 19, 1988.

2.5.1-309 Hoenstine, R.W., E. Lane, F. Rupert, J.W. Yon, and S.M. Spencer, "Mineral Resources of Marion County, Florida," Map Series No. 117, Florida Geological Survey, 1988.

2.5.1-310 Lane, E., R.W. Hoenstine, J.W. Yon, and S.M. Spencer, "Mineral Resources of Levy County, Florida," Map Series No. 116, Florida Geological Survey, 1988.

2.5.1-311 Yon, J.W., R.W. Hoenstine, and S.M. Spencer, "Mineral Resources of Citrus County, Florida," Map Series No. 115, Florida Geological Survey, 1988.

2.5.1-312 Donoghue, J.F., and W.F. Tanner, "Quaternary Terraces and Shorelines of the Panhandle Florida Region," in Fletcher, C.H., III, and J.F. Wehmiller, eds., *Quaternary Coasts of the United States: Marine and Lacustrine Systems*, Society for Sedimentary Geology, SEPM Special Publication No. 48, 1992, pp. 233 – 241.

2.5.1-313 Pirkle, E.C., W.H. Yoho, and C.W. Hendry, Jr., "Ancient Sea Level Stands in Florida," Geological Bulletin No. 52, 1970.

2.5.1-314 Alt, D., and H.K. Brooks, "Age of the Florida Marine Terraces," *The Journal of Geology*, Vol. 73, No. 2, 1965, pp. 406 – 411.

2.5.1-315 Randazzo, A.F., and D.L. Smith, "Subsidence-Induced Foundation Failures in Florida's Karst Terrain," in Beck, B.F., ed., "Sinkholes and the Engineering and Environmental Impacts of Karst," Proceedings of the Ninth Multidisciplinary Conference, Huntsville, Alabama, September 6-10, 2003, pp. 82 – 94.

2.5.1-316 Denizman, C., and A.F. Randazzo, "Post-Miocene Subtropical Karst Evolution, Lower Suwannee River Basin, Florida," *GSA Bulletin*, Vol. 112, No. 12, 2000, pp. 1804 – 1813.

2.5.1-317 Sinclair, W.C., and J.W. Stewart, "Sinkhole Type, Development, and Distribution in Florida," Map Series 110, Florida Geological Survey, 1985.

2.5.1-318 Klimchouk, A., "Towards Defining, Delimiting and Classifying Epikarst: Its Origin, Processes and Variants of Geomorphic Evolution," *Speleogenesis and Evolution of Karst Aquifers*, Vol. 2, No. 1, 2004, 13 pp.

2.5.1-319 Upchurch, S.B., and A.F. Randazzo, "Environmental Geology of Florida," in Randazzo, A.F., and D.S. Jones, *The Geology of Florida*, University Press of Florida, 1997.

2.5.1-320 Sinclair, W.C., J.W. Stewart, R.L. Knutilla, A.E. Gilboy, and R.L. Miller, "Types, Features, and Occurrence of Sinkholes in the Karst of West-Central Florida," U.S. Geological Survey, Water-Resources Investigations Report 85-4126, 1985.

2.5.1-321 Arthur, J.D., R.A. Lee, and L. Li, "Lithostratigraphic and Hydrostratigraphic Cross Sections through Levy-Marion to Pasco Counties, Southwest Florida," Florida Geological Society Open-File Report 81, 2001.

2.5.1-322 Faulkner, G.L., "Geohydrology of the Cross-Florida Barge Canal Area with Special Reference to the Ocala Vicinity, U.S. Geological Survey Water-Resources Investigations Report 1-73, 1973.

2.5.1-323 Southwest Florida Water Management District, "Aquifer Characteristics within the Southwest Florida Water Management District," Report 99-1, Fourth Edition, Revised February 2006.

2.5.1-324 Technos Inc., "Final Report, Geophysical Logging at the Levy County Florida Project, Levy County, Florida," for CH2M Hill, Inc., and Progress Energy Services, Technos Project No. 07-208, February 1, 2008.

2.5.1-325 Geovision Geophysical Services, "Draft Report, Boring Geophysics, Borings A-7, A-8, A19, A-20, I-1, I-2, I-3, I-4, I-5, I-6, I-7, I-8, I-9, and I-10, Progress Energy Florida Levy Nuclear Plant, Combined Operating License Application," Report 7087-01 rev. a, January 7, 2008.

2.5.1-326 Geovision Geophysical Services, "Draft Report, Deep Boring Geophysics, Borings AD-1, AD-2, AD-3, AD-4, I-1, I-3, I-4, I-6, I-8, and I-9, Progress Energy Florida Levy Nuclear Plant, Combined Operating License Application," Report 7087-03 rev. a, January 24, 2008.

2.5.1-327 Chen, C.S., Drilling Log of C.E. Robinson No. 1, Well W-2012, Humble Oil & Refining Co., well drilled November 1949, log interpreted December 31, 1964, Levy County, Florida.

2.5.1-328 Upchurch, S., Personal Communication via email, June 3, 2009.

2.5.1-329 Opdyke, N.D., D.P. Spangler, D.L. Smith, D.S. Jones, and R.C. Lindquist, "Origin of the Epeirogenic Uplift of Pliocene-Pleistocene Beach Ridges in Florida and Development of the Florida Karst," Geology, Vol. 12, 1984, pp. 226-228.

2.5.1-330 Willett, M.A., "Effect of Dissolution of the Florida Carbonate Platform on Isostatic Uplift and Relative Sea-Level Change," M.S. Thesis, Florida State University, 2006.

2.5.1-331 Scott, T.M., K.M. Campbell, F.R. Rupert, J.D. Arthur, R.C. Green, G.H. Means, T.M. Missimer, J.M. Lloyd, J.W. Yon, and J.G. Duncan, "Geologic Map of the State of Florida," Florida Geological Survey Map Series 146, scale approximately 1:1,000,000, 2001. Revised 2006, D. Anderson.

2.5.1-332 Knapp, M.S., "Environmental Geology Series - Gainesville Sheet," Florida Geological Survey Map Series 79, scale 1:250,000, 1 sheet, 1978.

2.5.1-333 Campbell, K.M., "Geologic Map of Levy County, Florida," Florida Geological Survey Open File Map Series No. 11, 1992.

2.5.1-334 Knapp, M. S., "Top of the Floridan Aquifer of North Central Florida," Florida Department of Natural Resources, Bureau of Geology, Map Series No. 92, scale 1:500,000, 1979.

2.5.1-335 Arthur, J.D., C. Fischler, C. Kromhout, J.M. Clayton, G.M. Kelley, R.A. Lee, L. Li, M. O'Sullivan, R.C. Green, and C.L. Werner, "Hydrogeologic Framework of the Southwest Florida Water Management District," Florida Geological Survey, Bulletin No. 68, 2008, 175 pp.

2.5.1-336 Coleman, N. M., "Gravity Investigation of Basement Structure in Northwest Peninsular Florida," M.S. thesis submitted to the University of South Florida, 1979, 70 pp.

2.5.1-337 Talwani, P., and I. Durá-Gómez, "Finding Faults in the Charleston Area, South Carolina: 2. Corroborative Data," unpublished manuscript submitted to *Seismological Research Letters* (in review), 62 pp.

2.5.1-338 Talwani, P., and I. Durá-Gómez, "A Revised Seismotectonic Framework for the Charleston, South Carolina Earthquakes," (abstract) 2008 AGU Fall Meeting, SF, CA, S42A-06, 2008.

2.5.1-339 Durá-Gómez, I., and P. Talwani, "Finding Faults in the Charleston Area, South Carolina: 1. Seismological Data," unpublished manuscript submitted to *Seismological Research Letters* (in review), 54 pp.

2.5.1-340 Talwani, P., "Macroscopic Effects of the 1886 Charleston Earthquake," Field trip #1, 2000, 6 pp.

2.5.1-341 Lennon, G., "Identification of a Northwest Trending Seismogenic Graben near Charleston, South Carolina," U.S. Nuclear Regulatory Commission Report, NUREG/CR-4075, 1986, 43pp.

2.5.1-342 Behrendt, J.C., R.M. Hamilton, H.D. Ackermann, and V.J. Henry, "Cenozoic Faulting in the Vicinity of the Charleston, South Carolina, 1886 Earthquake," *Geology*, Vol. 9, 1981, pp. 117 – 122.

2.5.1-343 Hamilton, R. M., J.C. Behrendt, and H.D. Ackermann, "Land Multichannel Seismic-Reflection Evidence for Tectonic Features near Charleston, South Carolina," *in* Gohn, G.S., ed., Studies Related to the Charleston, South Carolina, Earthquake of 1886—Tectonics and Seismicity: U.S. Geological Survey Professional Paper 1313, 1983, pp. 11 - 18.

2.5.1-344 Chapman, M.C., and J.N. Beale, "Mesozoic and Cenozoic Faulting Imaged at the Epicenter of the 1886 Charleston, South Carolina, Earthquake," *Bulletin of the Seismological Society of America*, Vol. 98, No. 5, 2008, pp. 2533 – 2542.

2.5.1-345 Electric Power Research Institute (EPRI), "Volumes 5 – 10, Seismic Hazard Methodology for the Central and Eastern United States, Tectonic Interpretations," Palo Alto, California, July 1986.

2.5.1-346 Petersen, M.D., A.D. Frankel, S.C. Harmsen, C.S. Mueller, K.M. Haller, R.L. Wheeler, R.L. Wesson, Y. Zeng, O.S. Boyd, D.M. Perkins, N. Luco, E.H. Field, C.J. Wills, and K.S. Rukstales, "Documentation for the 2008 Update of the United States National Seismic Hazard Maps," U.S. Geological Survey Open-File Report 2008-1128, 2008, 127 pp.

2.5.1-347 Dunn, M.M., and M.C. Chapman, "Fault Orientation in the Eastern Tennessee Seismic Zone: A Study Using the Double Difference Earthquake Location Algorithm," Seismological Research Letters, Vol. 77, No. 4, 2006, pp. 494 – 504.

2.5.1-348 Obermeier, S.F., R.B. Jacobson, J.P. Smoot, R.E. Weems, G.S. Gohn, J.E. Monroe, and D.S. Powars, "Earthquake-Induced Liquefaction Features in the Coastal Setting of South Carolina and in the Fluvial Setting of the New Madrid Zone," U.S. Geological Survey Professional Paper 1504, 1990.

2.5.1-349 Southern Nuclear Operating Company (SNC), 2007, "Response to March 15, 2007 RAI Letter No. 6 for the Vogtle ESP Application Involving Geology, Seismology, and Geotechnical Engineering, AR-07-0801, Enclosure 1," submitted April 16, 2007.

2.5.1-350 Frankel, A.D., M.D. Petersen, C.S. Mueller, K.M. Haller, R.L. Wheeler, E.V. Leyendecker, R.L. Wesson, S.C. Harmsen, C.H. Cramer, D.M. Perkins, and K.S. Rukstales, "Documentation for the 2002 Update of the National Seismic Hazard Maps," U.S. Geological Survey Open-File Report 02-420, 2002.

2.5.1-351 Dominion Nuclear North Anna, LLC (Dominion), "North Anna Early Site Permit Application, Response to Request for Additional Information No. 3," Serial No. 04-270 ESP/JDH Docket No. 52-008, 2004.

2.5.1-352 Duke Energy Carolinas, LLC, *William States Lee III Nuclear Station Final Safety Analysis Report*, Rev 0.

2.5.1-353 Schulte, S.M., and W.D. Mooney, "An Updated Global Earthquake Catalogue for Stable Continental Regions: Reassessing the Correlation with Ancient Rifts," *Geophysical Journal International,* Vol. 161, 2005, pp. 707-721.

2.5.1-354 Means, H., Personal Communication via email, May 28, 2009.

2.5.1-355 Upchurch, S., Personal Communication via email, May 28, 2009.

2.5.1-356 Tiling, G., "Aminostratigraphy of the Plio-Pleistocene of Florida," M.S. thesis submitted to the Department of Geology, University of South Florida, 2004, 71 pp.

2.5.1-357 Olson, S.L., and Hearty, P.J., "A Sustained +21 m Sea-level Highstand During MIS 11 (400 ka): Direct Fossil and Sedimentary Evidence From Bermuda," *Quaternary Science Reviews,* Vol. 28, 2009, pp. 271-285.

2.5.1-358 Roberts, D.L., Z. Jacobs, P. Karkanas, and C.W. Marean, "Onshore Expression of Multiple Orbitally Driven Late Quaternary Marine Incursions on the Ultra-stable Southern South African Coast," Quaternary International 167-168 Supplement, July 2007, pp. 345. Poster presented at the International Quaternary Association (INQUA) 2007 Congress.

2.5.1-359 Winkler, C.D., and J.D. Howard, "Correlation of Tectonically Deformed Shorelines on the Southern Atlantic Coastal Plain," *Geology*, Vol. 5, 1977, pp. 123-127.

2.5.1-360 Opdyke, N.D., D.P. Spangler, D.L. Smith, D.S. Jones, and R.C. Lindquist, "Origin of the Epeirogenic Uplift of Pliocene-Pleistocene Beach Ridges in Florida and Development of the Florida Karst," *Geology*, Vol. 12, 1984, pp. 226-228.

2.5.1-361 Willett, M.A., "Effect of Dissolution of the Florida Carbonate Platform on Isostatic Uplift and Relative Sea-Level Change," M.S. Thesis, Florida State University, 2006.

2.5.1-362 Pirkle, F.L., and L.J. Czel, "Marine Fossils from Region of Trail Ridge, A Georgia-Florida Landform," *Southeastern Geology*, Vol. 24, 1983, pp. 31 – 38.

2.5.1-363 Means, G.H., "A Marine-influenced Siliciclastic Unit (Citronelle Formation) in Western Panhandle Florida," M.S. thesis submitted to the Department of Geological Sciences, Florida State University, 2009,134 pp.

2.5.1-364 Scott, T., Geological Overview of Florida, Florida Geological Survey Open File Report No. 50, 1992, 81 pp.

2.5.1-365 Scott, T.M., "Text to Accompany The Geologic Map of Florida," Florida Geological Survey Open-File Report 80, Florida Geological Survey, 2001, 28 pp.

2.5.1-366 Scott, T.M., K.M. Campbell, F.R. Rupert, J.D. Arthur, R.C. Green, G.H. Means, T.M. Missimer, J.M. Lloyd, J.W. Yon, and J.G. Duncan, "Geologic Map of the State of Florida," Florida Geological Survey Map Series 146, scale approximately 1:1,000,000, 2001. Revised 2006, D. Anderson.

2.5.1-367 Knapp, M.S., "Environmental Geology Series - Gainesville Sheet," Florida Geological Survey Map Series 79, scale 1:250,000, 1 sheet, 1978.

2.5.1-368 Campbell, K.M., "Geologic Map of Levy County, Florida," Florida Geological Survey Open File Map Series No. 11, 1992.

2.5.1-369 Knapp, M. S., "Top of the Floridan Aquifer of North Central Florida," Florida Department of Natural Resources, Bureau of Geology, Map Series No. 92, scale 1:500,000, 1979.

2.5.1-370 Arthur, J.D., C. Fischler, C. Kromhout, J.M. Clayton, G.M. Kelley, R.A. Lee, L. Li, M. O'Sullivan, R.C. Green, and C.L. Werner, "Hydrogeologic Framework of the Southwest Florida Water Management District," Florida Geological Survey, Bulletin No. 68, 2008,175 pp.

2.5.1-371 Scott, T., Personal Communication via email, May 30, 2009.

2.5.1-372 Upchurch, S., Personal Communication via email, May 28, 2009.

2.5.1-373 Means, H., Personal Communication via email, May 28, 2009.

2.5.1-374 Winston, G.O., "Florida's Ocala Uplift is Not an Uplift," Bulletin of the American Association of Petroleum Geologists, v. 60, no. 6, 1976, p. 992-994.

2.5.1-375 Scott. T., Personal Communication via email, May 30, 2009.

2.5.1-376 Upchurch, S., Personal Communication via email, May 28, 2009.

2.5.1-377 Means, H., Personal Communication via email, May 28, 2009.

2.5.1-378 Frankel, A.D., M.D. Petersen, C.S. Mueller, K.M. Haller, R.L. Wheeler, E.V. Leyendecker, R.L. Wesson, S.C. Harmsen, C.H. Cramer, D.M. Perkins, and K.S. Rukstales, "Documentation for the 2002 Update of the National Seismic Hazard Maps," U.S. Geological Survey Open-File Report 02-420, 2002.

2.5.2-201 Electric Power Research Institute and Seismic Owners Group, "Seismic Hazard Methodology for the Central and Eastern United States," Technical Report NP-4726-A, 1986 and 1988, Electric Power Research Institute, Palo Alto, California, Vols. 1 – 10.

2.5.2-202 Electric Power Research Institute, "Probabilistic Seismic Hazard Evaluations at Nuclear Power Plant Sites in the Central and Eastern United States," Technical Report NP-6395-D, 1989, Palo Alto, California.

2.5.2-203 American Society of Civil Engineers/Structural Engineering Institute, "American Society of Civil Engineers, Seismic Design Criteria for Structures, Systems, and Components in Nuclear Facilities," ASCE Standard ASCE/SEI 43-05, 2005.

2.5.2-204 Seeber, L., and J.G. Armbruster, "The NCEER-91 Earthquake Catalog: Improved Intensity-Based Magnitudes and Recurrence Relations for U.S. Earthquakes East of New Madrid," NCEER-91-0021, 1992, National Center for Earthquake Engineering Research. Available at website: mceer.buffalo.edu/publications/reports/91-0021/, accessed October 25, 2007.

2.5.2-205 National Center for Earthquake Engineering Research, "NCEER Catalog for Central and Eastern United States," 2007, Website, folkworm.ceri.memphis.edu/catalogs/html/cat_nceer.html, October 25, 2007.

2.5.2-206 Mueller, C., M. Hopper, and A. Frankel, "Preparation of Earthquake Catalogs for the National Seismic-Hazard Maps: Contiguous 48 States," U.S. Geological Survey Open-File Report 97-464, 1997.

2.5.2-207 U.S. Geological Survey, "National Seismic Hazard Mapping Project," Websites, earthquake.usgs.gov/research/hazmaps/products_data/2002/catalogs/ and earthquake.usgs.gov/research/hazmaps/products_data/2002/catalogs/downloads/emb2001.txt, accessed October 2, 2008.

2.5.2-208 Tennessee Valley Authority, "Geotechnical, Geological, and Seismological (GG&S) Evaluations for the Bellefonte Site, North Alabama," Report prepared by CH2M HILL and Geomatrix Consultants, Rev. 1, March 2006.

2.5.2-209	Metzger, A.G., J.G. Armbruster, and L. Seeber, "Documentation, Location and Size — Estimation of 'New' Historical Earthquakes in the Central United States: Continuation," U.S. Geological Survey Contract No. 1434-HQ-97-GR-03064, Final Technical Report, March 2000.
2.5.2-210	Metzger, A.G., "Documentation, Location and Size — Estimation of 'New' Historical Earthquakes in the Central United States," U.S. Geological Survey Contract No. 1434-95-G-2604, Annual Summary, Vol. 37, Website, erp-web.er.usgs.gov/reports/annsum/vol37/cu/g2604.htm, accessed October 3, 2005.
2.5.2-211	Munsey, J.W., "Identification of 'New' Historic Earthquakes in the Central and Eastern United States through Online Keyword Searches," Unpublished Report of River Operations, February 2006, Tennessee Valley Authority.
2.5.2-212	Northern California Earthquake Data Center, "Advanced National Seismic System Catalog Search," 2003, Website, ncedc.org/anss/catalog-search.html, accessed October 25, 2007.
2.5.2-213	U.S. Geological Survey, National Earthquake Information Center, Website, neic.usgs.gov/neis/epic/epic_rect.html, accessed March 28, 2008.
2.5.2-214	Virginia Tech Seismological Observatory, Southeastern U.S. Seismic Network, Website, www.geol.vt.edu/outreach/vtso/anonftp/catalog/, accessed June 27, 2008.
2.5.2-215	International Seismological Centre, Website, www.isc.ac.uk/search/bulletin/unscript.html, accessed August 23, 2007.
2.5.2-216	Hanks, T.C., and H. Kanamori, "A Moment Magnitude Scale," *Journal of Geophysical Research*, Vol. 84, B5, 1979, pp. 2348 – 2350.
2.5.2-217	U.S. Geological Survey, 2008, Earthquake Hazards Program: Florida, Earthquake History, Website, earthquake.usgs.gov/regional/states/florida/history.php, accessed June 27, 2008.
2.5.2-218	U.S. Geological Survey, 2008, Earthquake Hazards Program: Historic Earthquakes, Charleston, South Carolina, Website, earthquake.usgs.gov/regional/states/events/1886_09_01.php, accessed April 1, 2008.

2.5.2-219 U.S. Geological Survey, 2008, Earthquake Hazards Program: South Carolina, Earthquake History, Website, earthquake.usgs.gov/regional/states/south_carolina/history.php, accessed April 1, 2008.

2.5.2-220 Nettles, M., "Two Unusual Seismic Events in the Gulf of Mexico in 2006" (abs.), Incorporated Research Institutions in Seismology, 2006, Annual Workshop Abstracts, 18th Annual Workshop, Tucson, AZ, June 8 – 10, 2006, p. 64.

2.5.2-221 Nettles, M., "Analysis of the 10 February 2006: Gulf of Mexico Earthquake from Global and Regional Seismic Data," Offshore Technology Conference, Houston, Texas, 30 April – 3 May, 2007, Paper OTC 19099, 2 pp.

2.5.2-222 Frohlich, C., "Seismicity of the Central Gulf of Mexico," *Geology*, Vol. 10, 1982, pp. 103 – 106.

2.5.2-223 U.S. Geological Survey, "Information Regarding Technical and Scientific Information on the September 10, 2006 Earthquake in the Gulf of Mexico," National Earthquake Information Center, 2007, Websites: earthquake.usgs.gov/eqcenter/eqinthenews/2006/usslav/ data files; for USGS Fast Moment Tensor Solution; neic.usgs.gov/neis/eq_depot/2006/eq_060910_slav/neic_slav_q .html; for Harvard Centroid Moment Tensor Solution; neic.usgs.gov/neis/eq_depot/2006/eq_060910_slav/neic_slav_h rv.html, accessed June 27, 2008.

2.5.2-224 U.S. Geological Survey, "Earthquake Summary Poster of the Gulf of Mexico Earthquake of 10 September 2006 — Magnitude 5.8," September 2006.

2.5.2-225 Harvard CMT Catalog, 072478A Gulf of Mexico, Website, www.globalcmt.org/cgi-bin/globalcmt-cgi-bin/CMT3/form?itype=ymd&yr=1978&mo=7&day=24&oyr=1978&omo=7&oday=24&jyr=1976&jday=1&ojyr=1976&ojday=1&otype=nd&nday=1&lmw=0&umw=10&lms=0&ums=10&lmb=0&umb=10&llat=-90&ulat=90&llon=-180&ulon=180&lhd=0&uhd=1000&lts=-9999&uts=9999&lpe1=0&upe1=90&lpe2=0&upe2=90&list=0, accessed March 27, 2008.

2.5.2-226 Gangophadhyay, A., and M. Sen, "Seismicity in the Northern Gulf of Mexico: A Possible Mechanism," *Geophysical Journal International*, paper submitted 2 January 2008, in review, 38 pp.

2.5.2-227 Sawyer, D.S., R.T. Buffler, and R.H. Pilger, Jr., "The Crust under the Gulf of Mexico Basin," in A. Salvador, ed., "The Gulf of Mexico Basin," Chapter 4, *The Geology of North America*, 1991, Vol. J, Geological Society of America, pp. 53 – 72.

2.5.2-228 Buffler, R. T., "Seismic Stratigraphy of the Deep Gulf of Mexico Basin and Adjacent Margins," in Salvador, A., ed., "The Gulf of Mexico Basin," Boulder, Colorado, Geological Society of America, *The Geology of North America*, Vol. J., 1991, pp. 353 – 387.

2.5.2-229 Watkins, J.S., G. MacRae, and G.R. Simmons, "Bipolar Simple Shear Rifting Responsible for Distribution of Mega-Salt Basins in Gulf of Mexico?," in Salt, Sediment and Hydrocarbons: Papers Presented at the Gulf Coast Section Society of Economic Paleontologists and Mineralogists Foundation, Sixteenth Annual Research Conference: Houston Texas, December 3-6, 1995.

2.5.2-230 Peel, F., "The Setting and Possible Mechanism of the 2006 Green Canyon Seismic Event," Offshore Technology Conference, Houston, Texas, 30 April – 3 May 2007, Paper OTC 19032, 4 pp.

2.5.2-231 Angell, M., and C. Hitchcock, "A Geohazard Perspective of Recent Seismic Activity in the Northern Gulf of Mexico," Offshore Technology Conference, Houston, Texas, 30 April – 3 May 2007, Paper OTC 19035, 8 pp.

2.5.2-232 Bechtel Group, Inc., "Seismic Hazard Methodology for the Central and Eastern United States, Volume 9: Tectonic Interpretations by Bechtel Group, Inc.," Technical Report NP-4726, 1986, prepared for the Seismic Owners Group and the Electric Power Research Institute, Palo Alto, California.

2.5.2-233 Dames & Moore, "Seismic Hazard Methodology for the Central and Eastern United States, Volume 6: Tectonic Interpretations by Dames & Moore," Technical Report NP-4726, 1986, prepared for the Seismic Owners Group and the Electric Power Research Institute, Palo Alto, California, Volume 6.

2.5.2-234 Law Engineering Testing Company, "Seismic Hazard Methodology for the Central and Eastern United States, Volume 7: Tectonic Interpretations by Law Engineering Testing Company," Technical Report NP-4726, 1986, prepared for the Seismic Owners Group and the Electric Power Research Institute, Palo Alto, California.

2.5.2-235 Rondout Associates, "Seismic Hazard Methodology for the Central and Eastern United States: Tectonic Interpretations by Rondout Associates," Technical Report NP-4726, 1986, prepared for the Seismic Owners Group and the Electric Power Research Institute, Palo Alto, California, Volume 10.

2.5.2-236 Weston Geophysical Corporation, "Seismic Hazard Methodology for the Central and Eastern United States: Tectonic Interpretations by Weston Geophysical Corporation," Technical Report NP-4726, 1986, prepared for the Seismic Owners Group and the Electric Power Research Institute, Palo Alto, California, Volume 5.

2.5.2-237 Woodward-Clyde Consultants, "Seismic Hazard Methodology for the Central and Eastern United States: Tectonic Interpretations by Woodward-Clyde Consultants," Technical Report NP-4726, 1986, prepared for the Seismic Owners Group and the Electric Power Research Institute, Palo Alto, California, Volume 8.

2.5.2-238 Savy, J.B., W. Foxall, N. Abrahamson, and D. Bernreuter, "Guidance for Performing Probabilistic Seismic Hazard Analysis for a Nuclear Plant Site: Example Application to the Southeastern United States: UCRL-ID-133494," prepared for the U.S. Nuclear Regulatory Commission, NUREG CR6607, 2002.

2.5.2-239 Senior Seismic Hazard Analysis Committee, composed of R.J. Budnitz, G. Apostolakis, D.M. Boore, L.S. Cluff, K.J. Coppersmith, C.A. Cornell, and P.A. Morris, "Recommendations for Probabilistic Seismic Hazard Analysis: Guidance on Uncertainty and Use of Experts," NUREG/CR-6372, prepared for the U.S. Nuclear Regulatory Commission, the U.S. Department of Energy, and the Electric Power Research Institute, April 1997.

2.5.2-240 Frankel, A.D., M.D. Petersen, C.S. Mueller, K.M. Haller, R.L. Wheeler, E.V. Leyendecker, R.L. Wesson, S.C. Harmsen, C.H. Cramer, D.M. Perkins, and K.S. Rukstales, "Documentation for the 2002 Update of the National Seismic Hazard Maps," U.S. Geological Survey Open-File Report 02-420, 2002.

2.5.2-241 Frankel, A., C. Mueller, T. Barnhard, D. Perkins, E.V. Leyendecker, N. Dickman, S. Hanson, and M. Hopper, "National Seismic-Hazard Maps: Documentation," U.S. Geological Survey Open-File Report 96-532, 1996.

2.5.2-242 South Carolina Department of Transportation, "Seismic Design Specifications for Highway Bridges, Seismicity Study Report," 2003, Website, www.dot.state.sc.us/doing/bridge/bridgeseismic.html, accessed June 30, 2008.

2.5.2-243 Southern Nuclear Company, "Update of Charleston Seismic Source and Integration with EPRI Source Models," 25144-006-V14-CY06-0006, Revision 002-20060908, 2006.

2.5.2-244 STP Nuclear Operating Company (STPNOC), "Application for a Combined License (COL) for Two Advanced Boiling Water Reactors (ABWRs), the Proposed South Texas Project Units 3 & 4, Rev 01," January 15, 2008.

2.5.2-245 Systems Energy Resources Inc. (SERI), "Early Site Permit Application for Grand Gulf Nuclear Station Site, Part 2 Site Safety Analysis Report," Rev 3, Jackson Mississippi.

2.5.2-246 Wells, D.L., and K.J. Coppersmith, "New Empirical Relationships among Magnitude, Rupture Length, Rupture Width, Rupture Area, and Surface Displacement," *Bulletin of the Seismological Society of America*, Vol. 84, No. 4, 1994, pp. 974 – 1002.

2.5.2-247 Youngs, R.R., and K.J. Coppersmith, "Implications of Fault Slip Rates and Earthquake Recurrence Models to Probabilistic Seismic Hazard Estimates," *Bulletin of the Seismological Society of America*, Vol. 75, 1985, pp. 939 – 964.

2.5.2-248 Youngs, R.R., F.H. Swan, M.S. Power, D.P. Schwartz, and R.K. Green, "Probabilistic Analysis of Earthquake Ground-Shaking Hazards Along the Wasatch Front, Utah," in "Assessment of Regional Earthquake Hazards and Risk Along the Wasatch Front, Utah," U.S. Geological Survey Professional Paper 1500-M, pp. M1 – M67.

2.5.2-249 McGuire, R.K., G.R. Toro, and W.J. Silva, "Engineering Model of Earthquake Ground Motion for Eastern North America," Electric Power Research Institute Technical Report NP-6074, 1988, Electric Power Research Institute, Palo Alto, California.

2.5.2-250 Boore, D.M., and G.M. Atkinson, "Stochastic Prediction of Ground Motion and Spectral Response Parameters at Hard-Rock Sites in Eastern North America," *Bulletin of the Seismological Society of America*, Vol. 77, No. 2, 1987, pp. 440 – 467.

2.5.2-251 Nuttli, O.W., Letter to J.B. Savy, "Seismic Hazard Characterization of 69 Nuclear Plant Sites East of the Rocky Mountains: Questionnaires," prepared by D.L. Bernreuter, J.B. Savy, R.W. Mensing, and J.C. Chen, NUREG/CR-5250, UCID-21517, 1986, Vol. 7.

2.5.2-252 Newmark, N.M., and W.J. Hall, "Earthquake Spectra and Design," 1982, Earthquake Engineering Research Institute, Berkeley, California.

2.5.2-253 Electric Power Research Institute (EPRI), "CEUS Ground Motion Project Final Report," Technical Report 1009684, 2004, Palo Alto, California.

2.5.2-254 Silva, W., N. Gregor, and R. Darragh, "Development of Regional Hard Rock Attenuation Relations for Central and Eastern North America," unpublished report by Pacific Engineering and Analysis, 2002, Website, http://pacificengineering.org.

2.5.2-255 Atkinson, G.M., and D.M. Boore, "Ground Motion Relations for Eastern North America," *Bulletin of the Seismological Society of America*, Vol. 85, No. 1, 1995, pp. 17 – 30.

2.5.2-256 Silva, W., N. Gregor, and R. Darragh, "Development of Regional Hard Rock Attenuation Relations for Central and Eastern North America, Mid-Continent and Gulf Coast Areas," unpublished report by Pacific Engineering and Analysis, 2003, Website, http://pacificengineering.org/rpts_page1.shtml.

2.5.2-257 Atkinson, G. M., and D.M. Boore, "Earthquake Ground-Motion Prediction Equations for Eastern North America," *Bulletin of the Seismological Society of America*, Vol. 96, No. 6, December 2006, pp. 2181 – 2205.

2.5.2-258 Electric Power Research Institute (EPRI), "Program on Technology Innovation: Truncation of the Lognormal Distribution and Value of the Standard Deviation for Ground Motion Models in the Central and Eastern United States," Technical Report 1014381, August 2006, Palo Alto, California.

2.5.2-259 Johnston, A.C., "Seismic Moment Assessment of Earthquakes in Stable Continental Regions — I: Instrumental Seismicity," *Geophysical Journal International*, Vol. 124, 1996, pp. 381 – 414.

2.5.2-260 Electric Power Research Institute (EPRI), "Guidelines for Determining Design Basis Ground Motions," Technical Report 102293, 1993, Palo Alto, California, Vol. 1.

2.5.2-261 Shearon Harris (HAR) COLA, February 2008.

2.5.2-262 Miller, A.C., and T.R. Rice, "Discrete Approximations of Probability Distributions," *Management Science*, Vol. 29, 1983, pp. 352 – 362.

2.5.2-263 McGuire, R.K., W.J. Silva, and C.J. Costantino, "Technical Basis for Revision of Regulatory Guidance on Design Ground Motions: Hazard- and Risk-Consistent Ground Motion Spectra Guidelines," NUREG/CR-6728, 2001, Nuclear Regulatory Commission, Washington, D.C.

2.5.2-264 Baker, J.W., and C.A. Cornell, "Spectral Shape, Epsilon and Record Selection," *Earthquake Engineering & Structural Dynamics*, Vol. 35, 2006, pp. 1077 – 1095.

2.5.2-265 Baker, J.W., and C.A. Cornell, "Correlation of Response Spectral Values for Multicomponent Ground Motions," *Bulletin of the Seismological Society of America*, Vol. 96, No. 1, 2006, pp. 215 – 227.

2.5.2-266 Baker, J. W., and N. Jayaram, "Correlation of Spectral Acceleration Values from NGA Ground Motion Models," *Earthquake Spectra*, Vol. 24, No.1, 2008, pp. 299-317.

2.5.2-267 Pacific Earthquake Engineering Research Center's (PEER) Next Generation Attenuation Project (NGA). Website, peer.berkeley.edu/products/nga_project.html, accessed July 16, 2008.

2.5.2-268 GeoVision, Inc., 2008, Final Report Boring Geophysics, Borings A-7, A-8, A-19, A-20, I-1, I-2, I-3, I-4, I-5, I-6, I-7, I-8, I-9, and I-10, Progress Energy Florida, Levy Nuclear Plant Combined Operating License Application, Final Report 7087-01, Rev 0, March 27, 2008.

2.5.2-269 GeoVision, Inc., 2008, Final Report Deep Boring Geophysics, Borings AD-1, AD-2, AD-3, AD-4, I-1, I-3, I-4, I-6, I-8, and I-9, Progress Energy Florida, Levy Nuclear Plant Combined Operating License Application, Report 7087-03, Rev 0, March 27, 2008.

2.5.2-270 Technos, Inc., 2008, Final Report Geophysical Logging at PEF Levy Nuclear Plant (LNP) Site, Levy County, Florida Site, March 14, 2008.

2.5.2-271 Vernon, R.O., Geology of Citrus and Levy Counties, Florida, *Florida Geological Society Bulletin* No. 33, 1951.

2.5.2-272 Silva, W.J., N. Abrahamson, G. Toro, and C. Costantino, "Description and Validation of the Stochastic Ground Motion Model," Report submitted to Brookhaven National Laboratory, Associated Universities, Inc., New York, 1996.

2.5.2-273 Silva, W.J., "Base Case and Recommended Limits of Modulus Reduction and Damping Relationships," Data files EPRIRR1L.MAT, EPRIRR1U.MAT, EPRISR1.MAT, EPRISR1L.MAT, and EPRISR1U.MAT, transmitted March 18, 2007.

2.5.2-274 Electric Power Research Institute (EPRI), "Assessment of a Performance-Based Approach for Determining the SSE Ground Motion for New Plant Sites," Vol. 2, Seismic Hazard Results at 28 Sites, Final Report, 1012045, May 2005.

2.5.2-275 Schnabel, P.B., J. Lysmer, and H.B. Seed, "SHAKE — A Computer Program for Earthquake Response Analysis of Horizontally Layered Sites," Earthquake Engineering Research Center, University of California, Berkeley, California, EERC 72-12, 1972.

2.5.2-276 Anderson, J.G., and S.E. Hough, "A Model for the Shape of the Fourier Amplitude Spectrum of Acceleration at High Frequencies," *Bulletin of the Seismological Society of America*, Vol. 74, 1984, pp. 1969 – 1993.

2.5.2-277 Silva, W.J., and R. Darragh, "Engineering Characterization of Earthquake Strong Ground Motion Recorded at Rock Sites," Electric Power Research Institute TR-102261, 1995, Palo Alto, California.

2.5.2-278 Keefer, D.L., and S.E. Bodily, "Three-Point Approximations for Continuous Random Variables," *Management Science*, Vol. 29, No. 5, 1983, pp. 595 – 609.

2.5.2-279 Silva, W.J., and K. Lee, "WES RASCALS code for synthesizing earthquake ground motions: State-of-the-Art for Assessing Earthquake Hazards in the United States Report 24," Miscellaneous Paper S-73-1, 1987, U.S. Army Corps of Engineers Waterways Experiment Station.

2.5.2-280 Electric Power Research Institute (EPRI), "Program on Technology Innovation: Use of Cumulative Absolute Velocity (CAV) in Determining Effects of Small Magnitude Earthquakes on Seismic Hazard Analyses," Technical Report 1014099, August 2006, Palo Alto, California.

2.5.2-281 Darendeli, M.B, "Development of a New Family of Normalized Modulus Reduction and Material Damping Curves," Ph.D Thesis, The University of Texas at Austin, 2001.

2.5.2-282 Menq, F.Y., "Dynamic Properties of Sandy and Gravelly Soils," Ph.D Thesis, The University of Texas at Austin, 2003.

2.5.2-283 Power, M., B. Chiou, N. Abrahamson, Y. Bozorgnia, T. Shantz, and C. Roblee, "An Overview of the NGA Project," *Earthquake Spectra*, Vol. 24, No. 1, 2008, p. 3-21.

2.5.3-201 Crone, A.J., and R.L. Wheeler, "Data for Quaternary Faults, Liquefaction Features, and Possible Tectonic Features in the Central and Eastern United States, East of the Rocky Mountain Front," U.S. Geological Survey Open-File Report 00-260, 2000.

2.5.3-202 Wheeler, R.L., "Known or Suggested Quaternary Tectonic Faulting, Central and Eastern United States — New Updated Assessments for 2005," U.S. Geological Survey Open-File Report 2005-1336, 2005.

2.5.3-203 Vernon, R.O., "Geology of Citrus and Levy Counties, Florida," *Florida Geological Society Bulletin* No. 33, 1951.

2.5.3-204 Florida Power Corporation, "Site and Environment," in *Crystal River Final Safety Analysis Report*, Chapter 2, 1976.

2.5.3-205 Aero-Metric, Inc., Survey Report Topographic Mapping for Sargent & Lundy and Progress Energy, Florida. Florida site, 2007, Sheboygan, Wisconsin.

2.5.3-206 Miller, J.A., "Hydrogeologic Framework of the Floridan Aquifer System in Florida and in Parts of Georgia, Alabama, and South Carolina," Regional Aquifer-System Analysis, U.S. Geological Survey Professional Paper 1403-B, 1986 [includes Plates 1 through 33].

2.5.3-207 Applin, P.L., and E.R. Applin, "Regional Subsurface Stratigraphy and Structure of Florida and Southern Georgia," *Bulletin of the American Association of Petroleum Geologists*, Vol. 28, No. 12, 1944, pp. 1673 – 1753.

2.5.3-208 Puri, H.S., "Zonation of the Ocala Group in Peninsular Florida," *Journal of Sedimentary Petrology*, Vol. 23, 1953, p. 130.

2.5.3-209 Randazzo, A.F., "The Sedimentary Platform of Florida: Mesozoic to Cenozoic," in Randazzo, A.F., and D.S. Jones, eds., *The Geology of Florida*, University Press of Florida, 1997, Chapter 4, pp. 39 – 56.

2.5.3-210 Scott, T.M., "Miocene to Holocene History of Florida," in Randazzo, A.F., and D.S. Jones, eds., *The Geology of Florida*, University Press of Florida, 1997, Chapter 5, pp. 57 – 67.

2.5.3-211 Florida Department of Transportation (DOT), Lineament Map of Florida, prepared by the Remote Sensing Section, State Topographic Office, 1973, approx. scale 1:1,000,000.

2.5.3-212 Culbreth, M.A., "Geophysical Investigation of Lineaments in South Florida," Master of Science thesis, Department of Geology, University of South Florida, April 1988.

2.5.3-213 Sowers, G.F., "Failures in Limestones in Humid Subtropics," *Journal of the Geotechnical Engineering Division*, Proceedings of the American Society of Civil Engineers, Vol. 101, No. GT8, 1975, pp. 771 – 787.

2.5.3-214 Benson, R.C., and L.J. La Fountain, "Evaluation of Subsidence or Collapse Potential Due to Subsurface Cavities," *Proceedings of the First Multidisciplinary Conference on Sinkholes, Orlando, Florida,* 15-17 October, 1984, pp. 201 – 215.

2.5.3-215 Tihansky, A.B., "Sinkholes, West-Central Florida: A Link between Surface Water and Ground Water," excerpted from Galloway, D., D.R. Jones, and S.E. Ingebritsen, *Land Subsidence in the United States*, U.S. Geological Survey Circular 1182, pp. 121 – 141.

2.5.3-216 Scott, T., e-mail message to CH2M HILL (e-mail attachment: Upchurch, S.B. 2008. "Fractures and Photolineaments: Introduction and Analysis Methodology," Internal document for SDII Global Corporation), June 4, 2009.

2.5.3-217 Arthur, J.D., C. Fischler, C. Kromhout, J.M. Clayton, G.M. Kelley, R.A. Lee, L. Li, M. O'Sullivan, R.C. Green and C.L. Werner, "Hydrogeologic Framework of the Southwest Florida Water Management District," Florida Geological Survey, Bulletin No. 68, 2008, 175 pp.

2.5.3-218 Scott, T.M., K.M. Campbell, F.R. Rupert, J.D. Arthur, R.C. Green, G.H. Means, T.M. Missimer, J.M. Lloyd, J.W. Yon, and J.G. Duncan, "Geologic Map of the State of Florida," Florida Geological Survey Map Series 146, scale approximately 1:1,000,000, 2001. Revised 2006, D. Anderson.

2.5.3-219 Knapp, M.S., "Environmental Geology Series - Gainesville Sheet," Florida Geological Survey Map Series 79, scale 1:250,000, 1 sheet, 1978.

2.5.3-220 Campbell, K.M., "Geologic Map of Levy County,Florida," Florida Geological Survey Open File Map Series No. 11, 1992.

2.5.3-221 Knapp, M. S., "Top of the Floridan Aquifer of North Central Florida," Florida Department of Natural Resources, Bureau of Geology, Map Series No. 92, scale 1:500,000, 1979.

2.5.3-222 Maddox, G.L., J.M. Lloyd, T.M. Scott, R. Copeland, "Florida's Groundwater Quality Monitoring Program Hydrogeologic Framework," Florida Geological Survey Special Publication 32, 1992, 104 pp.

2.5.3-223 Not used.

2.5.3-224 Florida Power Corporation, "Site and Environment," Chapter 2, *Crystal River Final Safety Analysis Report*, 1976.

2.5.3-225 Upchurch, S.B, Personal Communication via email, June 12, 2009.

2.5.3-226 Barnett, R.S., "Basement Structure of Florida and Its Tectonic Implications," *Transactions - Gulf Coast Association of Geological Societies*, Vol. XXV, 1975, pp. 122 – 142.

2.5.3-227 Scott, T.M., K.M. Campbell, F.R. Rupert, J.D. Arthur, R.C. Green, G.H. Means, T.M. Missimer, J.M. Lloyd, J.W. Yon, and J.G. Duncan, "Geologic Map of the State of Florida," Florida Geological Survey Map Series 146, scale approximately 1:1,000,000, 2001. Revised 2006, D. Anderson.

2.5.4.2-201 COLA Site Investigation Workplan for Levy County Site, Progress Energy, Florida, CH2M Document Control Number 338884-WKPL-001, Revisions 0 through 6, 2007.

2.5.4.2-202 American Society for Testing and Materials, "D4633-05: Standard Test Method for Energy Measurement for Dynamic Penetrometers," Revision Year 2005.

2.5.4.2-203 American Society for Testing and Materials, "D2113-06: Standard Practice for Rock Core Drilling and Sampling of Rock for Site Investigation," Revision Year 2006.

2.5.4.2-204 American Society for Testing and Materials, "D1586-99: Standard Test Method for Penetration Test and Split-Barrel Sampling of Soils," Revision Year 1999.

2.5.4.2-205 American Society for Testing and Materials, "D6032-02: Standard Test Method for Determining Rock Quality Designation (RQD) of Rock Core," Revision Year 2006.

2.5.4.2-206 International Society of Rock Mechanics, "Rock Characterization Testing and Monitoring, ISRM Suggested Methods,", ed. E.T. Brown, 1981, Pergamon Press, Oxford, England.

2.5.4.2-207 American Society for Testing and Materials, "D5731-07: Standard Test Method for Determination of the Point Load Strength Index of Rock and Application to Rock Strength Classifications," Revision Year 2007.

2.5.4.2-208 American Society for Testing and Materials, "D5079-02: Standard Practices for Preserving and Transporting Rock Core Samples," Revision Year 2006.

2.5.4.2-209 American Society for Testing and Materials, "D7012-04: Standard Test Method for Compressive Strength and Elastic Moduli of Intact Rock Core Specimens under Varying States of Stress and Temperatures," Revision Year 2004.

2.5.4.2-210 American Society for Testing and Materials, "D3967-05: Standard Test Method for Splitting Tensile Strength of Intact Rock Core Specimens," Revision Year 2005.

2.5.4.2-211 U.S. Army, "Rock Testing Handbook (RTH)," Part 1, RTH 102-93, "Recommended Practice for Petrographic Examination of Rock Cores," 1993.

2.5.4.2-212 American Society for Testing and Materials, "C1271-99: Standard Test Method for X-ray Spectrometric Analysis of Lime and Limestone," Revision Year 2006.

2.5.4.2-213 American Society for Testing and Materials, "D2216-05: Standard Test Methods for Laboratory Determination of Water (Moisture) Content of Soil and Rock by Mass," Revision Year 2005.

2.5.4.2-214 American Society for Testing and Materials, "D4318-05: Standard Test Methods for Liquid Limit, Plastic Limit, and Plasticity Index of Soils," Revision Year 2005.

2.5.4.2-215 American Society for Testing and Materials, "D422-63: Standard Test Method for Particle-Size Analysis of Soils," Revision Year 1963 (Reapproved 2002).

2.5.4.2-216 American Society for Testing and Materials, "D1140-00: Standard Test Methods for Amount of Material in Soils Finer than No. 200 (75-μm) Sieve," Revision Year 2006.

2.5.4.2-217 American Society for Testing and Materials, "D854-06: Standard Test Methods for Specific Gravity of Soil Solids by Water Pycnometer," Revision Year 2006.

2.5.4.2-218 American Society for Testing and Materials, "G57-06: Standard Test Method for Field Measurement of Soil Resistivity Using the Wenner Four-Electrode Method," Revision Year 2006.

2.5.4.2-219 American Society for Testing and Materials, "D4972-01: Standard Test Method for pH of Soils," Revision Year 2007.

2.5.4.2-220 American Society for Testing and Materials, "D2974-07a: Standard Test Methods for Moisture, Ash, and Organic Matter of Peat and Other Organic Soils," Revision Year 2007.

2.5.4.2-221 American Society for Testing and Materials, "D2435-04: Standard Test Methods for One-Dimensional Consolidation Properties of Soils Using Incremental Loading," Revision Year 2004.

2.5.4.2-222 American Society for Testing and Materials, "D4767-04: Standard Test Method for Consolidated Undrained Triaxial Compression Test for Cohesive Soils," Revision Year 2004.

2.5.4.2-223 American Society for Testing and Materials, "D6066-96: Standard Practice for Determining the Normalized Penetration Resistance of Sands for Evaluation of Liquefaction Potential," Revision Year 1996 (Reapproved 2004).

2.5.4.2-224 Sabatini, P.J., Bachus, R.C., Mayne, P.W., Schneider, J.A., and T.E. Zettler, *Geotechnical Engineering Circular No. 5 Evaluation of Soil and Rock Properties*, Report No. FHWI-IF-02-034, 2002.

2.5.4.2-225 S&ME, *Geotechnical Laboratory Testing, Levy County Site, Levy County, Florida*, S&ME Report No. 1433-07-266, 2008.

2.5.4.2-226 Dunham, R. J., "Classification of carbonate rocks according to depositional texture," in Ham, W. E. (Ed.), *Classification of Carbonate Rocks*, American Association of Petroleum Geologists Memoir,1, p. 108-121, 1962.

2.5.4.2-227 Hoek, E., C. Carranza-Torres, and B. Corkum, "Hoek-Brown Failure Criterion — 2002 Edition," In *Proceedings, NARMS-TAC Conference, Toronto,* Vol. 1.

2.5.4.2-228 Hoek, E., and Brown, E.T., "Practical Estimates of Rock Mass Strength." Int. J. Rock Mech. Min. Sci., Vol. 34, No. 8, pp. 1165-1186, 1997.

2.5.4.2-229 RocScience, computer program "RocLab version 1.031,"2007.

2.5.4.2-230 Kramer, S. L., *Geotechnical Earthquake Engineering*, Prentice Hall, Upper Saddle River, New Jersey 07458, 1996.

2.5.4.2-231 Mayne, P.W., B.R. Christopher, and J. DeJong. 2002. "Subsurface Investigations-Geotechnical Site Characterization." Prepared for the U.S. Department of Transportation. *Publication No. FHWA NHI-01-031*. May 2002.

2.5.4.2-232 Hoek, E., and M.S. Diederichs, "Empirical estimation of rock mass modulus," *International Journal of Rock Mechanics & Mining Sciences*, Vol. 43, p. 203–215, 2006.

2.5.4.2-233 Yang, K., *Analysis of laterally loaded drilled shafts in rock*, PhD Dissertation, The University of Akron, 2006.

2.5.4.2-234 USACE (1994). Design of Sheet Pile Walls, EM 1110-2-2504, Washington, D.C.

2.5.4.2-235 NAVFAC, "Soil Mechanics," Design Manual 7.01, Alexandria, VA, 1 September 1986..

2.5.4.2-236 Trautmann, C. and Kulhawy, F., 1987, in Kulhawy, F. and Mayne, P. (1990), Manual on Estimating Soil Properties for Foundation Design, Report EL-6800, prepared for Electric Power Research Institute, Palo Alto, CA.

2.5.4.2-237 Webb, D. (1969), in Das, B. (1983). Advanced Soil Mechanics, McGraw-Hill, New York.

2.5.4.2-238 Farrent, T. (1963), in Das, B. (1983). *Advanced Soil Mechanics*, McGraw-Hill, New York.

2.5.4.2-239 Begemann, H. (1974), in Das, B. (1983). *Advanced Soil Mechanics*, McGraw-Hill, New York.

2.5.4.2-240 Lambe, T. and Whitman, R. (1969). *Soil Mechanics*, John Wiley & Sons, Inc., New York.

2.5.4.4-201 GeoVision, "Final Report Boring Geophysics Borings A-7, A-8, A-19, A-20, I-1, I-2, I-3, I-4, I-5, I-6, I-7, I-8, I-9, AND I-10, Progress Energy Florida Levy Nuclear Plant Combined Operating License Application," GeoVision Report 7087-01, Rev 0, March 27, 2008.

2.5.4.4-202 GeoVision, "Final Report Deep Boring Geophysics Borings AD-1, AD-2, AD-3, AD-4, I-1, I-3, I-4, I-6, I-8 AND I-9, Progress Energy Florida Levy Nuclear Plant Combined Operating License Application," GeoVision Report 7087-03, Rev 0, March 27, 2008.

2.5.4.4-203 Technos Geophysical Logging Data Reports at PEF Levy at PEF Levy Nuclear Plant (LNP) Site, April 30, 2008, (Included in 338884-EDF-034).

2.5.4.4-204 American Society for Testing and Materials, "D5753-05: Standard Guide for Planning and Conducting Borehole Geophysical Logging," Revision Year 2005.

2.5.4.4-205 RocScience, Inc., Dips, Graphical and Statistical Analysis of Orientation Data, Verification Manual, 2008.

2.5.4.4-206 Holmén, J. G. and N. Outters, "Theoretical study of rock mass investigation efficiency." Goulder Associates, pp 231-235, May, 2002.

2.5.4.8-201 Youd, T. L., et al. "Summary Report From the 1996 NCEER and 1998 NCEER/NSF Workshops on Evaluation of Liquefaction Resistance of Soils," *Journal of Geotechnical and Geo-environmental Engineering*, ASCE, October 2001.

2.5.4.8-202 Novak, M. and F. Aboul-Ella, "Impedance Functions of Piles in Layered Media", Journal of Engineering Mechanics Division, ASCE, June 1978.

2.5.4.8-203 Seed H.B., Idriss I.M., Makdisi F., & Banerjee N., Representation of Irregular Stress Time Histories by Equivalent Uniform Stress Series in Liquefaction Analyses, Report No. EERC 75-29, October, 1975.

2.5.4.10-201 American Concrete Institute (ACI), Building Code Requirements for Reinforced Concrete, ACI 318-89 and Commentary ACI 318R-89, 1989.

2.5.4.10-202 Kulhawy, F.H., and P.W. Mayne, "Manual on Estimating Soil Properties for Foundation Design," Report EL-6800, Electric Power Research Institute, Palo Alto, California, 1990.

2.5.4.10-203 Mayne, P.W., Christopher, B.R., and DeJong, J., "Manual on Subsurface Investigations- Geotechnical Site Characterization" NHI Publication No. FHWA NHI-01-031, Washington D.C. 2002.

2.5.4.10-204 American Association of State Highway and Transportation Officials (AASHTO) "LRFD Bridge Design Specification", 2002.

2.5.4.10-205 Bowles, J.E, *Foundation Analysis and Design*, McGraw Hill, 4th edition, 1968.

2.5.4.10-206 American Association of State Highway and Transportation Officials (AASHTO), "Standard Specification for Highway Bridges," Washington D.C., 16th edition, 1996.

2.5.4.10-207 Kramer, Steven. *Geotechnical Earthquake Engineering*, Prentice Hall, 1996.

2.5.4.10-208 Terzaghi, K. and Peck, R.B., Soil Mechanics in Engineering Practice, John Wiley and Sons, Inc., New York, 1948.

2.5.4.10-209 Westinghouse Electric Company. APP-GW-GLR-044, Revision 1 (TR-85), "Nuclear Island Basemat and Foundation", February 3, 2009.

Attachment G

Revised Subsection 3.7 Text and and New Subsection 3.7 Tables and Figures

[22 pages following this cover page]

3.7 SEISMIC DESIGN

This section of the referenced DCD is incorporated by reference with the following departures and/or supplements.

Add Subsection 3.7.1.1.1 as follows:

3.7.1.1.1 Design Ground Motion Response Spectra

LNP SUP 3.7-3 Figure 2.5.2-296 shows the comparison of the scaled horizontal and vertical site-specific ground motion response spectra (GMRS) to the AP1000 certified design seismic design response spectra (CSDRS). The GMRS was developed as the Truncated Soil Column Surface Response (TSCSR) on the uppermost in-situ competent material (elevation 11 m (36 ft.) NAVD88) as described in Subsection 2.5.2.6.

Plant design grade will be established at elevation 15.5 m (51 ft.) NAVD88 by placing engineered fill above in-situ material. Performance based surface horizontal and vertical response spectra (PBSRS) at the design grade elevation were developed as described in Subsection 2.5.2.6. Figure 2.5.2-297 presents the comparison of the AP1000 CSDRS with the scaled PBSRS for horizontal and vertical ground motions. The CSDRS envelops the scaled horizontal and the vertical PBSRS.

Figures 3.7-206 and 3.7-207 show the conceptual grading plan and the conceptual grading section for the LNP site respectively. The plant Nuclear Island (NI) footprint (approximately 0.8 acres for each unit) is small compared to the approximately 347 acres where fill will be placed to raise the existing grade level. The existing grade in the plant footprint area is at approximate elevation 12.8 m (42 ft.) NAVD88. The design grade in the 347 acre fill area will vary from elevation 15.2 m (50 ft.) NAVD88 to elevation 14.3 m (47 ft.) NAVD88. The large extent of the fill area compared to the NI footprint and because the PBSRS is higher than the GMRS for the LNP site, the fill to design grade was included in the DC/COL-ISG-017 free field response analysis and the SSI analysis presented in Subsection 3.7.2.4.1.

The backfill provides lateral support to the drilled shafts supporting the Turbine Building (TB), Annex Building (AB), and Radwaste Building (RB). Thus, the backfill will be controlled engineered fill under the footprint of the TB, AB, and RB and to a lateral extent of ~30 ft. beyond the building footprint as shown in Figure 3.7-208. The remainder of the fill required for site grading shown in Figure 3.7-206 will not be controlled engineered fill. As shown in Figure 3.7-209, the TB, AB, and RB buildings are supported on 3 ft., 4 ft., and 6 ft. diameter drilled shafts. The seismic II/I interaction evaluations show that for drilled shafts up to 6 ft. in diameter, the lateral stiffness of the drilled shafts is primarily dependent on the soil property of the top 16 ft. of soil. The ~30 ft. lateral extent of the controlled engineered fill corresponds to the lateral extent of the passive wedge for engineered fill with a friction angle of 34 degrees as specified in Table 2.5.4.5-201.

Add Subsection 3.7.1.1.2 as follows:

3.7.1.1.2 Foundation Input Response Spectra

The nuclear island is supported on 10.7 meters (35 feet) of roller compacted concrete over rock formations at the site as described in Subsection 2.5.4.5. As described in Subsection 2.5.2.6.6, foundation input response spectra (FIRS) were developed at elevation -7.3 m (-24 ft.) NAVD88, the base of planned excavation beneath the nuclear island. This FIRS was scaled to ensure that the computed soil column outcropping response (SCOR) at the AP1000 foundation elevation 3.4 m (11 ft.) NAVD88 meets the 0.1g minimum ZPA requirement of 10 CFR 50 Appendix S. The scaled SCOR FIRS at elevation -7 m (-24 ft.) NAVD88 and at elevation 3.4 m (11 ft.) NAVD88 are shown on Figures 3.7-201 and 3.7-205 respectively.

As shown in Figure 2.5.2-358, the CEUS SSC horizontal and vertical FIRS are enveloped by the updated EPRI-SOG scaled horizontal and vertical FIRS used for site specific soil structure interaction analysis described in Subsection 3.7.2.4.1. Thus, the conclusions of the soil structure analysis presented in Subsections 3.7.2.4.1.5 and 3.7.2.4.1.6 are valid for the LNP site ground motions based on the CEUS SSC model.

The seismic Category II and non-seismic adjacent structures are supported on drilled shafts. The top of the basemat for the Annex Building, Radwaste Building, and the Turbine Building (except for the condenser pit area) is at design grade elevation 15.5 m (51 ft.) NAVD88. The PBSRS described in Subsection 3.7.1.1.1 (Figure 2.5.2-297 and Table 2.5.2-227) are used to compute the maximum relative displacements of the Annex Building, Turbine Building, and the Radwaste Building drilled shaft foundation with respect to the nuclear island to evaluate site-specific aspect of the seismic interaction of these buildings with the nuclear island.

As shown in Figure 2.5.2-357, the CEUS SSC PBSRS are enveloped by the updated EPRI-SOG scaled PBSRS used for site specific displacement of the Annex Building, Turbine Building, and the Radwaste Building as described in Subsections 3.7.2.8.1, 3.7.2.8.2, and 3.7.2.8.3. Thus, the conclusions in these subsections of no seismic interaction between the Annex Building, Turbine Building, and Radwaste Building and the NI are valid for the LNP site ground motions based on the CEUS SSC model.

Add the following subsections after DCD Subsection 3.7.2.4.

3.7.2.4.1 Site Specific Soil Structure Analysis

LNP SUP 3.7-6 3.7.2.4.1.1 Soil Profiles for Soil Structure Analysis

LNP SUP 3.7-3 For the Soil Structure Analysis (SSI) analysis of the nuclear island (NI) the best estimate (BE), lower bound (LB), and upper bound (UB) soil profiles presented in Tables 2.5.2-228, 2.5.2-229, and 2.5.2-230 respectively were considered. In addition, to account for the potential degradation of soil shear modulus due to foundation installation, an additional Lower LB case (LLB) was also considered in the SSI analysis. The foundation construction activities that may affect the in-situ soil properties include installation of the drilled shafts, installation of the diaphragm wall, and installation of the rock anchors for the diaphragm wall. The construction methods and construction inspections used for installation of the drilled shafts, diaphragm wall, and the diaphragm wall anchors will minimize the extent of soil disturbance and avoid cave in. The holes for the anchors will be advanced using drilling techniques designed to minimize the disturbance to the surrounding soil. Such techniques may include the use of a casing, or drilling with water or drilling slurry (not air). The boreholes for the diaphragm wall anchors will be backfilled as the casing is extracted after the anchors are set in rock to avoid cave in. Alternatively, the casings will be backfilled and left in place. The drilled shaft construction methods and construction inspections and testing will follow guidance in ACI 336.1-01 and ACI 336.3R-93.

The volume of soil being disturbed by the drilled shaft installation, and diaphragm wall anchor installation is < 5 percent of the total soil volume in the vicinity of the NI. Assuming the disturbed soil around the drilled shaft and diaphragm wall anchors to have a soil shear modulus equal to half of the shear modulus of the corresponding soil layers, the average reduction in the soil shear modulus of the soil volume in the vicinity of the NI is < 2.5 percent. Thus, for the LLB soil profile, in-situ soil was conservatively assigned a shear modulus equal to 90 percent of the LB soil case as presented in Table 3.7-201. As shown in Table 3.7-201, the fill layer shear modulus was not changed from the LB shear modulus because of the large variation from the BE case already considered i.e., the coefficient of variation for the LB fill shear modulus is in the range of 4.02 to 6.13 from the BE fill shear modulus as shown in Table 3.7-201. Rock layer shear modulus for the LLB soil profile are the same as for the LB soil profile because the construction activities do not degrade the rock layer shear modulus.

3.7.2.4.1.2 DC/COL-ISG-017 Free Field Analysis

Design grade (elevation 15.5 m [51 ft.] NAVD88) deterministic surface spectra were developed using Subsection 5.2.1 of the Interim Staff Guidance DC/COL-ISG-017 as described in Subsection 2.5.2.6. The design grade surface response spectra from the three soil columns (best estimate, lower bound, and the upper bound properties) were developed using the scaled SCOR FIRS for elevation -7.3 m (-24 ft.) NAVD88, the base of planned excavation beneath the nuclear island. The three soil property profiles were developed based on the variation in the randomized soil profiles used for developing PBSRS and complying with SRP 3.7.2.II.4 guidance on soil property variation for SSI analysis. The shear wave velocity profiles for the upper bound (UB), best estimate (BE) and lower bound (LB) soil profiles are shown in Figure 2.5.2-298. The soil column profile and soil properties are presented in Tables 2.5.2-228, 229, and 230 for BE, LB, and UB cases respectively. Both horizontal and vertical SSI input response spectra were developed.

The envelope of the deterministic surface spectra for horizontal and vertical motions from the UB, LB, and BE envelops the PBSRS as required by DC/COL-ISG-017. This comparison is shown on Figures 3.7-202, 203, and 204. Figures 3.7-202 and 203 also present the comparison of the AP1000 CSDRS with the deterministic surface spectra from the UB, BE, and LB soil columns for the North-South (H1) and the East-West (H2) directions. The CSDRS envelops the deterministic surface spectra from the three soil columns for horizontal motions. For the vertical ground motions, Figure 3.7-204 presents the comparison of the AP1000 CSDRS with the deterministic surface spectra from the three soil columns for the vertical motions. The CSDRS does not envelop the deterministic surface spectra from the three soil columns in the high frequency range (greater than approximately 30 Hz). Thus, a LNP site-specific SSI analysis was performed.

3.7.2.4.1.3 Input Time Histories for Soil Structure Analysis

Input time histories for the SSI analysis were created in two steps. First, time histories were spectrally matched to the scaled SCOR FIRS at the base of the planned excavation (elevation -7.3 m (-24 ft.) NAVD88) shown in Figure 3.7-201. Then these time histories were input into the four (UB, BE, LB, and LLB) free field soil columns (full height to elevation 15.5 m (51 ft.) NAVD88) as outcropping motions and then output as in-column motion at the base of the excavation for use in the SSI analysis. As part of this process, the surface motion was computed for each of the four soil profiles and the SCOR FIRS was enhanced at intermediate frequencies to ensure that the surface motion envelops the PBSRS. The selected seed time history was the 1992 Landers Earthquake, Villa Park Serrano Ave station, chosen from the CEUS record library provided by NUREG/CR 6728. The seed time history was selected based on the seismological properties and spectral shape of both horizontal and vertical components. The selected time history represents a distance recording of a large (M 7.3) earthquake consistent with the dominant contribution to Levy site hazard by the Charleston source. Figures 3.7-210, 3.7-211, 3.7-212, and 3.7-213 show the in-column SSI input X, Y, and Z time histories at elevation -7.3 m (-24 ft.) NAVD88 for the Best Estimate (BE), Upper Bound (UB), Lower Bound (LB), and the Lower Lower Bound (LLB) soil profiles respectively.

3.7.2.4.1.4 Soil Structure Analysis Models

The LNP specific SSI analyses utilize both three dimensional (3D) and two dimensional (2D) models and SASSI Subtraction and Direct methods for computing in-structure floor response spectra.

The Design-Basis 3D model consists of a NI20r-derived, 5-Layer, 75-foot embedded Finite Element Model (FEM) developed for the BE soil case using the SASSI Direct method of analysis. An 8-Layer, 75-foot embedded 3D FEM was developed for sensitivity analysis of the LNP BE, UB, LB and LLB site soil cases utilizing the SASSI Subtraction method, and to confirm that the BE case is the controlling soil case particularly in the high frequency range. The 3D models capture the three dimensional response effects for the various site soil cases; however, the models are limited by the mesh size and corresponding passing model frequency based on the LNP site profile shear wave velocity and layer thickness. Therefore, two 2D models were developed to address 3D mesh size modeling, potential frequency filtering due to the 3D model layering, and to evaluate the SASSI SITE profile lower boundary depth.

The 2D 'Coarse' model was created to simulate the 3D design-basis embedded model in 2D. The 2D 'Fine' model was created to meet the SASSI wavelength criteria consistent with the NRC Interim Staff Guidance DC/COL-ISG-01 (ISG-01) 50 hertz model refinement frequency, and meet the lower boundary criteria specified in ASCE 4-98 Section 3.3.3.2 of at least 8000 fps or three times the maximum foundation dimension (~750 feet). The 2D SSI analyses utilized the SASSI Direct method. The results of the 2D SSI analyses determine the frequency-dependent ratio of Fine-to-Coarse response spectra (≥ 1.0), (i.e. Bump Factor), which is subsequently applied to the 3D BE Design-Basis FRS for comparison to the AP1000 generic and HRHF FRS envelopes.

The Turbine Building (TB), Annex Building (AB), and Radwaste Building (RB) drilled shafts and the diaphragm wall was not modeled in the 3D SSI model. The absence of any adverse Category II/I interaction between the NI and the TB, AB, and RB for LNP is documented in Subsections 3.7.2.8.1, 3.7.2.8.2, and 3.7.2.8.3.

3.7.2.4.1.5 Soil Structure Analysis

SASSI SSI analyses using the 3D and 2D models were performed considering the simultaneous occurrences of the two horizontal and one vertical components of the time history. The input time history (Subsection 3.7.2.4.1.3) was applied as in-column motions at elevation -7.3 m (-24 ft.) NAVD88. The floor response time histories in the X, Y, and Z directions were obtained by algebraically combining the co-directional acceleration time histories from the three excitations. Floor response spectra (FRS) were generated for the six key AP1000 locations using 5 percent damping. These locations include: CIS at Reactor Vessel Support Elevation (Node 1761), ASB NE Corner at Control Room Floor (Node 2078), CIS at Operating Deck (Node 2199), ASB Corner of Fuel Building Roof at Shield Building (Node 2675), SCV near Polar Crane (Node 2788), and ASB Shield Building Roof Area (Node 3329).

The first SSI analysis was performed using the 3D 8-Layer embedded model and the BE, UB, LB and LLB soil profiles. The SASSI Subtraction method was used. The LNP specific broadened 5 percent damped FRS computed at the six key locations for the X, Y and Z directions are shown in Figures 3.7-214, 3.7-215, 3.7-216, 3.7-217, 3.7-218, and 3.7-219. The figures show that the LNP FRS are enveloped by the AP1000 generic FRS at all of the six NI key nodes. The FRS also confirm that the BE soil profile FRS are the controlling FRS in the critical high frequency range (≥ 25 Hz.) except for the horizontal spectra at node 2078. At this node, the AP1000 HRHF FRS provides sufficient additional margin.

The second SSI analysis was performed using the 2D "Coarse" and "Fine" models for the BE soil profile. The SASSI Direct method was used. The 5 percent damped FRS at the six key nodes were generated. Frequency dependent Bump Factors (≥ 1.0) were calculated from the FRS as the ratio of the 2D Fine model and the 2D Coarse model FRS at the six key nodes.

The third SSI analysis was performed using the 3D 5-layer embedded model for the BE soil profile. The SASSI Direct method was used. The 5 percent damped FRS at the six key nodes were generated. The frequency dependent Bump Factors calculated from the 2D model were applied to the 3D 5-layer model FRS along the frequency spectrum to amplify the 3D 5-layer model FRS. These factored FRS are compared to the AP1000 generic and HRHF (as necessary) FRS envelops at the six key locations in Figures 3.7-220, 3.7-221, 3.7-222, 3.7-223, 3.7-224, and 3.7-225. The HRHF FRS envelope is presented for 3D nodes 2078, 2199, and 2675 to demonstrate that additional margin exists at the three nodes in the high frequency region (20-50 Hz.). As shown in the figures, the LNP site-specific factored FRS are enveloped by the AP1000 generic and HRHF FRS envelopes at each of the six nodes with sufficient margin.

3.7.2.4.1.6 Bearing Pressure and Base Shear

Based on the SSI analysis, the maximum bearing pressure on the RCC bridging mat beneath the NI basemat for the BE, UB, LB and LLB soil profiles is 20.29 ksf. The maximum bearing pressure corresponds to the BE soil profile. The LNP site specific maximum bearing pressure is enveloped by the AP1000 soft rock site maximum bearing pressure of 24 ksf for soft rock sites.

Based on the SSI analysis, the maximum base shear on the RCC bridging mat for the BE, UB, LB and LLB soil cases is 77,600 kips. The maximum base shear corresponds to the BE soil profile. The maximum 77,600 kips base shear yields a base shear to vertical load ratio of 0.12 for the NI. This ratio is enveloped by the AP1000 maximum ratio of 0.55.

3.7.2.4.1.7 Sensitivity Evaluations for Regulatory Guide 1.60 Spectra FIRS

The Regulatory Guide 1.60 Foundation Input Response Spectra (FIRS) is anchored at peak ground accelerations for the scaled site-specific FIRS in Table 2.5.2-236 (0.1g horizontal and 0.0695g vertical). The scaled site-specific FIRS was developed using the updated EPRI SOG methodology and scaled to meet 10 CRF Part 50 Appendix S requirements. Tables 3.7-203 and 3.7-204 present the 5% damped site specific FIRS, the 5% damped Regulatory Guide 1.60 FIRS, and the ratio of the Regulatory Guide FIRS and the site specific FIRS at various frequencies for horizontal and vertical spectra respectively.

Sensitivity evaluations were performed to assess whether the FRS at the six key locations using the Regulatory Guide 1.60 FIRS instead of the scaled site-specific FIRS remains bounded by the Certified Seismic Design Response Spectra (CSDRS) FRS. The sensitivity evaluations were performed using conservative simplified methodology by scaling the entire site specific FRS by the ratio of the Regulatory Guide 1.60 FIRS and the scaled site specific FIRS at the predominant response frequency at the node/direction. The predominant response frequency was determined from the peaks in the site specific FRS at each of the six nodes in the X, Y, and Z directions. The site specific FRS at the six nodes in the X, Y, and Z directions are shown in Figures 3.7-214, 3.7-215, 3.7-216, 3.7-217, 3.7-218, and 3.7-219. For this evaluation the lowest predominant response frequency is used because it will yield a larger scaling factor and is thus conservative. Table 3.7-205 presents the predominant response frequencies at the six key nodes in the X, Y, and Z directions, the ratio of the Regulatory Guide 1.60 FIRS and the scaled site specific FIRS at the predominant response frequency (scaling factor), and the minimum margin for site specific FRS with respect to the CSDRS FRS when the whole site specific FRS is scaled by the scaling factor for the predominant response frequency for the node and direction. Because the scaling factors to develop the Regulatory Guide 1.60 FRS are always smaller than the available margin with respect to the CSDRS FRS, the Regulatory Guide 1.60 FRS will be bounded by the CSDRS FRS. In addition, because the Regulatory Guide 1.60 spectra has only a small frequency content above 20 Hz. and no frequency content above 33 Hz., the Regulatory Guide 1.60 FRS peaks in the high frequency range (>20 Hz.) will be lower than that obtained by the simple scaling used, thus providing additional margin with respect to the CSDRS FRS.

As stated in Subsections 2.5.4.5.4 and 2.5.4.10.1.1, the conceptual design of the RCC bridging mat is based on a bearing pressure of 8.9 kips per square foot [ksf] for static loading and 24.0 ksf for dynamic loading. The static bearing pressure is based on DCD Tier 1 Table 5.0.1. The dynamic bearing pressure is the maximum subgrade pressure at the AP1000 basemat that results from the generic AP1000 analysis for soft rock sites. For the subsurface rock bearing capacity calculations, the RCC self weight was included as an additional bearing pressure load of 5.16 ksf. The buoyancy effects due to the hydrostatic pressure acting at the bottom of the RCC were considered in this analysis. A base shear load of 136,000 kips based on the AP1000 generic analysis was applied at the top of the RCC bridging mat. Because the AP1000 generic analyses are based on the CSDRS (0.3g Regulatory Guide 1.60 spectra enhanced in the high frequency region), the RCC design is conservative for the Regulatory Guide 1.60 FIRS.

3.7.2.8.1 Annex Building

Add the following text to the end of DCD Subsection 3.7.2.8.1.

In DCD Subsection 3.7.2.8.1, the maximum displacement of the roof of the Annex Building is reported as 1.6 inches for response spectra input at the base of the building that envelops the SSI spectra for the six soil profiles and also the CSDRS. The Annex Building foundation (top of mat) is at design grade. Figure 2.5.2-297 shows a comparison of the LNP scaled performance based surface response spectra (PBSRS) at the plant design grade and the CSDRS. The CSDRS envelops the LNP PBSRS by a wide margin. Thus, the LNP Annex Building roof displacement relative to its foundation is expected to be less than the 1.6 inches in the DCD for the CSDRS. The computed probable maximum relative displacement during SSE between the NI and the Annex Building foundation mat is less than 2.5 cm (1 in.) for both the scaled Performance Based Surface Response Spectra (PBSRS) or the Regulatory Guide 1.60 spectra anchored at peak ground acceleration of 0.1g applied at the foundation elevation of the Annex Building as shown in Table 3.7-206. The probable maximum relative displacement calculation included the drilled shaft supported foundation mat displacements including the drilled shaft to drilled shaft interaction effects, additional displacement due to soil column displacement, and the NI displacement at design grade. The square root of the sum of squares (SRSS) method was used to compute the probable maximum relative displacement. Thus, the LNP Annex Building roof displacement during SSE is expected to be less than 2.6 inches. As stated in DCD Subsection 3.7.2.8.1, the minimum clearance between the structural elements of the Annex Building above grade and the nuclear island (NI) is 4 inches. Figure 3.7-226 shows the conceptual design detail for the interface between the Nuclear Island (NI) and the drilled shaft supported foundation mat of the Annex Building. This design detail provides a 5.0 cm (2 in.) gap between the Annex Building foundation and the NI consistent with DCD Subsection 3.8.5.1. The top of the diaphragm wall and controlled low strength material fill between the diaphragm wall and the NI wall is at least 1.5 m (5 ft.) below the bottom of the Annex Building foundation mat as stated in Subsection 2.5.4.5.1. Engineered fill is used from the top of the controlled low strength material fill to the bottom of the Annex Building foundation as stated in Subsection 2.5.4.5.4. This interface is designed to avoid hard contact between the NI and the Annex Building foundation mat resulting from the relative displacement between the NI and the Annex Building foundation mat during the seismic event. Thus, no seismic interaction between the Annex Building and the NI is expected.

3.7.2.8.2 Radwaste Building

Add the following text to the end of DCD Subsection 3.7.2.8.2.

LNP SUP 3.7-5

The computed probable maximum relative displacement between the NI and the Radwaste Building foundation mat is less than 2.5 cm (1 in.) for both the scaled ~~from a Performance Based Surface Response Spectra (~~PBSRS~~)~~ or the Regulatory Guide 1.60 spectra anchored at peak ground acceleration of 0.1g applied at the foundation elevation of the Radwaste Building as shown in Table

3.7-206~~is less than 2.5 cm (1 in.)~~. The probable maximum relative displacement calculation included the drilled shaft supported foundation mat displacements including the drilled shaft to drilled shaft interaction effects, additional displacement due to soil column displacement, and the NI displacement at design grade. The SRSS method was used to compute the probable maximum relative displacement. Figure 3.7-226 shows the conceptual design detail for the interface between the Nuclear Island (NI) and the drilled shaft supported foundation mat of the Radwaste Building. This design detail provides a 5.0 cm. (2 in.) gap between the Radwaste Building foundation and the NI consistent with DCD Subsection 3.8.5.1. The top of the diaphragm wall and controlled low strength material fill between the diaphragm wall and the NI wall is at least 1.5 m (5 ft.) below the bottom of the Radwaste Building foundation mat as stated in Subsection 2.5.4.5.1. Engineered fill is used from the top of the controlled low strength material fill to the bottom of the Radwaste Building foundation as stated in Subsection 2.5.4.5.4. This interface is designed to avoid hard contact between the NI and the Radwaste Building foundation mat resulting from the relative displacements during the seismic event. Thus, no seismic interaction between the Radwaste Building foundation mat and the NI is expected.

3.7.2.8.3 Turbine Building

Add the following text to the end of DCD Subsection 3.7.2.8.3.

LNP SUP 3.7-5

The computed probable maximum relative displacement between the NI and the Turbine Building foundation mat is less than 2.5 cm (1 in.) for both the ~~from a Performance Based Surface Response Spectra (~~PBSRS~~)~~ or the Regulatory Guide 1.60 spectra anchored at peak ground acceleration of 0.1g applied at the foundation elevation of the Turbine Building as shown in Table 3.7-206~~is less than 2.5 cm (1 in.)~~. The probable maximum relative displacement calculation included the drilled shaft supported foundation mat displacements including the drilled shaft to drilled shaft interaction effects, additional displacement due to soil column displacement, and the NI displacement at design grade. The SRSS method was used to compute the probable maximum relative displacement. Figure 3.7-226 shows the conceptual design detail for the interface between the Nuclear Island (NI) and the drilled shaft supported foundation mat of the Turbine Building. This design detail provides the 5.0 cm. (2 in.) gap between the Turbine Building foundation and the NI consistent with DCD Subsection 3.8.5.1. The top of the diaphragm wall and controlled low strength material fill between the diaphragm wall and the NI wall is at least 1.5 m (5 ft.) below the bottom of the Turbine Building foundation mat as stated in Subsection 2.5.4.5.1. Engineered fill is used from the top of the controlled low strength material fill to the bottom of the Turbine Building foundation mat as stated in Subsection 2.5.4.5.4. This interface is designed to avoid hard contact between the NI and the Turbine Building foundation mat resulting from the relative displacements during the seismic event. Thus, no seismic interaction between the Turbine Building foundation mat and the NI is expected.

3.7.2.8.4 Median Centered Adjacent Building Relative Displacements for 10^{-5} UHRS

As a sensitivity analysis, the median centered probable maximum relative displacements between the NI and the adjacent Turbine, Annex, and Radwaste Buildings' foundation mat were calculated for updated EPRI-SOG 10^{-5} UHRS. The drilled shaft supported foundation mat lateral displacements were obtained from 21 randomly selected soil profiles from the set of several hundred randomized soil profiles used to develop the updated EPRI-SOG 10^{-5} UHRS. The median shear wave velocity profile for the 21 soil profiles closely matches the median shear wave velocity profile for the entire set of randomized soil profiles used to develop the updated EPRI-SOG 10^{-5} UHRS as shown in Figure 3.7-227. The probable maximum relative displacement between the NI and the TB, AB, and the RB foundation mats was computed by combining the soil column displacements for UHRS, the NI displacement at the design grade, and the Turbine, Annex, and Radwaste Buildings' foundation mat displacements for updated EPRI-SOG 10^{-5} UHRS using the square root of the sum of squares (SRSS) method. The computed probable maximum median relative displacements between the NI and the adjacent Turbine, Annex, and Radwaste Buildings' foundation mat for updated EPRI-SOG 10^{-5} UHRS are less than 2.5 cm. (1 in.). Figure 3.7-226 shows the conceptual design detail for the interface between the Nuclear Island (NI) and the drilled shaft supported foundation mat of the Turbine Building. This design detail provides the 5.0 cm. (2 in.) gap between the Turbine, Annex, and Radwaste Buildings' foundation mat and the NI consistent with DCD Subsection 3.8.5.1. The top of the diaphragm wall and controlled low strength material fill between the diaphragm wall and the NI wall is at least 1.5 m (5 ft.) below the bottom of the Turbine Building foundation mat as stated in Subsection 2.5.4.5.1. Engineered fill is used from the top of the controlled low strength material fill to the bottom of the Turbine Building foundation as stated in Subsection 2.5.4.5.4. This interface is designed to avoid hard contact between the NI and the Turbine Building foundation resulting from the relative displacements during the seismic event. Thus, no seismic interaction between the Turbine, Annex, and the Radwaste Buildings' foundation mat and the NI is expected for updated EPRI-SOG 10^{-5} UHRS.

To evaluate the HCLPF capacity for no seismic interaction between the Annex Building, Turbine Building, and Radwaste Building foundation mats and the NI, the relative displacement between the NI and the Annex Building, Turbine Building, and Radwaste Building foundations was computed based on the updated EPRI-SOG 10^{-5} UHRS. As shown in Figures 3.7-228 and 3.7-229, 1.67*GMRS and 1.67*PBSRS developed using the CEUS SSC method and modified CAV filter are enveloped by the updated EPRI-SOG 10^{-5} UHRS. Thus, HCLPF capacity for no seismic interaction between the Annex Building, Turbine Building, and Radwaste Building foundation mats and the NI exceeds the 1.67*GMRS goal for the plant level HCLPF for the CEUS SSC ground motions.

3.7.2.12 Methods for Seismic Analysis of Dams

Add the following text to the end of DCD Subsection 3.7.2.12.

LNP COL 3.7-1

There are no existing dams that can affect the site interface flood level as specified in DCD Subsection 2.4.1.2 and discussed in FSAR Subsection 2.4.4.

3.7.4.1 Comparison with Regulatory Guide 1.12

Add the following text to the end of DCD Subsection 3.7.4.1.

STD SUP 3.7-1

Administrative procedures define the maintenance and repair of the seismic instrumentation to keep the maximum number of instruments in-service during plant operation and shutdown in accordance with Regulatory Guide 1.12.

3.7.4.2.1 Triaxial Acceleration Sensors

Add the following text to the end of DCD Subsection 3.7.4.2.1.

STD COL 3.7-5

A free-field sensor will be located and installed to record the ground surface motion representative of the site. It will be located such that the effects associated with surface features, buildings, and components on the recorded ground motion will be insignificant. The trigger value is initially set at 0.01g.

3.7.4.4 Comparison of Measured and Predicted Responses

Add the following text to the end of DCD Subsection 3.7.4.4.

LNP COL 3.7-2

Post-earthquake operating procedures utilize the guidance of EPRI Reports NP5930, TR-100082, and NP-6695, as modified and endorsed by the NRC in Regulatory Guides 1.166 and 1.167. A response spectrum check up to 10Hz and the cumulative absolute velocity will be calculated based on the recorded motions at the free field instrument. If the operating basis earthquake ground motion is exceeded or significant plant damage occurs, the plant must be shutdown in an orderly manner.

STD COL 3.7-2

In addition, the procedures address measurement of the post-seismic event gaps between the new fuel rack and walls of the new fuel storage pit, between the individual spent fuel racks, and from the spent fuel racks to the spent fuel pool walls, and provide for appropriate corrective actions to be taken if needed (such as repositioning the racks or analysis of the as-found condition).

3.7.4.5 Tests and Inspections

Add the following text to the end of DCD Subsection 3.7.4.5.

STD SUP 3.7-2 Installation and acceptance testing of the triaxial acceleration sensors described in DCD Subsection 3.7.4.2.1 is completed prior to initial startup. Installation and acceptance testing of the time-history analyzer described in DCD Subsection 3.7.4.2.2 is completed prior to initial startup.

3.7.5 COMBINED LICENSE INFORMATION

3.7.5.1 Seismic Analysis of Dams

LNP COL 3.7-1 This COL Item is addressed in Subsection 3.7.2.12.

3.7.5.2 Post-Earthquake Procedures

LNP COL 3.7-2
STD COL 3.7-2 This COL Item is addressed in Subsection 3.7.4.4.

3.7.5.3 Seismic Interaction Review

Replace DCD Subsection 3.7.5.3 with the following text.

STD COL 3.7-3 The seismic interaction review will be updated for as-built information. This review is performed in parallel with the seismic margin evaluation. The review is based on as-procured data, as well as the as-constructed condition. The as-built seismic interaction review is completed prior to fuel load.

3.7.5.4 Reconciliation of Seismic Analyses of Nuclear Island Structures

Replace DCD Subsection 3.7.5.4 with the following text.

STD COL 3.7-4 The seismic analyses described in DCD Subsection 3.7.2 will be reconciled for detailed design changes, such as those due to as-procured or as-built changes in component mass, center of gravity, and support configuration based on as-procured equipment information. Deviations are acceptable based on an evaluation consistent with the methods and procedure of DCD Section 3.7 provided the amplitude of the seismic floor response spectra, including the effect due to these deviations, does not exceed the design basis floor response spectra by more than 10 percent. This reconciliation will be completed prior to fuel load.

3.7.5.5 Free Field Acceleration Sensor

STD COL 3.7-5 This COL Item is addressed in Subsection 3.7.4.2.1.

3.7.6 REFERENCES

Add the following at the end of DCD Subsection 3.7.6:

201. Darendeli, M.B, Development of a New Family of Normalized Modulus Reduction and Material Damping Curves, Ph.D Thesis, University of Texas, Austin, 2001.

202. Menq, F.Y., Dynamic Properties of Sandy and Gravelly Soils, Ph.D Thesis, University of Texas, Austin, 2003.

203. Power, M., B. Chiou, N. Abrahamson, Y. Bozorgnia, T. Shantz, and C. Roblee, An Overview of the NGA Project, Earthquake Spectra, v. 24, p. 3-21, 2008.

Table 3.7-201
Lower Lower Bound (LLB) Soil Profile for SSI Analysis

LNP SUP 3.2-6
LNP SUP 3.7-3

Layer	Layer Thickness (ft.)	D(a) (ft.)	Unit Weight (kcf)	BE(c) V_s(b) (ft/sec)	LB(d) V_s(b) (ft/sec)	LB(d) G(g) (ksf)	LLB(e) G(g) (ksf)	LLB(e) - G(g) COV(f)	Description
1	2.5	2.5	110	836	373	476	476	4.02	Fill
2	2.5	5.0	110	824	342	400	400	4.81	Fill
3	2.5	7.5	110	796	315	339	339	5.38	Fill
4	3.5	11.0	110	788	300	307	307	5.92	Fill
5	2.0	13.0	110	796	301	310	310	5.97	Fill
6	2.0	15.0	110	786	294	296	296	6.13	Fill
7	3.5	18.5	120	1,503	1,123	4,702	4,232	0.99	In -situ Soil
8	2.5	21.0	120	1,500	1,115	4,632	4,169	1.01	In -situ Soil
9	1.0	22.0	120	1,500	1,115	4,632	4,169	1.01	In -situ Soil
10	3.5	25.5	120	1,501	1,074	4,301	3,871	1.17	In -situ Soil
11	3.5	29.0	120	1,496	1,070	4,270	3,843	1.17	In -situ Soil
12	6.7	35.7	120	1,482	1,111	4,596	4,137	0.98	In -situ Soil
13	4.3	40.0	120	1,476	1,100	4,507	4,056	1.00	In -situ Soil
14	2.4	42.4	120	1,476	1,100	4,507	4,056	1.00	In -situ Soil
15	8.3	50.7	130	2,267	1,851	13,830	12,447	0.67	In -situ Soil
16	8.3	59.0	130	2,266	1,850	13,822	12,440	0.67	In -situ Soil
17	7.2	66.2	130	2,254	1,841	13,680	12,312	0.67	In -situ Soil
18	7.2	73.4	130	2,251	1,838	13,639	12,275	0.67	In -situ Soil
19	1.6	75.0	138	2,772	2,264	21,960	19,764	0.67	In -situ Soil
20		> 75.0					Rock(i)		Rock

Notes:
a) D: Depth from Design Grade (EL +51 ft.) to bottom of Layer
b) Vs: Layer Shear wave velocity
c) BE: Best Estimate soil profile (Table 17 of Calculation LNG-0000-X7C-044 Rev. 1)
d) LB: Lower Bound soil profile (Table 18 of Calculation LNG-0000-X7C-044 Rev. 1)
e) LLB: Lower Lower Bound soil profile
f) COV: Coefficient of variation
g) G: Shear Modulus
i) Rock profile same as LB rock profile

Units:
ft.: Feet
kcf: Kips per cubic feet
ksf: Kips per square feet

LNP COL 2.5-9

Table 3.7-202
Median Soil Profile to 10^{-5} UHRS Relative Displacements Calculations

Layer	Thickness (ft)	Total Depth (ft)	Unit Weight (pcf)	Shear Wave Velocity (ft/sec)	Damping Ratio (%)	Compression Wave Velocity (ft/sec)	Elevation of Layer Base (ft)
1	2.5	2.5	110	828.7	1.5	1590.2	48.5
2	2.5	5	110	804.6	2.2	1590.2	46.0
3	2.5	7.5	110	761.9	2.9	1590.2	43.5
4	3.5	11	110	744.2	3.5	1590.2	40.0
5	2	13	110	742.7	3.9	5000.0	38.0
6	2	15	110	730.5	4.2	5000.0	36.0
7	3.5	18.5	120	1461.6	3.1	5600.0	32.5
8	2.5	21	120	1454.1	3.3	5600.0	30.0
9	1	22	120	1454.1	3.3	5600.0	29.0
10	3.5	25.5	120	1457.0	2.1	5600.0	25.5
11	3.5	29	120	1442.3	2.2	5600.0	22.0
12	6.9	35.9	120	1434.1	2.1	5600.0	15.1
13	4.1	40	120	1419.4	2.4	5600.0	11.0
14	2.8	42.8	120	1419.4	2.4	5600.0	8.2
15	8.4	51.2	130	2221.9	1.7	7550.0	-0.2
16	8.4	59.6	130	2221.2	1.8	7550.0	-8.6
17	7.1	66.7	130	2206.2	2.0	7550.0	-15.7
18	7.1	73.8	130	2202.1	2.0	7550.0	-22.8
19	1.2	75	138	2768.2	1.4	8700.0	-24.0
20	24.6	99.6	138	2768.2	1.4	8700.0	-48.6
21	47.4	147	138	2685.3	1.4	8550.0	-96.0
22	61.3	208.3	138	3369.3	1.4	10600.0	-157.3
23	17.9	226.2	138	3313.8	1.4	9450.0	-175.2
24	24.1	250.3	120	3204.8	1.8	7250.0	-199.3
25	24.6	274.9	120	3177.0	1.8	7250.0	-223.9
26	40	314.9	120	3522.5	1.3	7900.0	-263.9
27	42	356.9	120	3356.5	1.3	7900.0	-305.9
28	38.4	395.3	140	4130.9	0.9	8900.0	-344.3
29	59.4	454.7	140	3361.0	0.9	8100.0	-403.7
30	59.4	514.1	140	3712.0	0.9	9000.0	-463.1
31	242.7	756.8	140	4537.1	0.9	11000.0	-705.8
32	355.8	1112.6	140	5928.9	0.9	14400.0	-1061.6
33	249.4	1362	150	7276.9	0.7	17850.0	-1311.0
34	252.9	1614.9	150	5087.2	0.7	12350.0	-1563.9
35	148.3	1763.2	150	7277.1	0.7	17400.0	-1712.2
36	106.1	1869.3	150	6240.9	0.7	14900.0	-1818.3
37	199	2068.3	150	7165.6	0.7	17500.0	-2017.3
38	601.2	2669.5	150	5424.6	0.8	13000.0	-2618.5
39	149.2	2818.7	150	5949.2	0.8	14200.0	-2767.7
40	192.7	3011.4	150	6195.7	0.8	14950.0	-2960.4
41	652.3	3663.7	150	5155.8	0.8	12600.0	-3612.7
42	603.7	4267.4	150	5553.3	0.8	13450.0	-4216.4
43	96.6	4364	150	4797.8	0.8	11500.0	-4313.0
44	Halfspace	4364	169	9382.7	0.1	16100.0	-4313.0

Table 3.7-203
Ratio of Horizontal RG 1.60 FIRS and Site Specific (SS) FIRS

LNP SUP 3.7-6

Frequency (Hz)	Site Specific FIRS (g)	RG 1.60 FIRS (g)	RG 1.60 / SS FIRS Ratio
1.00	0.108	0.147	1.36
1.50	0.156	0.206	1.32
2.00	0.176	0.261	1.48
2.50	0.196	0.313	1.60
3.00	0.214	0.305	1.43
3.50	0.230	0.298	1.30
4.00	0.245	0.293	1.20
5.00	0.273	0.284	1.04
6.00	0.276	0.276	1.00
9.00	0.265	0.261	0.98
10.00	0.263	0.241	0.92
12.00	0.260	0.211	0.81
15.00	0.253	0.179	0.71
20.00	0.231	0.145	0.63
30.00	0.183	0.107	0.59
33.00	0.175	0.100	0.57
100.00	0.100	0.100	1.00

Table 3.7-204
Ratio of Vertical RG 1.60 FIRS and Site Specific (SS) FIRS

LNP SUP 3.7-6

Frequency (Hz)	Site Specific FIRS (g)	RG 1.60 FIRS (g)	RG 1.60/ SS FIRS Ratio
1.00	0.068	0.071	1.05
2.00	0.104	0.129	1.24
3.00	0.122	0.182	1.49
3.50	0.130	0.207	1.59
4.00	0.139	0.203	1.46
5.00	0.154	0.197	1.28
6.00	0.157	0.192	1.22
7.00	0.157	0.188	1.20
9.00	0.157	0.181	1.15
10.00	0.159	0.168	1.06
15.00	0.170	0.124	0.73
18.00	0.174	0.109	0.63
20.00	0.175	0.101	0.58
33.00	0.144	0.070	0.49
100.00	0.070	0.070	1.00

Table 3.7-205
Predominant Frequencies, Scale Factors for Regulatory Guide 1.60 FIRS, and CSDRS FRS Margin

LNP SUP 3.7-6

LNP SUP 3.7-3

Node / Direction	Predominant Frequency (Hz.)	Ratio RG 1.60 and Scaled FIRS	Minimum CSDRS FRS Margin
1761-X	3.0	1.43	>1.43
1761-Y	5.5	1.02	>1.02
1761-Z	5.0	1.28	>1.28
2078-X	20.0	0.63	>1.00
2078-Y	12.0	0.81	>1.00
2078-Z	20.0	0.58	>1.00
2199-X	20.0	0.63	>1.00
2199-Y	5.5	1.02	>1.02
2199-Z	20.0	0.58	>1.00
2675-X	30.0	0.59	>1.00
2675-Y	3.0	1.43	>1.43
2675-Z	6.0	1.22	>1.22
2788-X	5.0	1.04	>1.04
2788-Y	5.5	1.02	>1.02
2788-Z	18.0	0.63	>1.00
3329 X	3.5	1.30	>1.30
3329-Y	3.0	1.43	>1.43
3329-Z	7.0	1.20	>1.20

Table 3.7-206
Probable Maximum Relative Displacements between the Nuclear Island (NI) and Adjacent Buildings

LNP SUP 3.7-5

Adjacent Building	Probable Maximum Relative Displacement (in.)	
	Site Specific FIRS	RG 1.60 FIRS
Between NI and Annex Building	0.70	0.59
Between NI and Radwaste Building	0.77	0.64
Between NI and Turbine Building	0.40	0.35

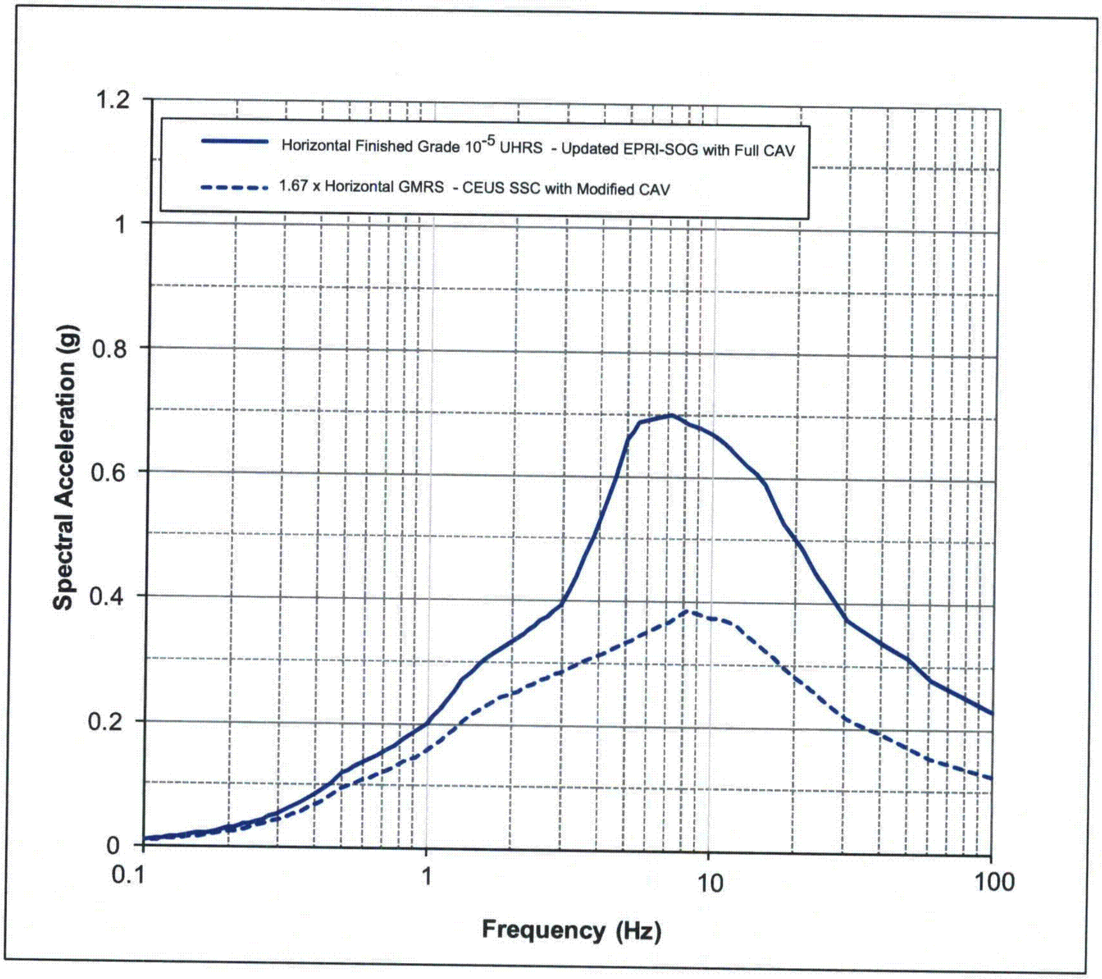

Progress Energy Florida

Levy Nuclear Plant
Units 1 and 2
Part 2, Final Safety Analysis Report

Comparison of the horizontal 10^{-5} UHRS using the Updated EPRI-SOG model with 1.67 x the GMRS using the CEUS SSC model with modified CAV

FIGURE 3.7-228

Rev 5

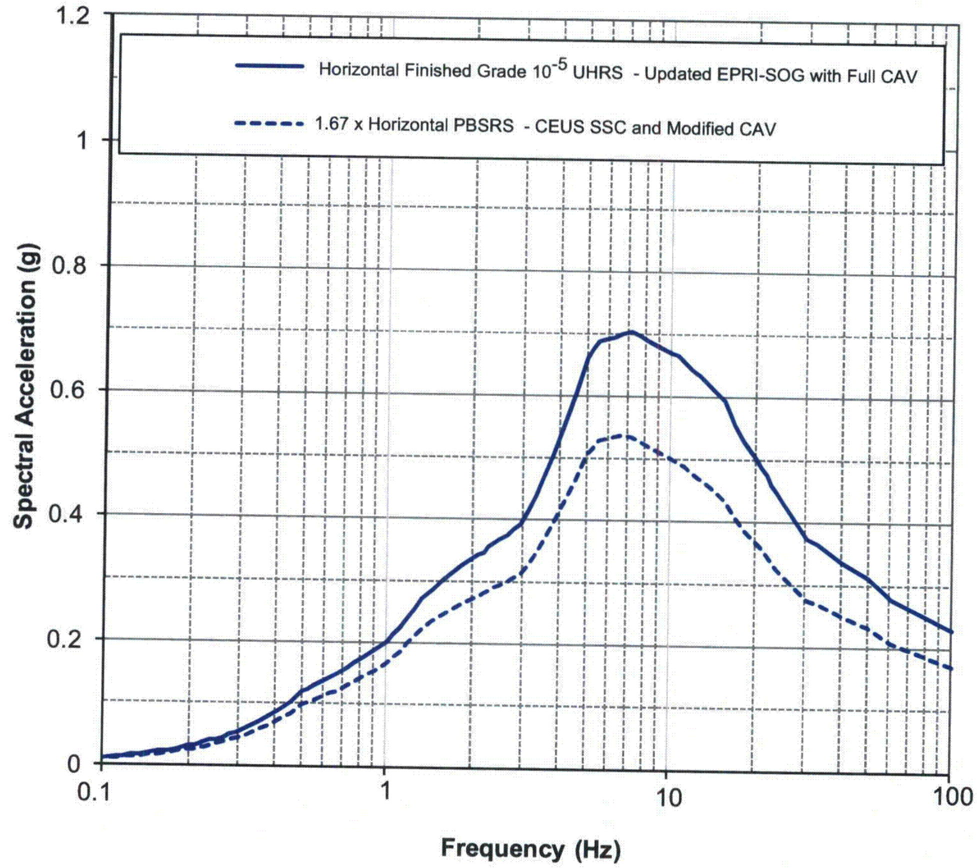

Progress Energy Florida

Levy Nuclear Plant
Units 1 and 2
Part 2, Final Safety Analysis Report

Comparison of the horizontal 10^{-5} UHRS using the Updated EPRI-SOG model with 1.67 x the PBSRS using the CEUS SSC model with modified CAV

FIGURE 3.7-229 Rev 5

Attachment H

Revised Subsection 19.55 Text and Table

[4 pages following this cover page]

19.55 SEISMIC MARGIN ANALYSIS

This section of the referenced DCD is incorporated by reference with the following departures and/or supplements.

Add the following Subsection after DCD Subsection 19.55.6.2:

19.55.6.3 Site-Specific Seismic Margin Analysis

LNP COL 19.59.10-6 The LNP GMRS was developed as the Truncated Soil Column Surface Response (TSCSR) on the uppermost in-situ competent material at elevation 11 m (36 ft.) NAVD88 as described in Subsection 2.5.2.6. Since plant design grade will be established at elevation 15.5 m (51 ft.) NAVD88 by engineered fill above in-situ material as noted in Subsection 2.5.4.5, performance based surface horizontal and vertical response spectra (PBSRS) at the design grade scaled to meet 10 CFR Part 50 Appendix S requirements were developed as described in Subsection 2.5.2.6. Both the LNP scaled GMRS and the scaled PBSRS are enveloped by the AP1000 Certified Seismic Response Spectra as documented in Subsection 2.5.2.6. In addition, LNP site-specific SSI analysis was performed to evaluate the effect of the LNP unique foundation conditions on seismic demand. It was determined that the LNP site-specific seismic floor response spectra (FRS) at the six key locations are enveloped by the AP1000 CSDRS based FRS at the six key locations. In addition, the LNP maximum bearing pressure is less than the CSDRS based maximum bearing pressure of 24 ksf for soft rock sites. For the 24 ksf bearing pressure, the LNP site specific bearing factor of safety is greater than the acceptable factor of safety for static and dynamic loadings (Subsection 2.5.4.10.1.1). The LNP SSI analysis results are documented in Subsection 3.7.1.1.1. Thus, LNP site unique foundation conditions do not lower the High Confidence Low Probability of Failure (HCLPF) values calculated for the certified design.

As shown in Figures 2.5.2-355 and 2.5.2-357, both the CEUS SSC GMRS and the PBSRS are enveloped by the AP1000 CSDRS. As discussed in Subsection 3.7.1.1.2, the CEUS SSC LNP site specific floor response spectra (FRS) at the six key locations are bounded by the CSDRS FRS. In addition, the CEUS SSC LNP site specific nuclear island maximum bearing pressure is less than the 24 ksf design value. Thus, LNP site unique foundation conditions and CEUS SSC ground motions do not lower the High Confidence Low Probability of Failure (HCLPF) values calculated for the certified design.

The soils under the LNP 1 and LNP 2 nuclear islands (NI) foundations will be excavated to rock and backfilled with Roller Compacted Concrete (RCC), as discussed in Subsection 2.5.4.5.3. For the NI, this eliminates any potential site-specific effects such as seismically induced liquefaction settlements, slope stability, foundation failure or relative settlements that would lower the HCLPF values calculated for the certified design. As described in Subsection 2.5.4.8, the LNP site-specific soil conditions also do not affect the nuclear island sliding and overturning stability based on Westinghouse analysis. Thus, LNP site-specific soil conditions do not lower the HCLPF values calculated for the certified design.

As described in Subsection 2.5.4.8, LNP site-specific liquefaction analysis (for PBSRS) was performed for soil beyond the nuclear island perimeter which will be left in place. Based on the liquefaction analysis, it was concluded that liquefiable zones under the LNP 1 and 2 footprints are confined to the northwest corner of the Unit 2 Turbine Building and in isolated random pockets under the remaining LNP 1 and 2 footprints. The LNP earthwork design will incorporate vertical and horizontal drains that will prevent liquefaction in the northwest corner of the Unit 2 Turbine Building and in isolated random pockets under the remaining LNP 1 and 2 footprints. The extent of these horizontal and vertical drains is shown in Figures 2.5.4.8-205 and 2.5.4.8-206. Liquefaction analysis was also performed for 10^{-5} uniform hazard response spectra (UHRS) for soil beyond the nuclear island perimeter which will be left in place as is described in Subsection 2.5.4.8. Based on this liquefaction analysis, it can be concluded that liquefiable zones under the LNP 1 and 2 footprints for 10^{-5} UHRS are confined soil zones where LNP earthwork design will incorporate vertical and horizontal drains that prevent liquefaction (Figures 2.5.4.8-205 and 2.5.4.8-206). ~~As stated previously, t~~The 10^{-5} UHRS is greater than 1.67 times the LNP scaled GMRS and the scaled PBSRS developed using the updated EPRI SOG model, and the GMRS and the PBSRS developed using the CEUS SSC model and modified CAV filter. Thus, liquefaction potential of soil beyond the nuclear island perimeter which will be left in place has the potential to drive the plant level HCLPF; however the soil liquefaction HCLPF exceeds the 1.67*GMRS goal for the plant level HCLPF.

Seismic Category II structures (Annex Building [AB] and the first bay of the Turbine Building [TB]) and nonsafety-related structures (rest of the TB and Radwaste Building [RB]) adjacent to the NI will be supported on drilled shaft foundations. The Seismic Category II/I interaction issues between the adjacent drilled shaft supported structures and the NI have been addressed in Subsections 3.7.2.8.1, 3.7.2.8.2, and 3.7.2.8.3. The probable maximum relative displacements between the NI and the adjacent Turbine, Annex, and Radwaste Buildings' foundation mat for the PBSRS and the 10^{-5} UHRS are less than the 50 mm (2.0 inch) gap between the NI and the adjacent buildings' foundation mats. The 10^{-5} UHRS is greater than 1.67 times higher than the LNP scaled GMRS and the scaled PBSRS developed using the updated EPRI SOG model, and the GMRS and the PBSRS developed using the CEUS SSC model and modified CAV filter. Thus, Seismic Category II/I interaction between the NI and the adjacent buildings has the potential to drive the plant level HCLPF; however the HCLPF for Seismic Category II/I interaction between the NI and the adjacent buildings exceeds the 1.67*GMRS goal for the plant level HCLPF.

The LNP RCC bridging mat is designed to span the postulated (conservative) design basis karst void of 10 ft. The failure of the RCC bridging mat can result in displacement of the AP1000 nuclear island foundation in excess of the maximum 6 in. displacements specified in DCD Tier 1 Table 5.0-1. In the AP1000 PRA-based Seismic Margin Assessment, the RCC bridging mat failure is conservatively assumed to fall within the gross structural collapse event modeled in the hierarchical event tree discussed in DCD Section 19.55. As gross structural collapse is assumed to directly lead to core damage, failure of the RCC bridging mat has the potential to drive the plant level high confidence low probability of failure (HCLPF) value. The HCLPF capacity of the RCC mat was calculated as ≥0.1~~2~~4g using the conservative deterministic failure margin (CDFM) methodology of Reference 19.55.7-201. The ≥0.1~~2~~4g HCLPF capacity of the RCC bridging mat ~~is 1.76 times the LNP site-specific GMRS peak ground acceleration; this~~ exceeds the overall plant HCLPF acceptance criteria of 1.67*scaled GMRS using the updated EPRI SOG model and the 1.67*GMRS developed using the CEUS SSC model and modified CAV filter.

Table 19.55-201 summarizes the HCLPF capacities of the LNP site-specific design features (e.g., RCC bridging mat, potential against soil liquefaction, and Seismic Category II/I interaction between the nuclear island and the adjacent buildings).

Thus, it can be concluded that the Seismic Margin Assessment analysis documented in Section 19.55 is applicable to the LNP site. Exceeding the HCLPF capacities for soil liquefaction and Seismic Category II/I interaction effects of buildings adjacent to the nuclear island will not affect the plant level HCLPF capacity. The RCC bridging mat HCLPF capacity, while potentially driving the plant-level HCLPF, exceeds the plant level HCLPF goal of 1.67*scaled GMRS using the updated EPRO SOG model and the GMRS developed using the CEUS SSC model and modified CAV filter.

19.55.7 REFERENCES

Add the following information at the end of DCD Subsection 19.55.7:

201. EPRI Report No. NP-6041-SL, “A Methodology for Assessment of Nuclear Power Plant Seismic Margin”, Revision 1, August 1991.

Table 19.55-201
HCLPF Capacities for LNP Site Specific Design Features

LNP COL 19.59.10-6

Description	HCLPF Capacity[(a)]	HCLPF/GMRS[(b)]	Basis
Soil Liquefaction Potential under Adjacent Buildings	> 0.~~12g~~14g	> 1.67 GMRS	(c)
Seismic II/I Interaction Potential	> 0.~~12g~~14g	> 1.67 GMRS	(d)
RCC bridging mat	≥0.~~12g~~14g	≥1.67 GMRS	(e)

Notes:

a) LNP scaled ~~site-specific~~ Ground Motion Response Spectra (GMRS) peak ground acceleration (PGA) is 0.~~0691g~~084g using updated EPRI SOG model (Subsection 2.5.2.6). The GMRS PGA using CEUS SSC model and modified CAV filter is 0.073g (Subsection 2.5.2.7).

b) HCLPF Capacity as a fraction of LNP ~~site-specific~~updated EPRI SOG scaled GMRS PGA.

c) Liquefaction potential of soils under the adjacent buildings was evaluated for the LNP ~~site-specific~~updated EPRI SOG 10^{-5} annual exceedance probability Uniform Hazard Response Spectra (10^{-5} UHRS). The LNP updated EPRI SOG 10^{-5} UHRS is greater than 1.67*scaled GMRS using the updated EPRI SOG model (Subsection 2.5.2.6) and the CEUS SSC GMRS with the modified CAV filter (Subsection 2.5.2.7).

d) Relative displacement between the NI and adjacent buildings for the LNP ~~site-specific~~updated EPRI SOG 10^{-5} UHRS is less than the gap provided. The LNP updated EPRI SOG 10^{-5} UHRS is greater than 1.67*scaled GMRS using the updated EPRI SOG model (Subsection 2.5.2.6) and the CEUS SSC GMRS with the modified CAV filter (Subsection 2.5.2.7).

e) HCLPF capacity calculated using conservative deterministic failure margin method of Reference 19.55.7-201.